Compartmental Differences in the Retinal Ganglion Cell Mitochondrial Proteome

by

Liam Steven Connor Lewis

Department of Pharmacology and Cancer Biology
Duke University

Defense Date: July 18th, 2024

Approved:

Dr. Vadim Arshavsky, Supervisor

Dr. Sidney Gospe III

Dr. Nikoleta Tsvetanova

Dr. Kris Wood

Dr. Laurie Sanders

Dissertation submitted in partial fulfillment of the requirements for the degree of Doctor of Philosophy in the Department of Pharmacology and Cancer Biology in The Graduate School of Duke University
2024

ABSTRACT

Compartmental Differences in the Retinal Ganglion Cell Mitochondrial Proteome

by

Liam Steven Connor Lewis

Department of Pharmacology and Cancer Biology
Duke University

Defense Date: July 18th, 2024

Approved:

Dr. Vadim Arshavsky, Supervisor

Dr. Sidney Gospe III

Dr. Nikoleta Tsvetanova

Dr. Kris Wood

Dr. Laurie Sanders

An abstract of a dissertation submitted in partial fulfillment of the requirements for the degree of Doctor of Philosophy in the Department of Pharmacology and Cancer Biology in The Graduate School of
Duke University
2024

Abstract

Retinal ganglion cells (RGCs) are projection neurons of the retina that are a nexus for integrating light signals originating from retinal photoreceptors and transmitting them to the visual processing centers of the brain. RGCs have a highly polarized morphology broadly divided into somatodendritic and axonal compartments. The drastically dissimilar structures and functions of these compartments implies that they face different bioenergetic and other physiological demands. As RGCs are known to be uniquely sensitive to dysfunction of mitochondria, it is believed that these organelles are key to maintaining RGC homeostasis and survival. Differences in mitochondrial biology are likely to be tailored to the specific physiological needs of each RGC compartment.

This dissertation focuses on identifying fundamental differences between RGC mitochondria in the somatodendritic and axonal compartments. Compartment-specific functional disparities between mitochondria may not only highlight unique physiological demands inherent to these compartments but also play a pathophysiological role in the development of RGC dysfunction and death in various optic neuropathies. We hypothesized that compartmental differences in mitochondrial biology would be reflected by dissimilarities in mitochondrial protein composition and therefore be amenable to interrogation using proteomics.

We describe an optimized protocol to isolate intact mitochondria separately from mouse RGC somatodendritic and axonal compartments by immunoprecipitating labeled mitochondria from novel RGC MitoTag mice. These genetically modified mice express a cytosol-facing GFP tag specifically on RGC mitochondria, allowing for GFP-based immunoprecipitation of mitochondria from the RGC somatodendritic compartment in the retina and from the axonal compartment in the optic nerve. Using liquid chromatography-mass spectrometry techniques, we identified several hundred proteins in the RGC somatodendritic and axonal mitochondrial immunoprecipitates,

including a number of proteins highly enriched or exclusively identified in either compartment. To validate these findings, we further analyzed three mitochondrial proteins with distinct compartmental enrichment profiles: superoxide dismutase (SOD2), enriched in the RGC somatodendritic compartment; sideroflexin-3 (SFXN3), expressed equally in both compartments; and trifunctional enzyme subunit α (HADHA), enriched in the RGC axonal compartment. The expression and localization profiles of these proteins within RGCs were assessed using immunofluorescence techniques and compared to the protein abundance data obtained in the proteomics analysis.

We subsequently explored RGC axon-specific metabolic programs after the identification of several enzymes involved in long-chain fatty acid catabolism as being enriched RGC axonal mitochondria. Metabolite profiling of mitochondria obtained in a compartment-specific manner from RGC MitoTag mice revealed an abundance of long-chain fatty acylcarnitine molecules primed for fatty acid oxidation in axonal mitochondria. Building from this finding, we performed RGC-specific genetic ablation of carnitine palmitoyltransferase 1, thereby depriving RGC mitochondria of the ability to import fatty acylcarnitine molecules to be used as metabolic substrates for the generation of cellular ATP. When assessing RGC abundance in the setting of chronic impairment of mitochondrial fatty acid import, there appeared to be a subtle trend towards decreased RGC survival in the mutant mice.

Our findings provide clues to compartment-specific distinctions in the roles of RGC mitochondria. While compartmentalized energy gradients have been previously identified in other neuronal populations, our work represents the first to pursue metabolic differences within a type of retinal neuron. Exploring how several optic nerve disease states impact mitochondrial proteomic differences in RGCs is the subject of ongoing work in the lab, with preliminary results described here.

Table of Contents

List of Tables

List of Figures

List of Abbreviations

AAV, Adeno-associated Virus

ADOA, Autosomal Dominant Optic Atrophy

ADP, Adenosine Diphosphate

AIS, Axon Initial Segment

ATP, Adenosine Triphosphate

CAT, Carnitine O-acetyltransferase

CNS, Central Nervous System

COX4, Cytochrome C Oxidase, subunit 4

Cpt, Carnitine Palmitoyltransferase 1

DNA, Deoxyribonucleic Acid

ER, Endoplasmic Reticulum

ERG, Electroretinogram

ETC, Electron Transport Chain

FACS, Fatty acyl-CoA Ligase

FADH2, Flavin Adenine Dinucleotide

FAO, Fatty Acid β-Oxidation

GCL, Ganglion Cell Layer

GFP, Green Fluorescent Protein

GTP, Guanosine Triphosphate

HADHA, Trifunctional Enzyme, subunit A

HADHB, Trifunctional Enzyme, subunit B

ILM, Inner Limiting Membrane

IMM, Inner Mitochondrial Membrane

IMS, Intermembrane Space

INL, Inner Nuclear Layer

IOP, Intraocular Pressure

IPL, Inner Plexiform Layer

KHC, Kinesin Heavy Chain

LC-MS/MS, Liquid Chromatography-tandem Mass Spectrometry

LGN, Lateral Geniculate Nucleus

LHON, Leber Hereditary Optic Neuropathy

MAM, Mitochondria-Associated Membrane

MDV, Mitochondria Derived Vesicles

MPC, Mitochondrial Pyruvate Carrier

NADH, Nicotinamide adenine dinucleotide

NDUFS4, NADH dehydrogenase [ubiquinone] iron-sulfur protein 4

OMA1, Mitochondrial metallopeptidase OMA1

OMM, Outer Mitochondrial Membrane

ON, Optic Nerve

ONL, Outer Nuclear Layer

OPA1, Dynamin-like GTPase OPA1

OPL, Outer Plexiform Layer

OXHPOS, Oxidative Phosphorylation

PINK1, Serine/Threonine Protein Kinase 1

PTEN, Phosphatidylinositol 3,4,5-trisphosphate 3-phosphatase and dual-specificity protein phosphatase

RBPMS, Ribosomal Binding Protein, Multiple Splicing 1

RGC, Retinal Ganglion Cell

RNFL, Retinal Nerve Fiber Layer

ROS, Reactive Oxygen Species

RPE, Retinal Pigment Epithelium

SC, Superior Colliculus

SFXN3, Sideroflexin-3

SOD2, Superoxide Dismutase [Mn]

TCA, Tricarboxylic Acid Cycle

VDAC, Voltage-dependent Anion-selective Channel

VLCAD, Very long-chain acyl-CoA dehydrogenase

Acknowledgements

My time as a graduate student in the Pharmacology & Cancer Biology (PCB) program at Duke University has been nothing short of fulfilling and fun. I have made countless friends and memories at Duke and am forever grateful to those individuals who continuously supported me.

I must first thank Andrew Ottens, PhD, from Virginia Commonwealth University. While at VCU, Dr. Ottens ("Dr. O") served as my undergraduate research mentor from 2014-2016, and eventually my mentor for the VCU Post-Baccalaureate Research Education Program (PREP) from 2017-2018. I am incredibly grateful for your advice about alternative careers in science and truly following my passions and curiosity. Your desire to create supportive environments for your students and foster an atmosphere of acceptance and fun is why I continued to pursue graduate school and neurobiology-related research. Thank you also to David Sherwood, PhD, for being a great introduction to Duke University as my first laboratory rotation. Thank you for nurturing such a supportive lab environment and continuing to stay in touch throughout my graduate school journey.

Thank you to my lab-mates – Howard Bomze, PhD, Samantha Wilkison, PhD, and Cora Bright – for always providing advice and tips, pertaining to lab or life. Thank you for always listening to my frustrations, and always wanting to go to a happy hour or lunch. Throughout all the difficult times in our lab, I am grateful to have such a great group of individuals to lean on.

Thank you to my friends from the Cell & Molecular Biology (CMB) and Duke BioCoRE programs, especially Pia, Ale, and Fabi. Our social gatherings and happy hours to vent about the trials and tribulations of graduate school were always a constant source of enjoyment.

I am forever thankful to my family – especially my mom, dad, and step-dad. I can't begin to imagine how much time and energy it has taken over the years for you all to support me through school. Thank you for working so tirelessly to extend me opportunities in life that I could never have dreamed of. Dad, thank you for always being so curious about science and my research. Thank you for exposing me to science fiction and outlandish theories since I was a child. Mom, thank you for allowing me to have a “secret lab” under the stairs as a kid – I would never be here without you.

Finally, thank you to my girlfriend, Taryn Hayes, for being involved (begrudgingly or not) through every step of graduate school. Without you and your support, I don’t believe I would ever have made it through this program. I am forever in awe of your positivity and will to persevere through any situation. I look so forward to building our future together and seeing where our careers take us in life.

1. Introduction

1.1 Rationale

Mitochondria are energy-producing organelles that are key to cellular development, maintenance, and, ultimately, death. These organelles exist in almost all cells of eukaryotic organisms and are typically distributed throughout the cell, actively transported to and positioned at various sites to perform important cellular and metabolic functions (Altmann 1894). Chief among the cellular functions performed by mitochondria is oxidative metabolism, with the enzymatic reactions of the tricarboxylic acid (TCA) cycle and the ATP-producing electron transport chain (ETC) occurring within mitochondria. Mitochondria are also involved in the biosynthesis of important cellular biochemical components such as phospholipids, heme, and neurotransmitters (Nunnari and Suomalainen 2012; Wang, Xu et al. 2019). Additionally, mitochondria have important roles in the management of cellular reactive oxygen species (ROS) generation, apoptosis regulation, calcium buffering, and local protein translation **(Figure 1)** (Kiedrowski and Costa 1995; Green and Reed 1998; Cioni, Lin et al. 2019; Norat, Soldozy et al. 2020).

Neurons are highly metabolically active cells and, as such, are heavily reliant on mitochondria. These cells are divided into distinct compartments that are highly differentiated in their functional capacities and differ greatly in their morphologies and overall volumes. It is important to note that on average, neuronal axons are ~20,000 times longer than the greatest dimension of the somas from which they arise. This extreme architecture necessitates a high level of compartment-specific functional regulation (Wang, Medress et al. 2012) (**Figure 2)**. This includes the proper genesis, maintenance, and removal of cellular organelles functioning in each area of the neuron, in order to coordinate a harmonization of supplying the cell with sufficient materials for physiological homeostasis, including meeting the local ATP demands.

Mitochondrial oxidative metabolism is the primary biochemical process that supports the energy needs of neurons, responsible for producing ~90% of the cell's ATP stores (Cooper and Adams 2022). The importance of oxidative metabolism in neurons is emphasized by the fact that while it accounts for only 2% of the body's mass, the central nervous system (CNS) consumes 20% of the body's oxygen (Attwell and Laughlin 2001). Mitochondria are present to some extent in every portion of the neuron to support local bioenergetics. Accordingly, some mitochondria must be kept in the cell soma, while the remaining mitochondria must be trafficked and positioned within the dendrites, axons, and synapses.

The focus of this dissertation is to gain insight into compartmentalized mitochondrial functions in a particular type of neuron: the retinal ganglion cell (RGC). RGCs are projection neurons which transmit visual information from the retina to the CNS. In our initial work, detailed in Chapter 2, we uncover differences in the proteomes of mitochondria localizing to the somatodendritic and axonal compartments of the RGC, and we validate the differential abundance of three proteins – SOD2, SFXN3, and HADHA – using immunofluorescence methods. We then investigate an axon-specific signature of mitochondrial fatty acid oxidation (described in Chapter 3) and study the effects of RGC-specific loss of Cpt1a, the protein responsible for importing fatty acid molecules across the mitochondrial outer membrane. Our work sheds on light potential compartmentalized mitochondrial functions which may influence the neurodegenerative properties of optic neuropathies.

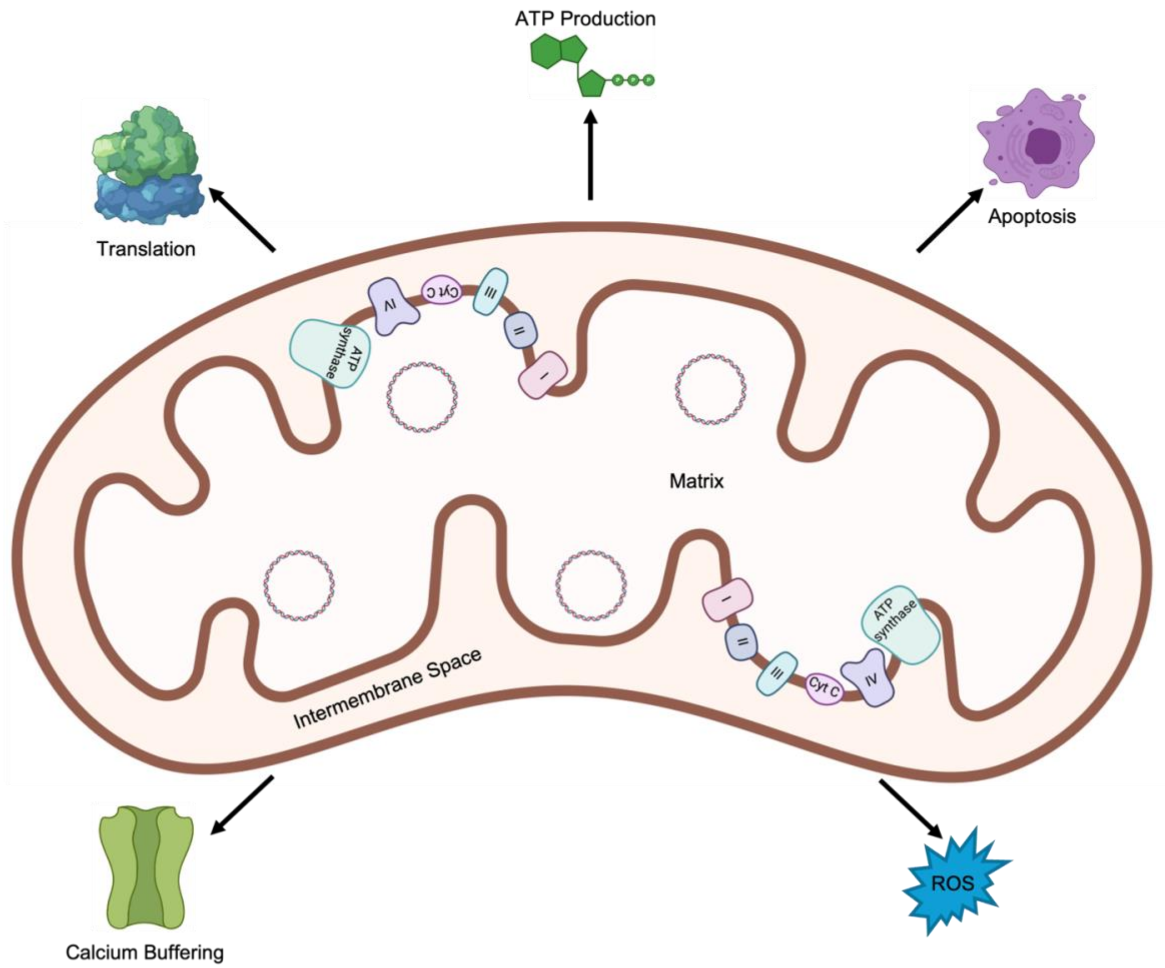

Figure 1. Mitochondria are double-membrane organelles fulfilling numerous cellular functions. Mitochondria contain their own circular mitochondrial DNA within the matrix. The enzymatic reactions of the TCA cycle in the matrix and the Electron Transport Chain in the inner mitochondrial membrane facilitate ATP production through oxidative phosphorylation. Additionally, mitochondria play pivotal roles in buffering cellular calcium, production of reactive oxygen species (ROS), serving as a site of local protein translation, and regulating apoptosis.

1.2 Mitochondria

1.2.1 Mitochondrial Composition

Mitochondria are delineated by two discrete lipid bilayers: the outer mitochondrial membrane (OMM), which faces the cytosol, and inner mitochondrial membrane (IMM). Between the two membranes is the intermembrane space, and entirely enclosed by the IMM is the mitochondrial matrix. As described later, the IMM and intermembrane space are key to ATP generation by the electron transport chain. The IMM contains many infoldings (cristae) in order to maximize surface area for this purpose. The mitochondrial matrix contains the enzymes of the TCA cycle. In addition, mitochondria contain their own mitochondrial DNA (mtDNA) and ribosomes, both localizing within the matrix. Despite having these components necessary for replication and protein synthesis, mitochondria are not truly autonomous: normal mitochondrial biology is also dependent on the import of proteins whose genes are encoded in the nuclear genome.

Proteins localized to mitochondria are highly specialized and provide a variety of organellar functions, such as import of metabolic substrates across the mitochondrial membranes, fatty acid oxidation to produce acetyl-CoA, the enzymatic reactions of the TCA cycle, and electron transport ultimately resulting in reduction of O_2 to H_2O and the generation of ATP. Moreover, mitochondrial dynamics (e.g. fusion, fission, transport) are regulated by specific proteins on the outer mitochondrial membrane. To perform these varied functions, mitochondria have a core proteome consisting of around 1,500 proteins. Vertebrate mtDNA only encodes for 15 proteins (13 OXPHOS subunits and 2 mitochondrial ribosome components), while the vast majority of mitochondrial proteins are encoded by the nuclear genome and targeted to the mitochondria (Alston, Rocha et al. 2017). Not surprisingly, it has been established that there is great amount of heterogeneity in the mitochondrial proteomes between different tissues (i.e. liver, heart, brain), yet the heterogeneity of mitochondrial protein compositions within cells has only begun to be investigated (Pagliarini, Calvo et al. 2008).

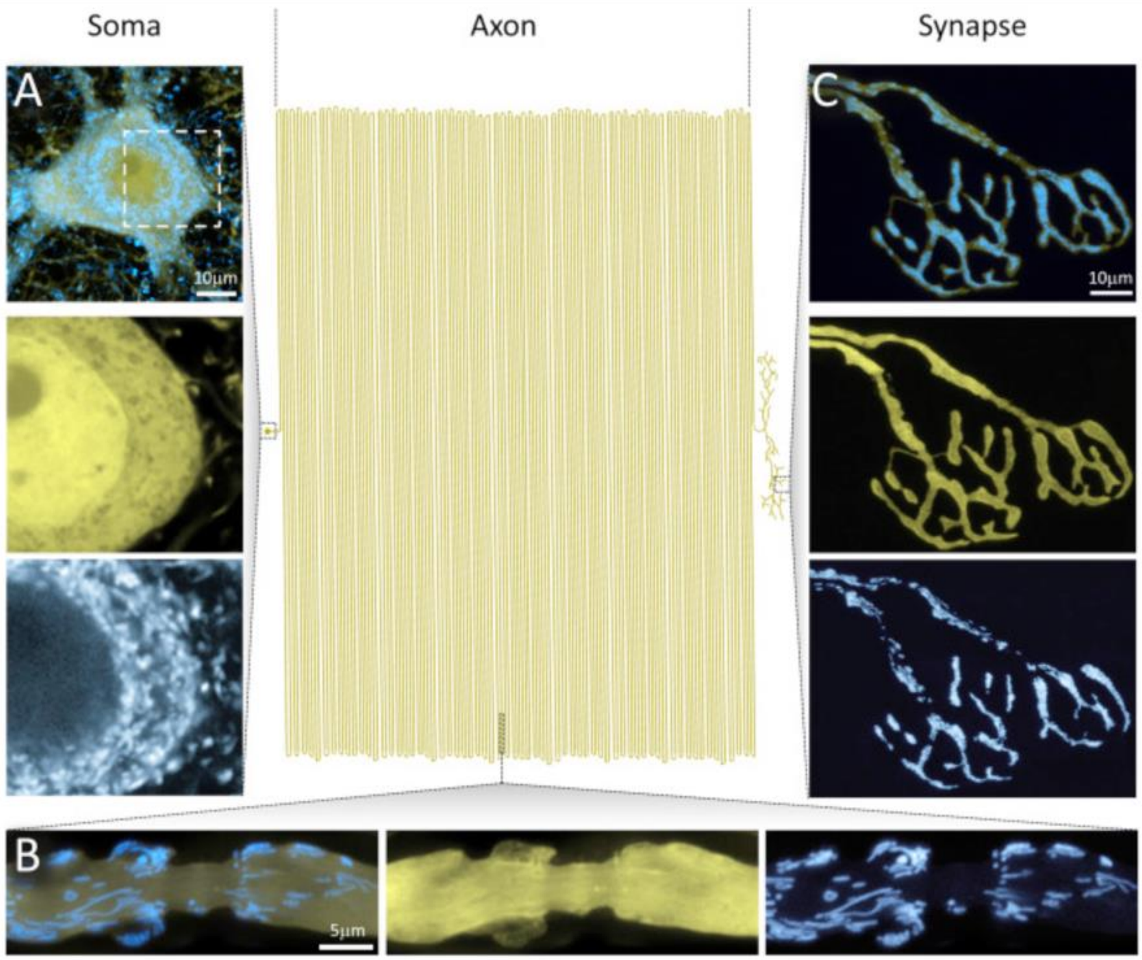

Figure 2. Compartmentalization of projection neurons and mitochondrial positioning. The central diagram depicts a projection neuron to scale, with the axon dwarfing all other compartments. Insets: (A) A cell soma with perinuclear mitochondria (blue); (B) mitochondria positioned on either side of a node of Ranvier along the axon; (C) dense accumulation of mitochondria at the synaptic terminal. Adapted from (Misgeld and Schwarz 2017).

1.2.2 Mitochondrial Dynamics

Mitochondrial positioning and function are regulated through processes like trafficking, fusion and fission, and quality control mechanisms such as mitophagy and membrane budding via mitochondria-derived vesicles (MDVs) **(Figure 3)**. In large, polarized cells, such as RGCs and other projection neurons, mitochondria are transported on microtubules via large motor/adaptor complex proteins. Kif5B (Kinesin family member 5B) or Kinesin Heavy Chain (KHC) is a member of the Kinesin-1 family and contains motor domains that allow for anterograde transport of mitochondria away from the cell's center(Schwarz 2013), whereas dynein/dynactin motor proteins are responsible for retrograde movement towards the center. A set of GTPase proteins, Miro (RhoT1/2) and Milton (Trak1/2) are responsible for coupling the motor adaptor proteins KHC and dynein/dynactin to mitochondria (Stowers, Megeath et al. 2002; Brickley, Smith et al. 2005; Fransson, Ruusala et al. 2006; Glater , Megeath et al. 2006).

Mitochondrial size, shape, morphology, and quality are adjusted through fusion and fission processes in response to local homeostatic needs and other stimuli (Yu and Pekkurnaz 2018). Because mitochondria are structurally complex, the fission and fusion processes require a multitude of proteins working together in a coordinated fashion. The OMM and IMM are phospholipid bilayers that are structurally and functionally distinct (Funai, Summers et al. 2020). During the process of OMM fusion, Mitofusin 1 and Mitofusin 2 (Mfn1/2) are tethered to mitochondria and allow for the fusion of the OMM of two distinct mitochondria through GTP hydrolysis (Chen, Detmer et al. 2003; Qi, Yan et al. 2016). Genetic deletion of Mfn1 and Mfn2 lead to neurodevelopmental abnormalities and embryonic lethality – primarily due to neuron death and mitochondrial fragmentation/transport deficiencies from the loss of mitochondrial fusion capacity (Chen, McCaffery et al. 2007). OMM fission is mediated by a GTPase protein, Dynamin-related protein 1 (Drp1), and its receptor proteins: mitochondrial fission protein 1 (Fis1), mitochondrial fission factor (Mff), and mitochondrial dynamics proteins of 49 and 51 kDa (MiD49/ MiD51) (Losón, Song et al. 2013). Once recruited to the OMM, Drp1 oligomerizes and forms helices around the surface of mitochondria, resulting in membrane constriction and triggering mitochondrial fission (Friedman, Lackner et al. 2011). This Drp1 activity can be additionally modulated through post-translation modification (Chang and Blackstone 2010). As mentioned earlier, OPA1, a dynamin-like GTPase, is responsible for regulating both IMM fusion and fission (Yu and Pekkurnaz 2018). OPA1, encoded by a single gene, is post-transcriptionally proteolyzed to a long and short isoform (L-OPA1 and S-OPA1). L-OPA1 accumulation is responsible for triggering IMM fusion, while S-OPA1 drives fragmentation of mitochondria (Ban, Ishihara et al. 2017). Importantly, the cleavage of L-OPA1 to S-OPA1 is regulated by the proteases OMA1 and YME1LA, in a cellular stress-dependent manner (Ishihara, Fujita et al. 2006). The exquisite coordination and regulation of OMM and IMM fusion/fission processes highlights how mitochondria can alter their morphology in response to cellular stimuli and stress to manage bioenergetic and functional capacities.

Mitochondria maintain their intrinsic homeostasis in similar manners to cells, by degrading and removing damaged components that are detrimental to their function. In mitochondria this occurs via two distinct mechanisms: regulated autophagy of whole mitochondria ('mitophagy') (Youle and Narendra 2011) and release of mitochondria-derived vesicles (MDVs). MDVs are cargo-carrying vesicles that are transferred from mitochondria to other organelles through the process of "budding." MDVs can allow for the selective removal of mitochondrial components. Soubannier et al, showed that MDVs targeted to lysosomes contained oxidized mitochondrial proteins, such as VDAC and Complex III subunits (Soubannier, Rippstein et al. 2012). Mammalian mitophagy can occur via two independent pathways: NIX- and Pink1/Parkin-mediated pathways. NIX is a selective autophagy receptor which accumulates on the surface of mitochondria. NIX binds to MAP1 light chain 3 (LC3), which sequesters mitochondria into autophagosomes(Schweers, Zhang et al. 2007; Novak, Kirkin et al. 2010). Pink1/Parkin-mediated mitophagy is believed to be involved in the degradation and removal of damaged or stressed mitochondria. While Nix and Pink1/Parkin both stimulate the mitophagy pathway, evidence suggests Nix may be a redundant and compensatory pathway – highlighted in the Pink1/Parkin loss-of-function experiments (Koentjoro, Park et al. 2017).The mitochondrial kinase, PTEN-induced putative kinase protein 1 (PINK1), phosphorylates the E3-ubiquitin ligase, Parkin, which is then translocated to and accumulates on the mitochondrial surface (Narendra, Tanaka et al. 2008). Parkin accumulation induces polyubiquitination, causing mitochondria to be engulfed by membranes that then fuse with lysosomes. Beyond simply removing old and damaged mitochondria, mitophagy plays a role in adjusting mitochondrial quantities in changing metabolic landscapes and during specialized developmental milestones (Kissová, Deffieu et al. 2004; Schweers, Zhang et al. 2007; Tal, Winter et al. 2007).

The converse of mitophagy, mitochondrial biogenesis offers a method of replenishment of the mitochondrial pool (Piantadosi, Carraway et al. 2008). As alluded to before, the proteins that comprise the mitochondria are both nuclear- and mitochondria encoded. Because mitochondrial biogenesis requires the coordinated transcription and translation of nuclear- and mitochondria-encoded DNA, mitochondrial biogenesis typically occurs in close proximity to the cell nucleus (Davis and Clayton 1996), and the level of mitochondrial biogenesis can vary from cell-to-cell based on local environmental factors. Peroxisome proliferation factor-activated γ coactivator 1α (PGC-1α) – the master regulator of mitochondrial biogenesis (Fernandez-Marcos and Auwerx 2011) – has been found to become up-regulated in RGCs and astrocytes localized to the inner retina and optic nerve head after a metabolic or oxidative stress (Guo, Dason et al. 2014). On the other hand, decreased PGC-1α levels – thus decreased capacity for mitochondrial biogenesis – was observed in the ganglion cell layer of older mice with experimental glaucoma (Guo, Dason et al.

2014). The capacity for effective mitochondrial quality control likely influences the ability of RGCs and other neurons to weather pathological stressors.

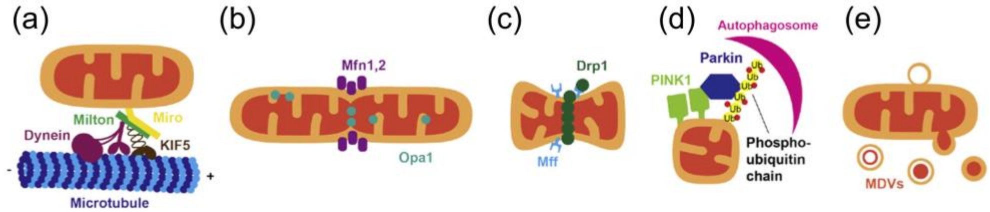

	Transport	Fusion	Fission	Mitophagy	Mitochondria Derived Vesicles (MDVs)
Proteins involved	Miro1, Miro2, Milton, Syntaphilin, KIF5, Dynein	Mfn1, Mfn2, MitoPLD, L-Opa1	Drp1, S-Opa1 Mff, Fis1	NIX, PINK1, Parkin	Vps35, PINK1, Parkin
Function	Regulation of mitochondrial transport on cytoskeleton (Microtubules, actin filaments)	Fusion of two or more mitochondria fused together to become a mitochondrion	Division of a mitochondrion into several mitochondria	Removal of damaged mitochondria for quality control	Generation of small vesicle carrying mitochondrial proteins and lipids to other intracellular organelles
Effects	Intracellular redistribution of mitochondria	Elongation OXPHOS ↑	Fragmentation Mediates mitophagy Glycolysis ↑	Less number of mitochondria	Mediates partial removal of mitochondrial proteins Lipid transport

Figure 3. Overview of Mitochondrial Dynamics and Quality Control Mechanisms. (A) Mitochondrial transport via microtubules is mediated through mitochondrial adaptor proteins Miro and Milton. The adaptor proteins interact with KIF5 and Dynein to transport mitochondria in anterograde and retrograde directions, respectively. (B,C) Mitochondrial fusion (B) and fission (C) are regulated by the fusion proteins Mfn1/1, MitoPLD, and L-Opa1 and by the fission proteins Drp1, S-Opa1, Mff, and Fis1. (D) The process of eliminating defective mitochondria – mitophagy – is modulated through Nix, PNK1, and Parkin protein interactions on the mitochondrial outer membrane. (E) Mitochondrial-derived vesicles (MDVs) form through Vps35, PINK1, and Parkin interactions to achieve removal of mitochondrial components. Adapted from (Yu and Pekkurnaz 2018).

1.2.3 Oxidative Metabolism in Mitochondria

Regular neuronal functions including action potential initiation and propagation utilize ATP generated primarily through the aerobic respiration. Aerobic respiration uses glucose as the major energy substrate and proceeds through three stages: glycolysis, the TCA cycle, and oxidative phosphorylation.

In glycolysis, a series of enzymatic reactions in the cytosol converts glucose, a 6-carbon molecule) into two molecules of pyruvate (a 3-carbon molecule) while additionally generating ATP and nicotinamide adenine dinucleotide (NADH). Pyruvate is then shuttled from the cytosol into the mitochondria via the essential mitochondrial pyruvate carrier (MPC), which is formed by a heterodimer of MPC1 and MPC2 (Bricker, Taylor et al. 2012; Herzig, Raemy et al. 2012).

Within the mitochondrial matrix, all three carbons of pyruvate are oxidized to CO_2, the first when pyruvate is into acetyl-CoA, the major input into the TCA cycle. In the TCA Cycle, acetyl-CoA combines with oxaloacetate to form citrate, and then a successive chain of chemical reactions ultimately oxidizes both carbons derived from acetyl-CoA into CO_2, with a concomitant reduction of NAD+ to NADH and FAD to $FADH_2$ (Chalecka, Kazberuk et al. 2021). It is important to note that while mainly derived from glycolysis and pyruvate metabolism, acetyl-CoA can also be generated within the mitochondria from other sources, such as through the metabolism of fatty acids and amino acids (Ronnett, Kim et al. 2005; Bonora, Patergnani et al. 2012; Torres, Tobón-Cornejo et al. 2023). The three NADH and one $FADH_2$ molecules produced in the TCA cycle then provide critical reducing power to the electron transport chain (ETC) in the IMM.

In the ETC, electrons from NADH and $FADH_2$ are passed through a chain of large protein complexes to generate ATP. As electrons pass from Complex I to Complex III to Complex IV and ultimately onto O_2 to generate H_2O, the energy released is coupled to the extrusion of hydrogen ions from the mitochondrial matrix to the intermembrane space to generate a proton gradient. This gradient is the proton-motive force used by Complex V (ATP Synthase) to generate ATP through the phosphorylation of ADP while dissipating the proton gradient. It is important to note that the ETC is the major source for ROS generation in cells – this is a normal physiological process but can be exacerbated in pathological conditions (Indo, Davidson et al. 2007; Raimondi, Ciccarese et al. 2020). While the proteins that comprise the ETC reside within the IMM, the integrity of the IMM is responsible for maintaining the proton-motive force necessary for ATP generation (Fedorenko, Lishko et al. 2012).

1.2.4 Mitochondrial-Associated Membranes (MAMs)

Mitochondria are involved in complex structural and functional relationships with other organelles in the cell. The contact sites where mitochondria are tethered to other organelles is called mitochondria-associated membranes (MAMs). Mitochondria can form MAMs with the endoplasmic reticulum, lysosomes, and peroxisomes to carry out a number of functions.

The ER is a dynamic organelle that is the site of protein synthesis and folding, calcium storage and release, and lipid synthesis. Mitochondrial and ER functions may be intimately linked through MAMs. Mitochondria-ER contact sites are important in the resource sharing between the two organelles, such as metabolite, nutrient, ion, and lipid allocation. Mfn2 has been heavily implicated in the formation of mitochondria-ER contact sites, through the direct physical tethering of the two organelles. Prior studies have highlighted the importance of Mfn2 in the development and maintenance of these MAMs. Silencing of Mfn2 in mouse embryonic fibroblasts and HeLa cells leads to an increased distance between mitochondria and ER, with a concurrent decrease in calcium uptake in the ER (De Brito and Scorrano 2008; Naon, Zaninello et al. 2016). Mitochondria-ER contact sites also create metabolic connections between the organelles. Liver-specific deletion of Mfn2 in mice induced ER stress through the generation of ROS, which led to glucose intolerance.

Fission sites of mitochondria can also often be indicated by tubular ER and actin cytoskeleton which aid in the Drp1-Mff fission complex. Mitochondria fission which occurs at mitochondria-ER contact sites allows critical mitochondrial inheritance and transfer of phospholipids from mitochondria to ER for membrane restructuring and organization (Friedman, Lackner et al. 2011).

Lysosomes are acidic degradation organelles, primarily responsible for the degradation of autophagy- and endocytosis-derived macromolecules. Recent studies have highlighted functional properties of lysosome-mitochondria contact sites. Vacuole and mitochondria patch (vCLAMP) sites are regulated vacuolar tethering complex (HOPS) subunit Vps39/Vam6 and the Rab GTPase Ypt7 (Hönscher, Mari et al. 2014). Active metabolite transfer, such as with amino acids, ions, and lipids occur at lysosome-mitochondria contact sites (Hönscher, Mari et al. 2014; Ballabio 2016). During amino acid starvation experiments, lysosomal biogenesis and storage of amino acids is induced by decreased mTOR activity. This decreased activity causes decreased translation in mitochondrial fission process protein 1 (MTFP1), leading to mitochondrial elongation (Abu-Remaileh, Wyant et al. 2017; Morita, Prudent et al. 2017). These fluctuations in mitochondrial dynamics influence the activity of the electron transport chain, and ultimately the survival of the cell. This evidence suggests functional crosstalk between mitochondria and lysosomes through mTOR signaling in addition to their core degradation properties.

Peroxisomes are critical organelles involved in ROS management, fatty acid oxidation, and amino acid degradation – and are inextricably linked to mitochondria through metabolic processes. Emerging evidence suggests physical and functional connection between peroxisomes and mitochondria (Cohen, Klug et al. 2014). Peroxisomes have been shown to co-immunoprecipitate with mitochondria (Islinger, Lüers et al. 2006) and to localize to mitochondria-ER contact sites with Pex11 – a peroxisomal factor involved in biogenesis and division (Ušaj, Brložnik et al. 2015). Peroxisomes have also been shown to be functionally linked to mitochondria through ROS signaling and oxidative stress. Indeed, inducing peroxisomal dysfunction through the loss of Pex5 – the peroxisome oxidative stress sensor – in mouse hepatocytes, led to impaired mitochondrial respiration, depleted mtDNA concentrations, and an increase in mitochondrial biogenesis (Peeters, Shinde et al. 2015). The potential for physical connections between mitochondria and other organelles like ER, lysosomes, and peroxisomes is likely to be reflected in the breadth of proteins identified in proteomic analyses of purified mitochondria, as will be discussed in Chapter 3.

1.2.5 Mitochondrial Dysfunction

Mitochondrial dysfunction occurs when mitochondria are unable to carry out essential functions within the cell, leading to diminished ATP generation, increased ROS production and oxidative stress, and impaired calcium buffering. In a neuronal context, mitochondrial dysfunction is a common cause of neurodegeneration. Mitochondrial damage progressively accumulates within cells if it occurs at a rate that overwhelms the cell's ability to sequester and degrade mitochondria through mitophagy(Norat, Soldozy et al. 2020).

Mitochondrial DNA (mtDNA) is subject to mutation just like nuclear DNA (nDNA). While mitochondria have their own DNA quality control mechanisms including an ability to repair broken strands, (Liao, Chen et al. 2022) it is generally less robust than nuclear DNA repair. mtDNA damage, if unchecked, can lead to increased generation of ROS, (Nakabeppu, Tsuchimoto et al. 2007), which can cause oxidative damage to mitochondrial lipids, protein, and DNA (Angelova, Esteras et al. 2021). Due to its proximity to the ETC, mtDNA is even more susceptible to oxidative damage than nDNA (Yakes and Van Houten 1997), and its damage may result in a vicious cycle, mitochondrial dysfunction leading to greater ROS production and then to even greater mitochondrial damage. Mitochondrial-produced ROS may also further exacerbate mitochondrial dysfunction through the oxidation and damage of nDNA, which encodes a majority of mitochondrial proteins(Tanaka, Kovalenko et al. 1996).

1.3 Neuronal Compartmentalization

Neurons are the primary cells of the nervous system and are responsible for rapid communication of information between cells via synapses. Neurons can vary drastically in morphology, size, and function but are typically highly compartmentalized cells that can be broadly divided into dendritic, somatic, axonal, and synaptic compartments (Misgeld and Schwarz 2017). Dendrites are responsible for receiving information from other neurons and the extracellular environment, while the axonal and synaptic compartments communicate to more distal neurons **(Figure 4)**. Dendrites typically exist as numerous projections from the neuronal soma and contain neurotransmitter receptors and ion pumps and channels in their plasma membrane in order to receive extrinsic signals and generate an initial electric response. The soma or cell body houses the nucleus, most cellular organelles, including mitochondria, and is where the bulk of protein biogenesis processes occur.

The axon is classically a single long projection emanating from the soma. It can be further characterized based on their myelination patterns. All axons contain an axon initial segment (AIS), a thin, unmyelinated region (10-60 µm) past the origin of the axon (axon hillock) (Debanne, Campanac et al. 2011; Kole and Stuart 2012). The AIS contains a dense concentration of ion channels, from which the action potential is generated and then propagated through the remaining axon segment (Chang and Blackstone 2010; Kole and Stuart 2012). The local clustering of sodium (Na^+), potassium (K^+), and calcium (Ca^{2+}) ion channels allows for a massive, transient inward current of ions that causes a rapid, local depolarization event to initiate the propagation of the action potential throughout the rest of the axon (**Figure 5**) (Boiko, Van Wart et al. 2003; Lorincz and Nusser 2008). Nodes of Ranvier are interspersed, focally unmyelinated regions along the length of the axon(Debanne, Campanac et al. 2011). These nodes have a similar ion channel and supporting protein composition as the AIS, allowing for additional sites of rapid depolarization to continue moving the action potential to the terminal end of the axon(Yang, Ogawa et al. 2007; Rasband 2010). At the synaptic terminal, neurotransmitters are released across the synaptic cleft to the neighboring cell, allowing for inter-cellular communication of neuronal signals. Projection neurons can span lengths of millimeters to greater than a meter in length in some species, which can create spatial energy gradients along their length (Quintela-López, Shiina et al. 2022).

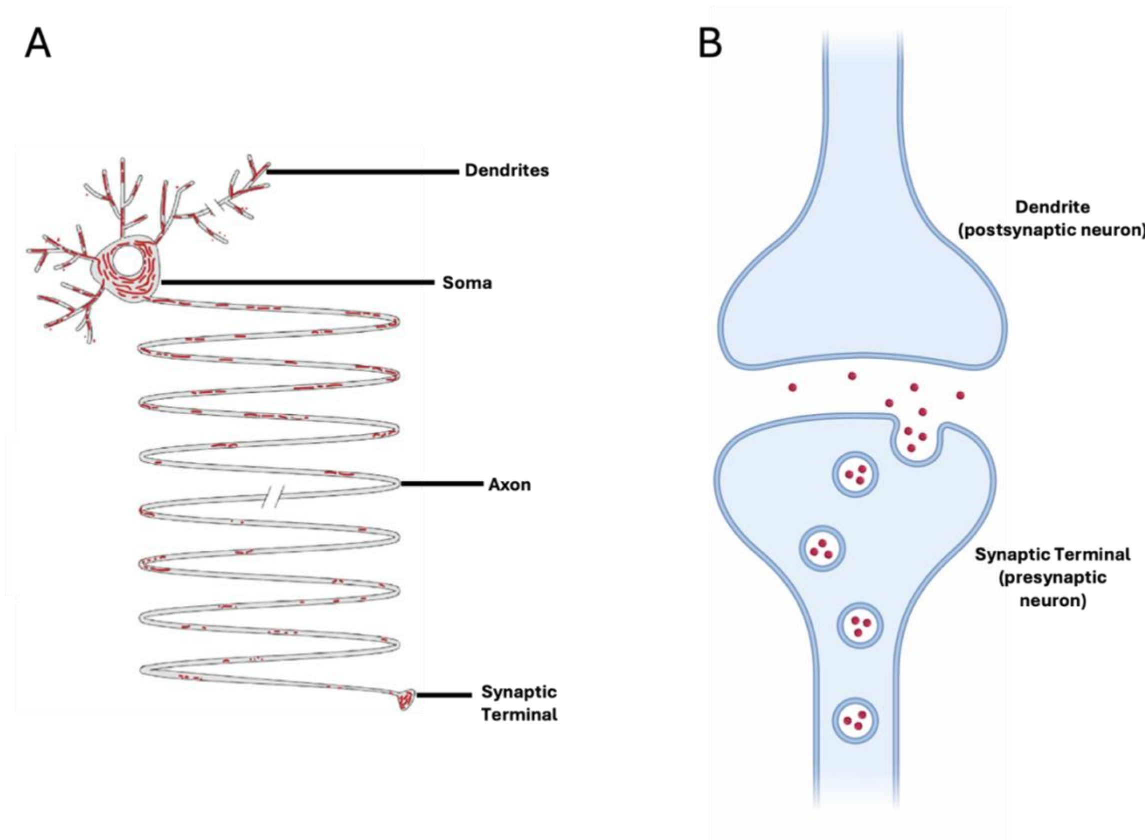

Figure 4. Neurons are highly polarized cells with a microanatomy designed to optimize receipt and transmission of signals. (A) Mitochondria (depicted in red) populate and provide essential cellular functions within the major neuronal compartments. (B) Synaptic communication between neurons is mediated by release of synaptic vesicles containing neurotransmitters from the synaptic terminal of the presynaptic neuron and the stimulation of receptors on the plasma membrane on the dendrites of postsynaptic cells. Adapted from (Pekkurnaz and Wang 2022).

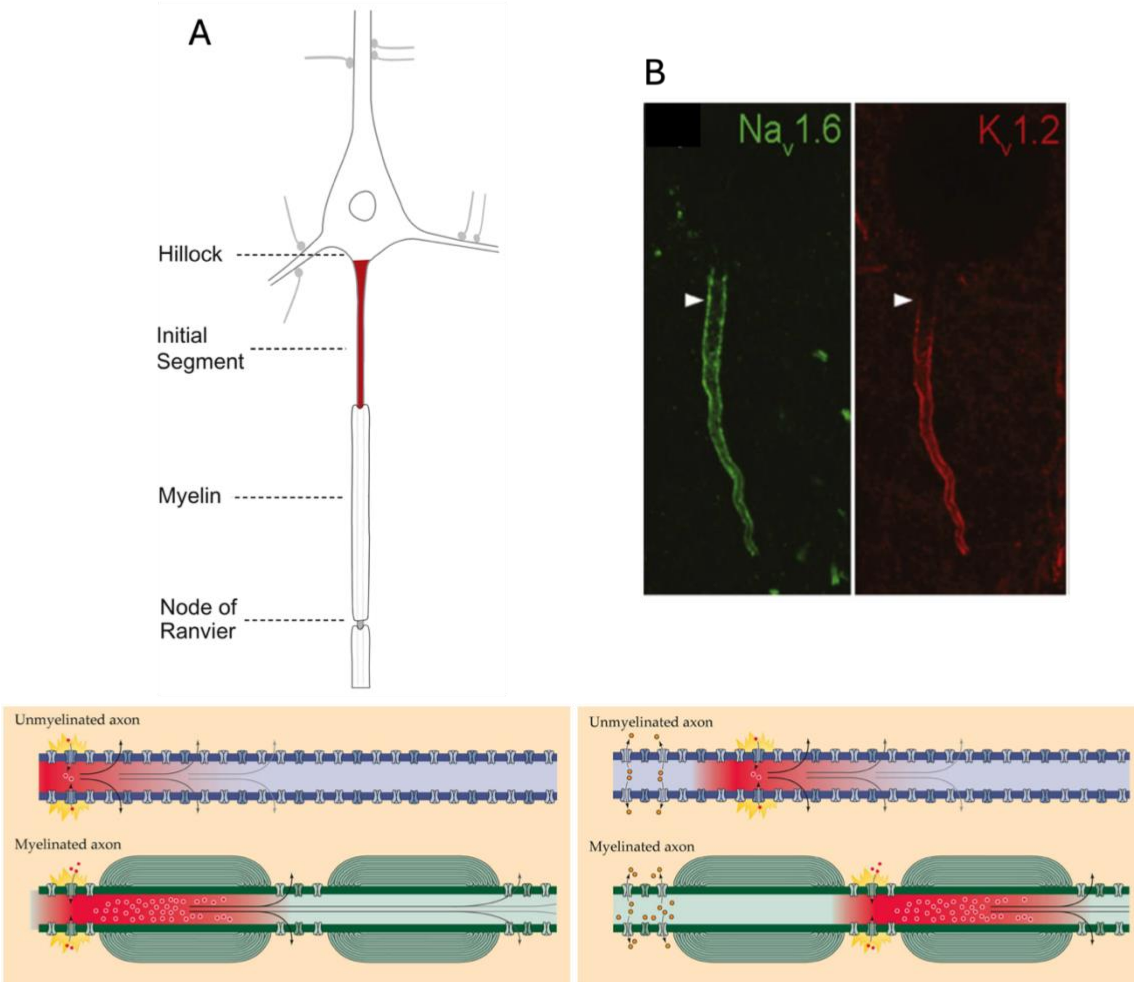

Figure 5. The axon initial segment and nodes of Ranvier allow for action potentials to propagate to the synapse. (A) Schematic of a neuron, highlighting the axon initial segment, where action potentials are generated and then transmitted down the axon via salutatory conduction along nodes of Ranvier. (B) Confocal microscopy images of a cultured neuron showing prominent expression of the voltage-gated sodium channel 1.6 (green) and voltage-gated potassium channel 1.2 (red) on the plasm membrane of the axon initial segment. (C) Propagation of the action potential in unmyelinated and myelinated axons. Nodes of Ranvier allow faster and more efficient conductance of action potentials compared to unmyelinated axons. Adapted from (Kole and Stuart 2012)

1.4 The Afferent Visual System

The afferent visual system is the most external and accessible portion of the CNS. The neural retina allows visual perception of light signals based on the stratification and coordination of six principal neuronal cell types – rod photoreceptors, cone photoreceptors, bipolar cells, horizontal cells, amacrine cells, and retinal ganglion cells – and two macroglia cell types – Müller Glia and astrocytes **(Figure 6A and 6B)** (Wässle 2004; Baden, Euler et al. 2020). The retina is specifically subdivided into nine distinct layers from the innermost to outermost retina – the inner limiting membrane (ILM), retinal nerve fiber layer (RNFL), ganglion cell layer (GCL), inner plexiform layer (ILM), inner nuclear layer (INL), outer plexiform layer (OPL), outer nuclear layer (ONL), photoreceptor inner segment/outer segment layer (IS/OS), and retinal pigment epithelium (RPE) **(Figure 6C)** (Masland 2012). Once photons are received by photoreceptors (rods and cones), the process of phototransduction leads to light-induced hyperpolarization of the cells, reducing the synaptic release of glutamate to the second-order neurons, bipolar cells (Burns and Arshavsky 2005). The horizontal and amacrine cells are responsible for integrating and modulating the visual signal as it passes from photoreceptors to the bipolar cells or the bipolar cells to RGCs, respectively (Firl, Ke et al. 2015; Chapot, Euler et al. 2017). RGCs are then responsible for ultimately processing and transmitting visual stimuli via their axons in the optic nerve (ON) to post-synaptic neurons in the lateral geniculate nucleus (LGN) and superior colliculus (SC), the primary downstream visual targets of RGCs (Hattar, Kumar et al. 2006; Huberman, Wei et al. 2009).

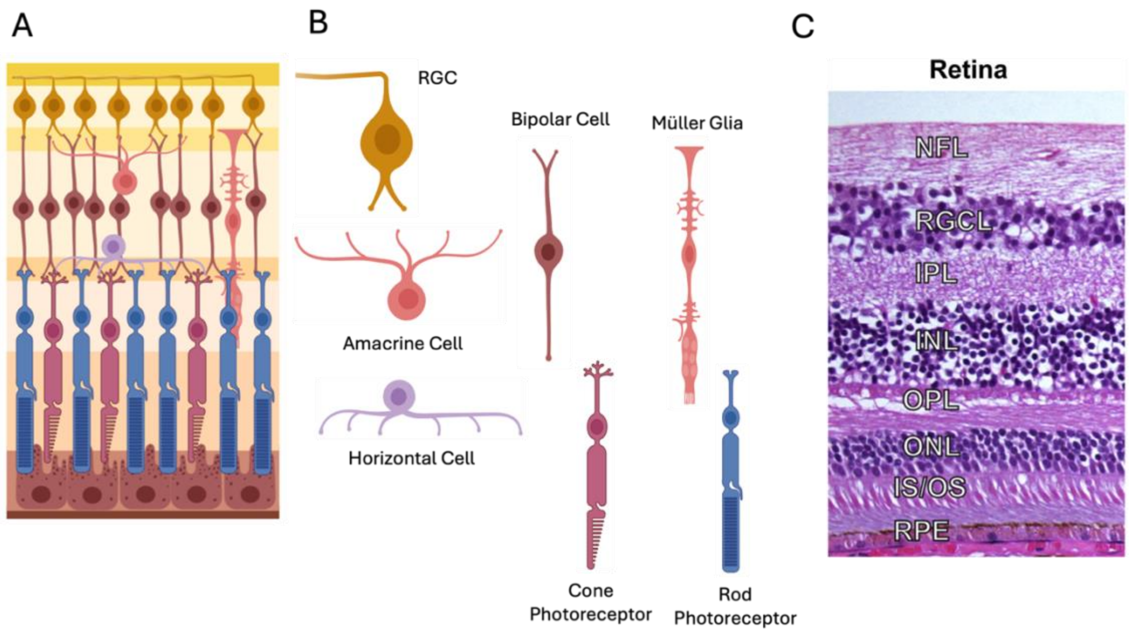

Figure 6. Retinal Microanatomy. (A,B) Distribution of major cell types within the neural retina, with the identities of each cell type depicted in (B). (C) Retinal cross section demonstrating the stratified nature of the retina. Photoreceptor nuclei localize to the outer nuclear layer (ONL), while their inner segments and outer segments (IS/OS) are in the deepest layer of the retina, adjacent to the retinal pigment epithelium (RPE). At the outer plexiform layer (OPL) the photoreceptors synapse with bipolar cells, the nuclei of which localize to the inner nuclear layer (INL). The bipolar cells synapse with retinal ganglion cell (RGC) dendrites in the inner plexiform layer (IPL), while the RGC somas localize to the ganglion cell layer (RGCL) and the axons course toward the optic nerve head in the nerve fiber layer (NFL), the inner-most layer of the retina. Adapted from (Yu, Cringle et al. 2013).

The ON is a crucial component of the mammalian visual system pathway. It contains RGC axons exiting the retina along with several supporting cells – endothelial cells, oligodendrocytes, astrocytes, microglia, and neuron glial 2 (NG2) cells **(Figure 7A and 7B)**. Endothelial cells modulate blood flow to the ON tissue through vasoconstriction and vasodilation while oligodendrocytes ensheathe the RGC axons in myelin to allow for efficient signal conductance (Furchgott and Zawadzki 1980; Mayoral, Etxeberria et al. 2018). ON glial cells, such as astrocytes and microglia, are critical to ON homeostasis, regulating angiogenesis, providing metabolic and structural support to RGC axons, facilitating cellular debris removal, and managing inflammatory responses (Sun, Lye-Barthel et al. 2009; Bouzier-Sore and Pellerin 2013; Lee, Han et al. 2017; Chen, Luo et al. 2019; Perelli, O'Sullivan et al. 2021). NG2 cells were previously considered to be adult oligodendrocyte progenitor cells, but in addition to their progeny-generating capacity, NG2 cells have recently become appreciated for their roles in axon-glial signaling, glial scar formation, node of Ranvier interactions, and modulating the tissue inflammatory response through microglia interactions (Parolisi and Boda 2018).

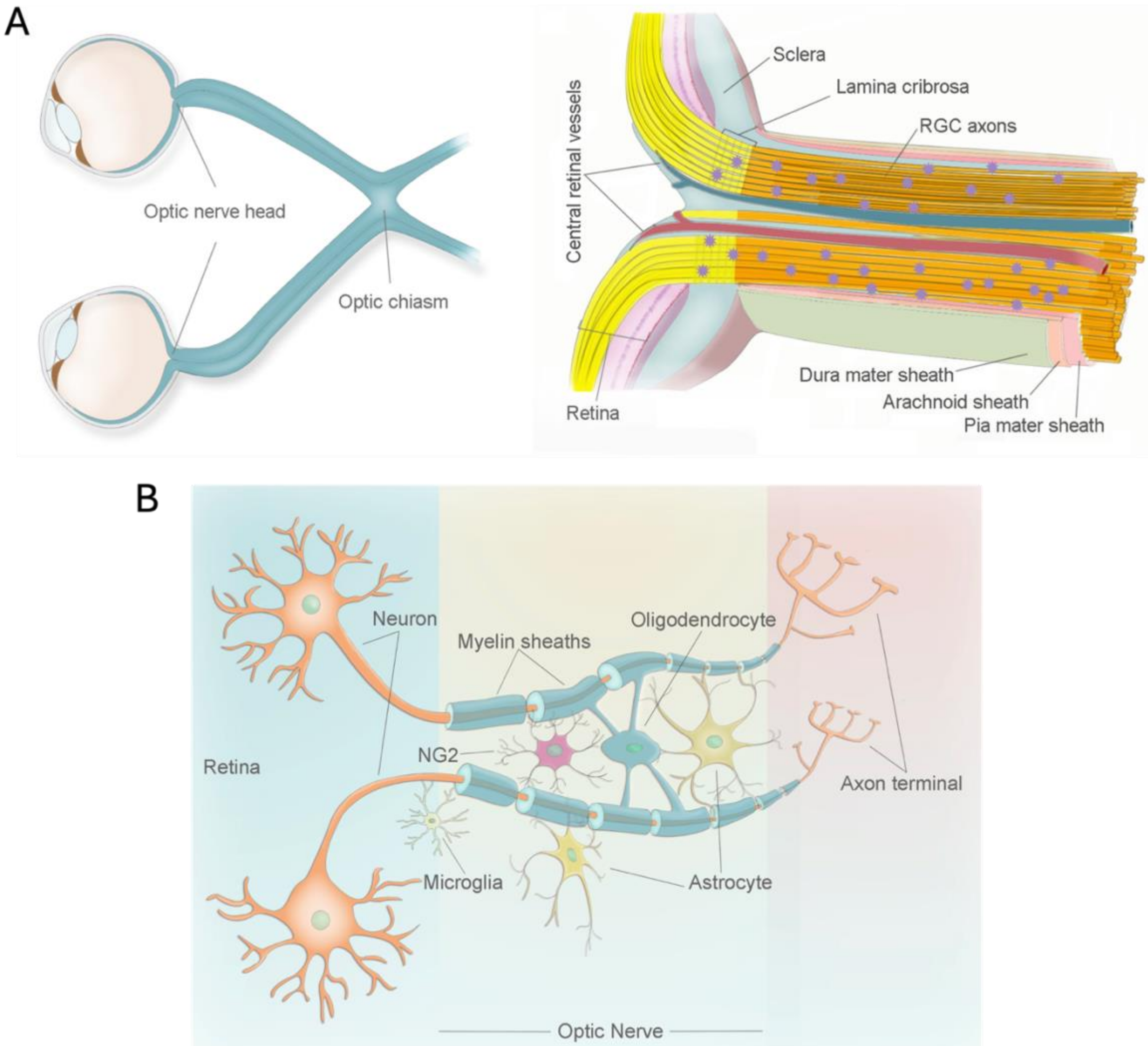

Figure 7. Optic Nerve Anatomy. (A) Left panel: The optic nerve is a white matter tract of the central nervous system, leaving the posterior of each eye and projecting to the brain. The two optic nerves join at the optic chiasm, where there is a decussation of approximately half of the axons from each optic nerve to the contralateral side. Right panel: depiction of retinal ganglion cell axon bundles within the eye (yellow) and upon exiting the eye (orange). Similar to the brain itself, the optic nerve is surrounded by a meningeal sheath consisting of pia, arachnoid, and dura mater. The lamina cribrosa is found where the axons are traversing the sclera to leave the eye. (B) Illustration highlighting varieties of supporting cells (Oligodendrocyte, Astrocyte, Microglia, and NG2) associated with RGC axons in the optic nerve. Adapted from (Yazdankhah, Shang et al. 2021).

1.5 Retinal Ganglion Cells (RGCs)

1.5.1 Compartmentalization of RGCs

RGCs are a population of projection neurons of the mammalian visual system and have the highest degree of cellular compartmentalization of any retinal cell type. RGC somas localize near the inner surface of the retina in the GCL, while their dendrites penetrate deeper into the IPL, where they receive inputs from bipolar cells and amacrine cells. RGC axons travel across the retinal surface, converging at the optic nerve head at the posterior aspect of the retina. There, they bundle and leave the back of the eye as the ON **(Figure 8A)**. The RGC axons within the most proximal aspect of the ON are initially unmyelinated for 250 μm and then ensheathed in myelin for the remainder of their route through the optic chiasm to the LGN and SC, interrupted only by interspersed nodes of Ranvier (Wilkison, Bright et al. 2021). The unmyelinated ON region immediately posterior to the eye cup is termed the lamina cribrosa in humans and glial lamina in mice. Here there exists a honeycomb-like network made of collagen and astrocytes that serves as channels for RGC axon bundles to pass through (Sun, Lye-Barthel et al. 2009) **(Figure 8B)**. Because of the unique cytoarchitecture and highly polarized energy demand, RGCs are highly dependent on mitochondrial function and generation of ATP to carry out normal cellular processes.

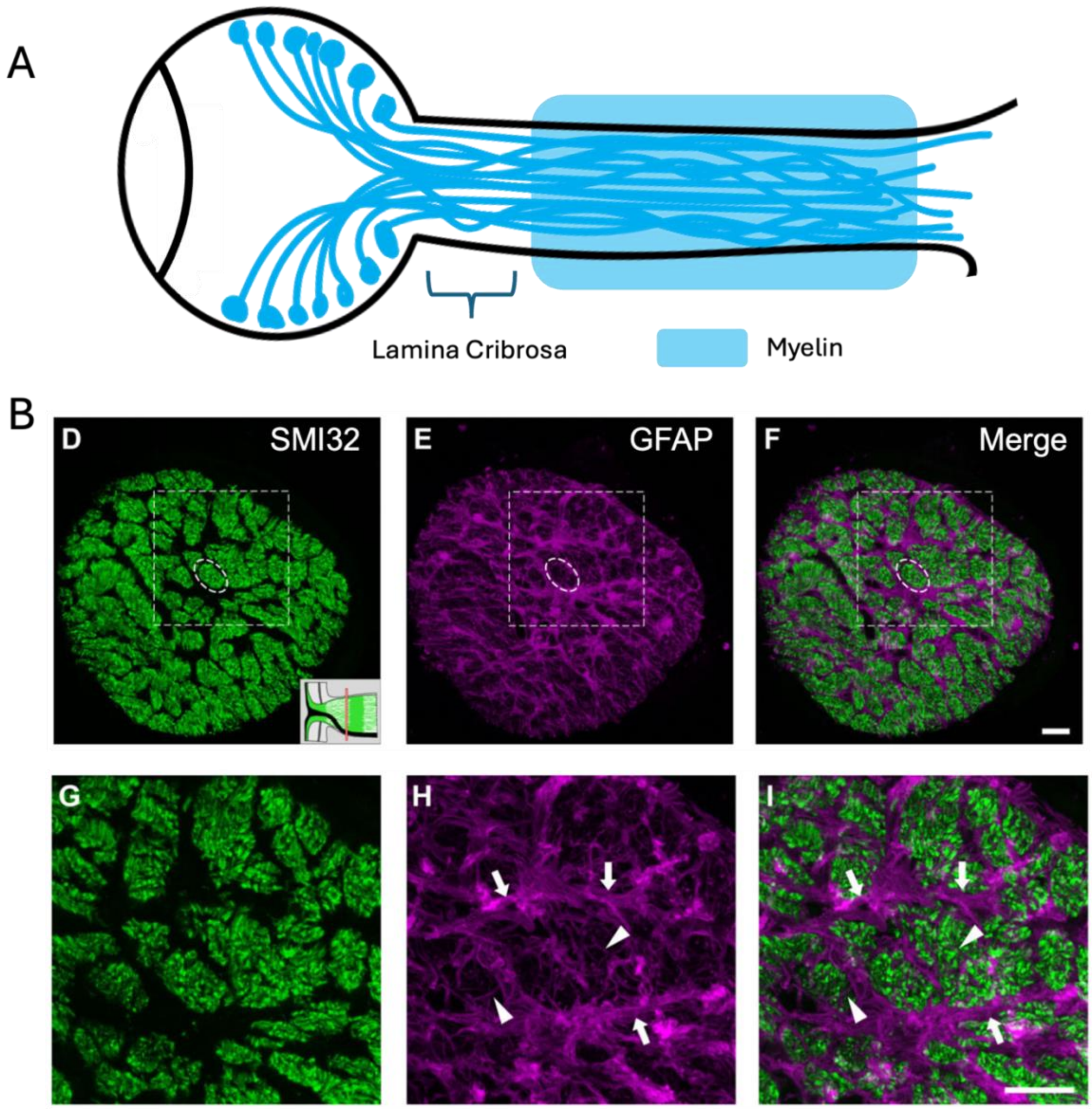

Figure 8. Optic nerve anatomy at the lamina cribrosa (glial lamina). (A) Schematic showing the unmyelinated RGC axons at the lamina cribrosa as they exit the eye. Throughout the remainder of the optic nerve projection, the vast majority of RGC axons are myelinated (blue shade). (B) Mouse optic nerve cross section at the glial lamina (the location of the section is depicted in the inset of the upper left panel). RGC axons are labeled with SMI32 (green) and traverse as bundles through a honeycomb-like network of astrocytes (labeled with GFAP, magenta). Scale bar = 20 μm. Adapted from (Sun, Lye-Barthel et al. 2009)

1.5.2 Bioenergetic Requirements of RGCs

Due to their varied morphology with extensive dendritic arbors and long-trajectory axons, coupled with the high rate of visual information received, processed, and transmitted, the energy demand of RGCs is very high. In humans, RGC axons are up to 50 mm in length from their retinal origin to synaptic targets in the brain, while the RGC soma is only 1/10,000 the length and surface area of the axon (Mikelberg, Drance et al. 1989). It has been shown that a significant and disproportionate amount of energy is required at intraretinal and brain synapses (Vos, Lauwers et al. 2010; Faria-Pereira and Morais 2022), and the proximal portions of RGC axons that are unmyelinated within the retina and in the glial lamina have larger energy demands than their myelinated counterparts because of their inability to perform more efficient saltatory conduction of action potentials (Wang, Dong et al. 2003). The high rate of energy consumption and the limited diffusion capacity of ATP molecules would ordinarily create a significant energy gradient along the course of the RGC, leading to the suggestion that mitochondria must be positioned at specific sites within the cell to meet local energy demands (Flood, Lee et al. 2023).

1.5.3 RGC Vulnerability to Stress

RGCs are uniquely vulnerable to stress and damage induced by mitochondrial deficits, as evidenced by the implication of mitochondrial dysfunction in the pathophysiology of numerous optic neuropathies characterized by degeneration of RGCs and ultimately vision loss. Some of these mitochondrial optic neuropathies are hereditary, caused by mutations in genes crucial to mitochondrial dynamics and bioenergetics. Leber Hereditary Optic Neuropathy (LHON) is a maternally inherited optic neuropathy in which a precipitous degeneration of RGCs results in rapid and profound vision loss, typically occurring in previously healthy adolescents and young adults. LHON is among the most common human diseases with a mitochondrial inheritance pattern – with a prevalence of 1:30,000-50,000 individuals (Rosenberg, Nørby et al. 2016; Yu-Wai-Man, Griffiths et al. 2016). Initiation and progression of LHON results from a missense mutation to mtDNA encoding subunits of the mitochondrial respiratory complex I (NADH:ubiquinone oxidoreductase), a major component of the primary site of input of reducing power into the electron transport chain. Approximately 90% of LHON cases are due to three specific mtDNA mutations: m.1178G>A (MTND4), m.3460G>A (MTND1), and m.14484T>C (MTND6) (Sundaramurthy, SelvaKumar et al. 2021). Although an LHON-causing mitochondrial mutation is present in virtually all cells of LHON patients, in most cases only RGCs are significantly compromised and manifest pathology.

Another optic neuropathy that results in functional loss due to mitochondrial mutation is Autosomal Dominant Optic Atrophy (ADOA). ADOA occurs due to a mutation in Optic Atrophy 1 (OPA), a dynamin-related guanosine triphosphatase (GTPase) that is responsible for mitochondrial inner membrane fusion and cristae formation and remodeling. It is also key to the fusion of mitochondrial membranes to create larger mitochondria organelles or mitochondrial networks. OPA1 is also expressed across all cell types, yet vision loss from RGC degeneration is similarly one of the few pathologies encountered in patients with ADOA. The prevalence of ADOA is 1:12,000-50:000, with vision loss typically presenting in the first two decades of life and in most cases slowly progressing over decades. Opa1 is a nuclear-encoded gene, with >200 distinct mutations implicated in ADOA. The pathogenic mechanism of ADOA is believed to be haploinsufficiency of the OPA1 protein. It is theorized that the distinct morphology and energy requirements of RGCs are partly to blame for the susceptibility of RGCs to OPA1 insufficiency. Although controversial, there is some evidence that Opa1 deficiency in ADOA may impair oxidative phosphorylation and complex I function specifically (Zanna, Ghelli et al. 2008; Yu-Wai-Man, Trenell et al. 2011). Because RGC axons only become myelinated after the lamina cribrosa, the unmyelinated portions of axons may require more energy inputs than is available with the loss of Opa1 protein in ADOA. Impairment of this energetic supply to RGCs may compromise cellular health and cause degeneration.

Glaucoma is another neurodegenerative disease specific to RGCs. It is a progressive optic neuropathy with many risk factors including increased age, elevated intraocular pressure (IOP), elevated blood pressure (hypertension), heart disease, and traumatic injury to the eye. Age and elevated IOP are the primary risk factors for developing glaucoma, and IOP remains the only modifiable risk factor for glaucoma to date. There are many varieties of glaucoma, with the most prevalent worldwide being open-angle glaucoma, where IOP is chronically elevated. The direct cause of RGC degeneration and vision loss in the context of IOP elevation is not entirely understood, but it is thought that the pathogenesis begins at the site of the lamina cribrosa as the unmyelinated RGC axons leave the eye. Following elevated IOP, RGCs exhibit a decrease in axonal transport across the lamina cribrosa, disruption of trophic factor transport, glial activation, increased oxidative stress, and mitochondrial dysfunction (Cooper, Crish et al. 2016). Similar to LHON, in glaucoma, lymphocytes derived from glaucoma patients exhibited a complex-I-driven ATP synthesis (Lee, Sheck et al. 2012). Systemic mitochondrial deficiency might suggest a possible mitochondrial influence to the RGC susceptibility in glaucoma. Interestingly, a recent study highlighted the effect of mitochondrial dysfunction in the DBA/2J model – the canonical glaucomatous mouse model which exhibits progressive IOP elevation and subsequent RGC and vision loss. In this study, elevated IOP, caused an age-dependent decrease in retinal NAD^+ and glutathione concentrations (Williams, Harder et al. 2017). These molecules are important for efficient oxidative phosphorylation and maintenance of cellular ROS. Oral supplementation of Vitamin-B_3/nicotinamide, a precursor of NAD^+, was neuroprotective and mitigated RGC loss in this mouse model. This suggests that modulating mitochondrial function may be beneficial even in optic neuropathies that do not result specifically from mitochondria-related genetic mutations.

2. Compartmentalization of Retinal Ganglion Cell Mitochondria

2.1 Study Background and Objectives

Like all projection neurons, RGCs have a highly polarized anatomy(Andrews, Griffiths et al. 1999; Yu, Cringle et al. 2013). RGC somas localize to the ganglion cell layer (GCL) of the inner retina, while their dendritic arbors extend deeper into the inner plexiform layer (IPL), receiving inputs from presynaptic neurons within their receptive fields. In contrast, the axon of each RGC courses along the innermost retinal nerve fiber layer (RNFL) before converging with other RGC axons and exiting the eye to project via the optic nerve to post-synaptic targets in the brain (Bao 2008; Dhande, Stafford et al. 2015; Guo, Zhou et al. 2021). Due to the extreme morphological polarization between RGC compartments, bioenergetic and other physiological demands differ considerably across the cell (Richard, Philip et al. 1999; Barron, Griffiths et al. 2004). Accordingly, it would be interesting to evaluate whether divergent mitochondrial protein compositions exist between the subcellular compartments in order to meet the specific local needs.

Mitochondrial dysfunction appears to play a key role in the pathogenesis of the most common optic neuropathy, glaucoma—both in primary open-angle glaucoma associated with high intraocular pressure and in the less common variant, normal tension glaucoma (Buono, Foroozan et al. 2002; Lee, Sheck et al. 2012; Lascaratos, Chau et al. 2015; Van Bergen, Crowston et al. 2015). In both forms of glaucoma, RGC death and vision loss are the consequence of a degenerative process that begins in a proximal region of the optic nerve called the lamina cribrosa in humans or glial lamina in mice (Carelli, Ross-Cisneros et al. 2004; Varma, Vajaranant et al. 2016; Ito and Di Polo 2017). Mitochondrial dysfunction, manifesting as disrupted ATP production and oxidative stress, has been associated with high intraocular pressure in glaucoma patients and in glaucoma mouse models, as well as in the setting of aging, a key risk factor for glaucoma (Yu Wai Man, Chinnery et al. 2005; Quigley 2011; Carelli, La Morgia et al. 2017). Intriguingly, a recent study in aged glaucomatous mice demonstrated RGC neuroprotection by boosting the level of nicotinamide adenine dinucleotide (NAD^+), a key cofactor required for mitochondrial ATP production and maintenance of mitochondrial membrane potential (Williams, Harder et al. 2017). These findings strongly imply a central role for mitochondria in the glaucomatous neurodegeneration of RGCs. However, it is unknown whether axon-specific molecular regulation of mitochondrial function impacts the degeneration of RGCs. The significance of this question is highlighted by a landmark study demonstrating that, whereas deletion of the key pro-apoptosis protein BAX in the DBA/2J glaucoma mouse model completely abrogates RGC soma degeneration, it fails to provide long-term protection to RGC axons in the optic nerve (Libby, Li et al. 2005). This result strongly suggests the existence of compartment-specific molecular pathways leading to degeneration in glaucoma (Ito and Di Polo 2017).

The goal of this study was to define physiologically relevant, compartment-specific signatures of the RGC mitochondrial proteome. Using an optimized RGC immuno-isolation procedure (‘mitocapture’), we purified GFP-labeled mitochondria from the axonal and somatodendritic compartments of RGC-specific MitoTag mice. Isolated mitochondria were subjected to proteomic analysis aiming to identify proteins differentially expressed in the mitochondria of these compartments, with subsequent validation using immunolocalization techniques.

2.2 Results

RGC MitoTag mice exhibit expression of GFP-labeled mitochondria throughout RGC somatodendritic and axonal compartments

Previous work has established a protocol for immuno-isolating labeled mitochondria from CNS tissue *in vivo* using a genetically-modified mouse line (Fecher, Trovò et al. 2019). The

'MitoTag' mouse can be crossed with transgenic mouse lines carrying tissue-specific Cre recombinase drivers to achieve labeling of mitochondria with a cytosol-facing GFP targeted to the outer mitochondrial membrane ('GFP-OMM'; **Figure 9A**). Mitochondria from the cell type of interest can then be isolated from crude mitochondrial preparations obtained from complex tissues (Fecher, Trovò et al. 2019; de Mello, Fecher et al. 2023).

To explore the heterogeneity and complexity of compartment-specific RGC mitochondrial populations, we purified RGC mitochondria from the optic nerve containing axonal mitochondria and from retinal tissue enriched in mitochondria localized to the somatodendritic compartments. This was achieved by specifically tagging RGC mitochondria with the GFP-OMM MitoTag. The MitoTag mouse line was bred with the *Vglut2-Cre* line, in which expression of Cre recombinase is driven by the promoter for the vesicular glutamate transporter *Vglut2 (Vong, Ye et al. 2011)*. This promoter begins to drive Cre expression in the retina by embryonic day 13 (our unpublished data), and we have previously been shown that it achieves Cre-mediated DNA recombination in >96% of RGCs and in only in a small subset of other retinal neurons but not in glia (Wang, Klingeborn et al. 2020). Histological characterization of retinal flat mounts from the *Vglut2-Cre;GFP-OMM*$^{fl/fl}$ mouse (henceforth denoted 'RGC MitoTag' mouse) demonstrated the expected expression of the GFP-OMM construct (green) in both RGC somas and axons co-labeled with Class III β-tubulin, Tuj1 (red, **Figure 9B**). In retinal cross-sections, GFP-OMM expression was observed in the RGC axons located in the RNFL, RGC somas in the GCL and dendrites in the IPL (**Figure 9C**, *left panel*). Higher magnification images highlight GFP labeling of mitochondria in RGC somas and proximal dendrites, as well as in axonal projections co-labeled for Tuj1 (**Figure 9C**, *right panels*). As expected, some GFP-OMM signal was also observed in the outer plexiform layer, corresponding to a subpopulation of horizontal cells expressing *Vglut2-Cre* (**Figure 9C**).

GFP-OMM expression within the optic nerve was very robust (**Figure 9D**). To confirm that this signal arose from RGC axonal mitochondria, we performed intravitreal injections on adult RGC MitoTag mice with adeno-associated virus (AAV2) carrying a MitoDsRed-Flex-Switch. By transducing the somas of RGCs in this way, we could achieve expression of this fluorescent Cre reporter and ultimately label mitochondria throughout all RGC cellular compartments. As expected, along the length of the optic nerve, MitoDsRed co-localized extensively with the *Vglut2-Cre*-dependent GFP-OMM construct expressed endogenously by RGCs in this mouse line (**Figure 9D**, *insets*).

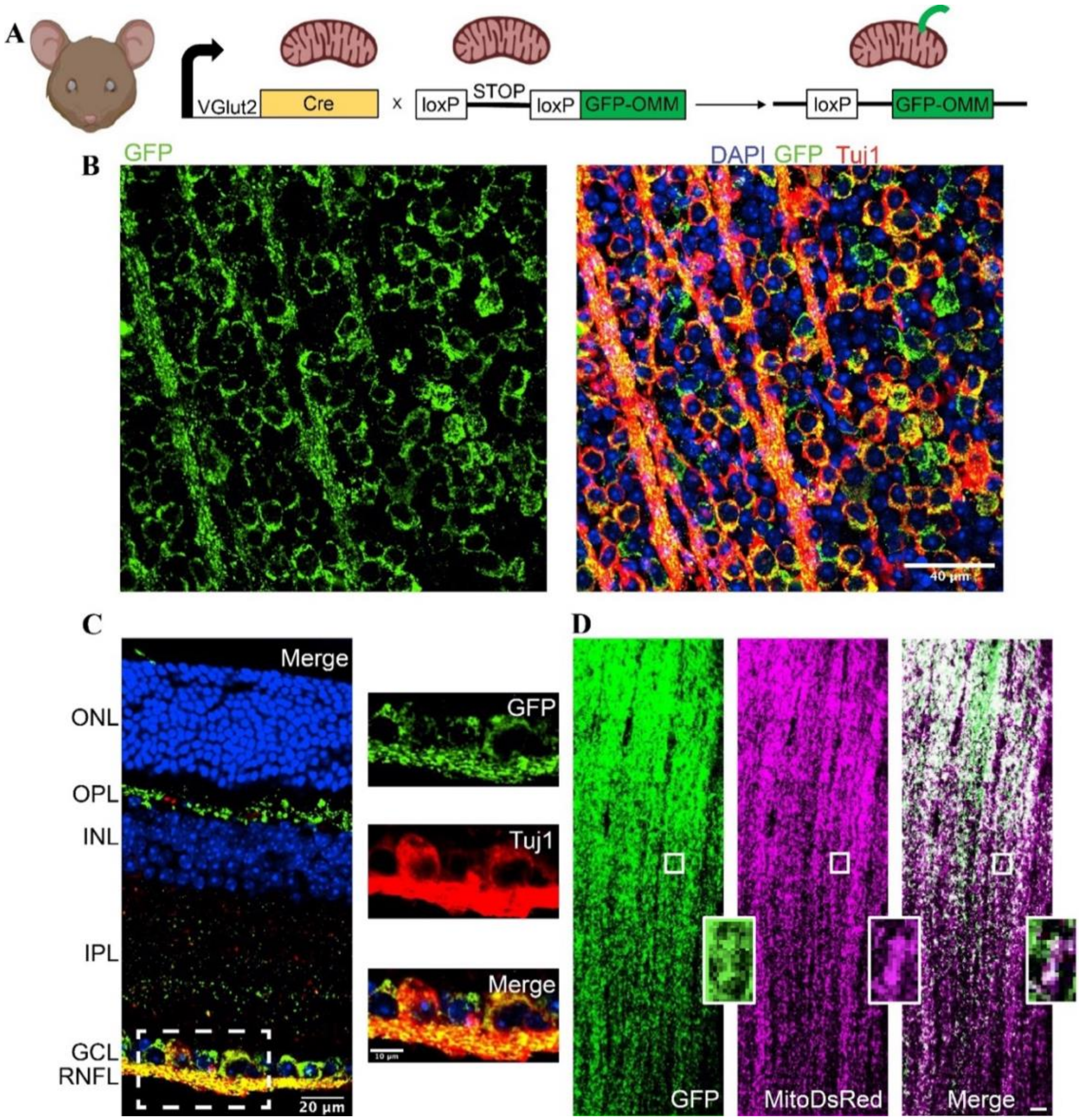

Figure 9. Characterization of the *Vglut2-Cre;GFP-OMM* (RGC MitoTag) mouse. A. Schematic of the genetic cross between *Vglut2-Cre* and *GFP-OMM*$^{fl/fl}$ mice to generate RGC MitoTag mice in which the STOP codon is excised to allow expression of the GFP-OMM construct in RGCs. B. Retinal flat mount from an adult RGC MitoTag mouse showing expression of the GFP-OMM construct (green) in nearly all RGCs (labeled with Tuj1, red). C. RGC MitoTag retinal cross-section showing *Vglut2*-Cre-driven expression of GFP-OMM (green) in retinal ganglion cell somas, dendrites, and axons in the inner retina (bottom of image), with expression of the construct also noted in some horizontal cells in the outer plexiform layer. Inset panels show co-localization of GFP-OMM with Tuj1 in RGC somas and axons. Abbreviations: ONL, outer nuclear layer; OPL, outer plexiform layer; INL, inner nuclear layer; IPL, inner plexiform layer; GCL, ganglion cell layer; RNFL, retinal nerve fiber layer. D. RGC MitoTag optic nerve longitudinal section showing *Vglut2-Cre*-driven GFP-OMM expression (green) co-localizing with MitoDsRed (magenta) in RGCs transduced by AAV2-MitoDsRed-Flex-Switch. Inset images show co-localization of GFP-OMM and MitoDsRed within a bundle of RGC axons. Scale bar = 20 µm.

Compartment-specific isolation of RGC mitochondria

Having confirmed extensive RGC-specific expression of the GFP-OMM construct in RGC MitoTag mice, we next explored whether we could use this mouse line to characterize compartment-specific RGC mitochondrial populations. **(Figure 10A)**. Because the exit of the optic nerve from the eye represents a clear anatomic landmark, distal to which only the RGC axonal compartment is present, purifying RGC mitochondria from harvested optic nerve tissue would allow assessment of mitochondria derived exclusively from axons. Conversely, RGC mitochondria purified from retinal tissue would be greatly enriched for those localizing to the somatodendritic compartments. We therefore tested whether tagged RGC mitochondria could be specifically isolated from retinal and optic nerve specimens. Pooled retinas or optic nerves from three mice were homogenized, and differential centrifugation was performed to obtain a crude mitochondrial fraction containing mitochondria and other subcellular organelles from all cells present in the harvested tissue. Incubation of this preparation with paramagnetic nanobeads conjugated to an anti-GFP antibody allowed immunoprecipitation of RGC-derived mitochondria from the crude mixture.

We used western blot analysis to assess the efficiency and specificity of our purification procedure **(Figure 10B)**. To control for nonspecific binding of cellular material to the beads, the purification was also performed on retinal and optic nerve tissue obtained from WT C57Bl/6J mice. The GFP-OMM construct was efficiently immunoprecipitated from the input of both the somatodendritic and axonal RGC MitoTag preparations, along with three other mitochondrial marker proteins: the voltage-dependent anion channel (VDAC), which localizes to the outer mitochondrial membrane, and subunits of respiratory complex I (NDUFS4) and complex IV (COX4), both localized to the inner mitochondrial membrane **(Figure 10B)**. As expected, minor fractions of these three proteins immunoprecipitated, as greater proportions derive from unlabeled, non-RGC mitochondria. Importantly, control samples from WT ocular tissues showed negligible precipitation of mitochondrial proteins, indicating low levels of their non-specific binding to the beads. To determine whether purified mitochondria remained intact, we examined the pellets from the immunoprecipitations using transmission electron microscopy and found that the majority of immuno-isolated membranous structures were indeed mitochondria with well-preserved ultrastructure **(Figure 10C)**. Additional membranous structures were also observed, likely representing the endoplasmic reticulum, which is known to establish contact sites with mitochondria (Maddison, Malik et al. 2023; Yu, Courjaret et al. 2024).

A concern with whole-organelle isolation is that mitochondria from other cell types within a specimen may be recovered nonspecifically alongside RGC mitochondria via clumping during the organelle isolation procedure (Meeusen, McCaffery et al. 2004; Ahier, Onraet et al. 2021; Bodenstein, Powlowski et al. 2023). To assess the extent to which our mitocapture procedure may be affected by such clumping, we performed a mixing experiment to determine qualitatively the extent of non-specific pulldown of unlabeled mitochondria. We generated *Vglut2-Cre;GFP-OMM*$^{fl/fl}$*;ndufs4*$^{-/-}$ mice, in which the GFP-OMM construct is expressed in RGCs of mice with a global deletion of the complex I accessory subunit NDUFS4. Optic nerves obtained from these mice as well as from WT mice and RGC MitoTag mice with intact NDUFS4 were processed to derive mitochondrial samples. Samples from *Vglut2-Cre;GFP-OMM*$^{fl/fl}$*;ndufs4*$^{-/-}$ mice and WT mice were combined at a 1:1 ratio ('Mixed' sample), and anti-GFP immunoprecipitation was performed separately on *Vglut2-Cre;GFP-OMM*$^{fl/fl}$*;ndufs4*$^{-/-}$, Mixed, WT and regular RGC MitoTag samples. Western blot analysis demonstrated a high level of specificity of the RGC Mitocapture assay **(Figure 10D)**. When mitochondria tagged with GFP-OMM but lacking NDUFS4 were mixed with WT (non-tagged) mitochondria, no NDUFS4 protein was co-precipitated with the GFP-OMM-positive, NDUFS4-negative mitochondria. This indicates that an overwhelming majority of mitochondrial proteins recovered in the RGC Mitocapture assay were indeed derived from the cell type of interest.

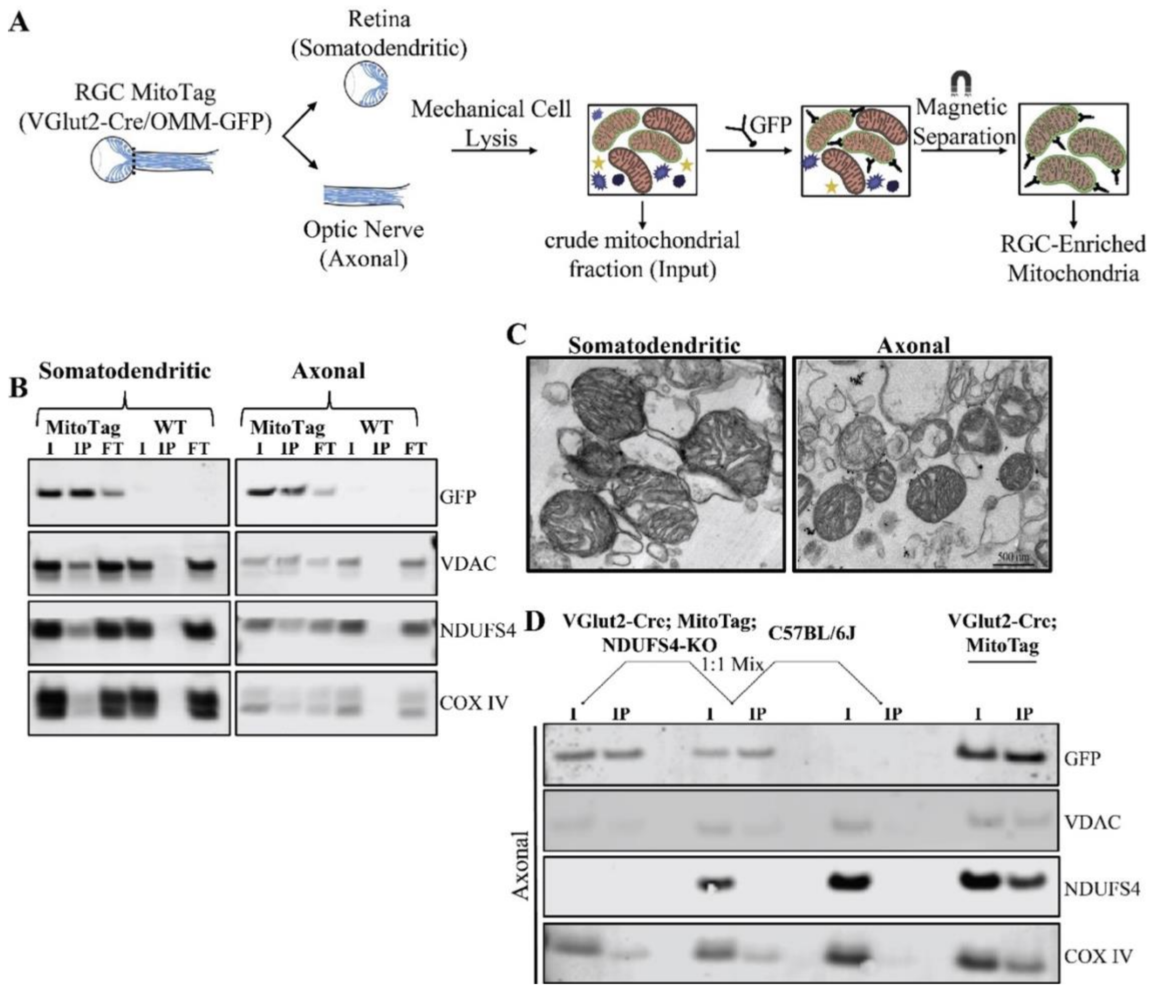

Figure 10. Characterization of the efficiency and specificity of the RGC Mitocapture assay. A. Schematic highlighting the workflow for the RGC Mitocapture procedure of obtaining RGC-enriched mitochondrial populations from separate RGC compartments through GFP-based immunopurification. B. Representative western blot showing immunoprecipitation of GFP-OMM-tagged mitochondria from RGC somatodendritic and axonal compartments of RGC MitoTAG mice compared to control WT mice lacking the tag. Native mitochondrial proteins VDAC, NDUFS4, and COX4 co-precipitated in RGC MitoTAG but not WT samples. I, input; IP, immunoprecipitate; FT, flow through. C. Representative transmission electron micrographs of isolated mitochondria from RGC somatodendritic and axonal compartments. D. Western blot from a mixing experiment assessing the specificity of the RGC mitocapture assay. Crude mitochondrial fractions from the optic nerves of *Vglut2-Cre;GFP-OMM*$^{fl/fl}$;*NDUFS4*$^{fl/fl}$ and C57BL/6J (WT) mice were mixed at a 1:1 ratio and immunoprecipitated with an anti-GFP antibody. Input fraction from RGC MitoTag optic nerve was used as a positive control.

Compartment-specific heterogeneity of RGC mitochondrial proteins

Having confirmed the efficiency and specificity of the RGC Mitocapture procedure, we characterized mitochondrial proteomes of RGC somatodendritic and axonal compartments using liquid chromatography-mass spectrometry (LC-MS/MS). The analysis was performed on four biological replicates, each with six retinas or optic nerves pooled from three RGC MitoTag mice or WT controls. The data summarized in **Figure 11A** and Supplementary Tables S1 and S2 include proteins identified from at least 2 unique peptides with p-value ≤ 0.05 whose abundance in RGC MitoTag preparations exceeded the abundance in WT controls by ≥ 1.5. Based on these criteria, 471 somatodendritic and 357 axonal proteins were identified in at least 3 of 4 biological replicates. Among these proteins, 282 were identified in both compartments, 189 in the somatodendritic compartment and 75 in the axonal compartment (Supplementary Tables S3, S4, S5). Using Mitocarta 3.0 (Rath, Sharma et al. 2021) and Uniprot ID Mapping (Consortium 2020), we determined that 36% of all proteins identified in the somatodendritic compartment and 43% of proteins identified in the axonal compartment are known mitochondrial proteins, making them the most highly represented population in these preparations **(Figure 11B)**. Additionally, 10% of somatodendritic and 9% of axonal proteins were identified as ER-localized proteins, as expected from the known physical contacts between ER and mitochondria (Maddison, Malik et al. 2023). It is conceivable that at least some of the other identified proteins may have multiple subcellular localizations or were similarly precipitated due to physical contacts between tagged mitochondria and other cellular structures.

For proteins identified in both somatodendritic and axonal compartments, a volcano plot was constructed to compare their relative abundances **(Figure 11C)**. To account for any differences in the total amount of mitochondrial material present in each preparation, the total ion intensity of all peptides representing each protein was normalized to that of GFP. The GFP-normalized values were averaged across all biological replicates and the ratios between the two compartments were calculated for each protein. We identified a total of 19 and 18 mitochondrial proteins that were differentially enriched by >2.0-fold in the somatodendritic and axonal compartments, respectively **(Tables I and II)**. In addition, 13 mitochondrial proteins were identified in at least 3 of 4 replicates in one compartment but not in a single replicate from the opposing compartment **(Table III)**.

We next sorted proteins confidently identified in either the somatodendritic or axonal compartment according to their reported functions **(Table IV)**. Notably, two groups of proteins enriched in the somatodendritic compartment are components of the electron transport chain and those related to antioxidant defenses. Among proteins enriched in the axonal compartment is a group related to fatty acid metabolism.

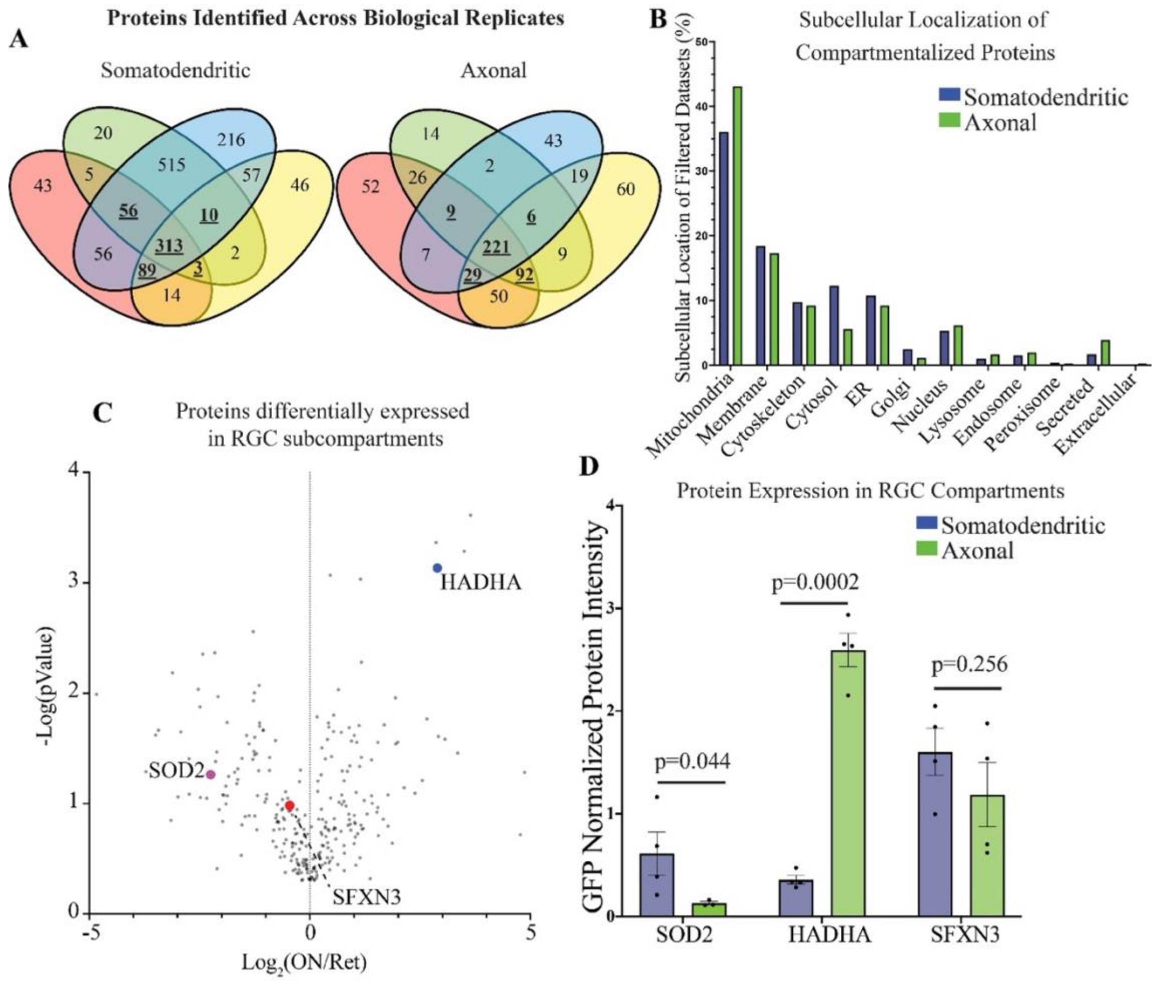

Figure 11. Proteomic profiling of mitochondria isolated from RGC somatodendritic and axonal compartments. A. Venn diagrams depicting proteins identified in 4 biological replicates for each compartment. Proteins identified in at least 3 of the 4 replicates are bolded and underlined. B. Assigned subcellular localizations of proteins identified in each compartment C. Volcano plot showing the relative abundance of proteins identified in both RGC somatodendritic (Ret) and axonal (ON) compartments. Proteins to the left of the vertical line are more abundant in the somatodendritic compartment and those to the right are more abundant in the axonal compartment. Colored dots represent proteins that underwent immunohistochemical validation: SOD2 (purple), SFXN3 (red), and HADHA (blue). D. Comparison of GFP-normalized protein abundance for SOD2, SFXN3, and HADHA between the somatodendritic and axonal compartments. A two tailed t-test was performed for each comparison. The GFP-normalized protein abundance for each replicate is depicted as an individual data point.

Table I. Mitochondrial Proteins Enriched in the Somatodendritic Compartment

Protein Name	Gene Abbreviation	Ret/ON
Creatine Kinase b-type	Ckb	7.60
Superoxide Dismutase [Mn]	Sod2	4.69
Cytochrome C Oxidase subunit 4 isoform 1	Cox4i1	4.16
Peroxiredoxin-5	Prdx5	3.93
ATP Synthase Subunit O	Atp5p0	3.58
Citrate Synthase	Cs	3.15
NADH dehydrogenase [ubiquinone] 1 alpha subcomplex subunit 10	Ndufa10	3.10
NADH dehydrogenase [ubiquinone] iron-sulfur protein 7	Ndufs7	2.93
NADH dehydrogenase [ubiquinone] iron-sulfur protein 3	Ndufs3	2.90
Mycophenolic acid acyl-glucuronide esterase	Abhd10	2.76
Elongation Factor Tu	Tufm	2.70
NAD Kinase 2	Nadk2	2.59
Leucine-rich PPR motif-containing protein	Lrpprc	2.42
3-hydroxyisobutyrate dehydrogenase	Hibadh	2.39
Mitochondrial import receptor subunit TOM70	Tomm70	2.317
Mitochondrial-processing peptidase subunit alpha	Pmpca	2.30
ATP synthase F(0) complex subunit B1	Atp5pb	2.20
Prohibitin-2	Phb2	2.08
Glutaminase Kidney Isoform	Gls	2.03

19 mitochondrial proteins enriched by >2.0-fold in RGC somatodendritic mitochondria. Ret/ON values are the ratios of GFP-normalized protein abundances in these compartments averaged across replicates.

Table II. Mitochondrial Proteins Enriched in the Axonal Compartment

Protein Name	Gene Abbreviation	ON/Ret
Peroxiredoxin-3	Prdx3	130.29
Isocitrate Dehydrogenase [NADP]	Idh2	11.27
NAD(P) Transhydrogenase	Nnt	10.19
Mitochondrial Trifunctional Enzyme, Subunit A	HADHA	7.25
Mitochondrial Trifunctional Enzyme, Subunit B	HADHB	5.84
Tricarboxylate Transport Protein	Slc25a1	3.97
Very long-chain specific acyl-coA dehydrogenase	Acadvl	3.21
NAD-dependent Malic enzyme	Me2	2.93
Aldehyde Dehydrogenase	Aldh2	2.64
Succinyl-CoA:3-ketoacid coenzyme A transferase 1	Oxct1	2.35
3-hydroxyacyl-CoA dehydrogenase type-2	Hsd17b10	2.25
Aldehyde Dehydrogenase X	Aldh1b1	2.20
ADP/ATP translocase 1	Slc25a4	2.19
Pyruvate Carboxylase	Pc	2.09
Acylglycerol Kinase	Agk	2.04
Glutamate dehydrogenase 1	Glud1	2.00
NADH-ubiquinone oxidoreductase chain 4	Mtnd4	2.00

18 mitochondrial proteins enriched by >2.0-fold in RGC axonal mitochondria. ON/Ret values are the ratios of GFP-normalized protein abundances in the corresponding compartments averaged across replicates.

Table III. Mitochondrial Proteins Identified in a Single Compartment

Protein Name	Gene Abbreviation	Compartment Identified In
ATP Synthase, subunit D	Atp5d	Somatodendritic
Hexokinase-2	HK-2	Somatodendritic
Tyrosine-tRNA ligase, mitochondrial	Yars2	Somatodendritic
3-hydroxyisobutyryl-CoA hydrolase, mitochondrial	Hibch	Somatodendritic
Mitochondrial import inner membrane translocase subunit TIM50	Timm50	Somatodendritic
Succinate dehydrogenase [ubiquinone] iron-sulfur subunit, mitochondrial	Sdhb	Somatodendritic
Mitochondrial Rho GTPase 2	Rhot2	Somatodendritic
Elongation factor G, mitochondrial	Gfm1	Somatodendritic
Thioredoxin-related transmembrane protein 1	Tmx1	Somatodendritic
Caseinolytic peptidase B protein homolog	Clpb	Somatodendritic
Alpha-aminoadipic semialdehyde dehydrogenase	Aldh7a1	Axonal
Delta-1-pyrroline-5-carboxylate dehydrogenase	Aldh4a1	Axonal
Choline transporter-like Protein 1	Slc44a1	Axonal

13 mitochondrial proteins identified in either the somatodendritic or axonal compartment in at least 3 biological replicates.

Table IV. Functional Analysis of Compartment-Enriched Mitochondrial Proteins

	Proteins Enriched in Somatodendritic		**Proteins Enriched in Axonal**	
	# Proteins Identified	Proteins Identified (Gene Abbreviation)	# Proteins Identified	Proteins Identified (Gene Abbreviation)
Electron Transport Chain	8	Ndufa10, Ndufs7, Cox4i1, Ndufs3, Atp5pb, Atp5po, **Sdhb, Atp5d**	1	Mtnd4
Lipid Metabolism	0	-	5	Hadha, Hadhb, Acadvl, Agk, Hsd17b10
ROS Management	4	Sod2, Prdx5, Abhd10, **Tmx1**	1	Prdx3
Other Metabolic Proteins	7	Cs, Ckb, Gls, Hibadh, **Hibch,** NADK2, **HK2**	13	Idh2, Pc, Aldh1b1, Oxct1, Aldh2, Slc25a4, Me2, Glud1, Nnt, **Aldh4a1, Aldh7a1, Slc25a1, Slc44a1**
Other	10	Tufm, Tomm70, Pmpca, Phb2, Lrpprc, **Clpb, Gfm1, Rhot2, Timm50, Yars2**	0	-

Functional classification of 29 and 20 mitochondrial proteins identified in the somatodendritic or axonal compartments, respectively

Histological validation of compartment-specific expression of RGC mitochondrial proteins

In the next set of experiments, we validated some of our proteomic findings using immunofluorescence analysis. We selected three mitochondrial proteins to confirm their compartment-specific enrichment: mitochondrial superoxide dismutase (SOD2, found to be enriched in the somatodendritic compartment); sideroflexin 3 (SFXN3, equally distributed between compartments); and trifunctional enzyme subunit α (HADHA, enriched in the axonal compartment) **(Figure 11D)**. We immunolabeled retinal and optic nerve cross-sections from RGC MitoTag mice with antibodies against each protein. In order to limit our analysis to protein expressed by RGCs but not other cell types, we used *ImageJ* to identify pixels containing signal for both GFP and protein of interest to create a GFP-localized mask for each protein (Rueden, Schindelin et al. 2017; Schroeder, Dobson et al. 2021). We then quantified the signal intensity for each protein of interest relative to that of GFP-OMM as a measure of the abundance of each protein within RGC mitochondria **(Figure 12A and 12B)**. Consistent with the proteomic data, this immunofluorescence analysis showed a statistically significant enrichment of SOD2 in the somatodendritic compartment and HADHA in the axonal compartment, while no statistically significant difference in SFXN3 abundance was observed between the two RGC compartments **(Figure 12C)**.

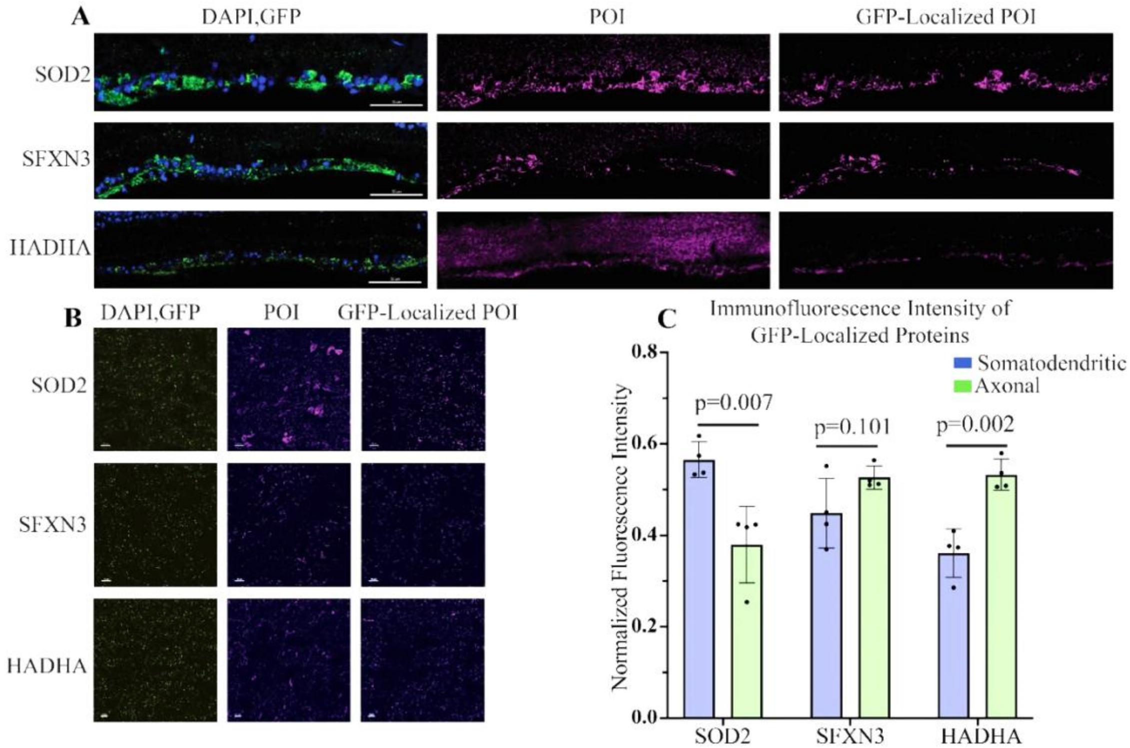

Figure 12. Histological validation of compartment-specific protein abundance in RGC mitochondria. A,B. Retinal (A) and optic nerve cross sections (B) from RGC MitoTag mice showing *Vglut2-cre*-dependent expression of GFP-OMM in RGCs (left panels, green), endogenous expression of proteins of interest (POI; middle panels, magenta), and POI expression solely within GFP-positive mitochondria (right panels, magenta). Protein identities are indicated to the left. Scale bars, 50 µm (A) and 20 µm (B). C. Comparison of GFP-normalized fluorescence intensities of SOD2, SFXN3 and HADHA in retinal and optic nerve sections from RGC MitoTag mice (N=4 replicates for each tissue). A two tailed t-test was performed for each comparison. The GFP-normalized fluorescence intensities for each replicate are depicted as individual data points.

Age-related heterogeneity of RGC mitochondrial proteins

Because age is a major risk factor for the development of glaucoma (Quigley 2011), we proceeded to use the Mitocapture procedure to isolate and characterize mitochondria from young and aged mice. RGC somatodendritic and axonal mitochondria were separately immunopreciptated from 3-month-old and 12-month old RGC MitoTAG mice as well as 3-month-old WT mice as controls (N=3 mice per group for each of two biological replicates). We again used western blot to validate the efficiency and specificity of our isolations. The GFP-OMM construct was immunoprecipitated from the input of both the somatodendritic and axonal RGC MitoTag preparations for both age groups, along with the inner mitochondrial membrane proteins COX4 and NDUFS4 (**Figure 13A**). The failure of COX4 and NDUFS4 to be immunoprecipated from WT control preparations confirmed excellent specificity of the purifications.

As before, using LC-MS/MS, we analyzed proteins with at least 2 unique peptides, a p-value ≤ 0.05, and whose abundance in RGC MitoTag preparations exceeded the abundance in WT controls by ≥ 1.5. Across the two biological replicates and among both age groups, there were 468 and 275 proteins identified in the somatodendritic and axonal compartments, respectively. Using the Mitocarta 3.0 and Uniprot ID Mapping protein databases, we determined that 38% of all proteins identified in the somatodendritic compartment and 52% of proteins identified in the axonal compartment are known mitochondrial proteins (**Figure 13B**). For proteins identified in the somatodendritic and/or axonal compartments in both replicates for the 3- and 12-month-old mice, a volcano plot was constructed to compare the relative abundances at the two ages (**Figure 13C**). As before, normalization of the total ion intensity of all peptides for each protein to that of GFP was performed to account for differences in total mitochondrial material present in each preparation. The GFP-normalized values were averaged across two biological replicates and the ratios between the two age groups were calculated for each protein. We determined that the relative abundances of SOD2, SFXN3, and HADHA were all decreased in the mitochondria of the somatodendritic compartment of the 12-month-old mice relative to their counterparts in the 3-month-old mice, while that of HADHA was also decreased in the axonal compartment (**Figure 13D**). Interestingly, this was part of an overall trend of decreased protein abundance in RGC mitochondria immunoprecipated from older mice, with 80% of all proteins less abundant in somatodendritic mitochondria and 91% less abundant in axonal mitochondria at 12 months compared to 3 months. The age-related changes in the abundance and activities of specific proteins are likely to be important in explaining the progression of optic neuropathies like glaucoma and will each require experimental validation. However, our general observation of decreased mitochondrial protein abundance at 12 months may be consistent with the known age-related global decline in mitochondrial function (Sohal and Sohal 1991; Cottrell, Blakely et al. 2001; Williams, Harder et al. 2017).

2.3 Conclusion

In this study, we employed a novel approach to isolate and characterize intact mitochondria derived from distinct subcellular compartments of a specific cell type. Using LC-MS/MS, we identified mitochondrial proteins enriched in either the somatodendritic or the axonal compartments of RGCs. Remarkably, many of the proteins with compartment-specific enrichment belong to groups with distinct mitochondrial activities, which suggests the existence of local differences in mitochondrial physiology in these neurons. Our approach should be readily adaptable to the compartment-specific analysis of organelles from any projection neurons obtained from living tissues.

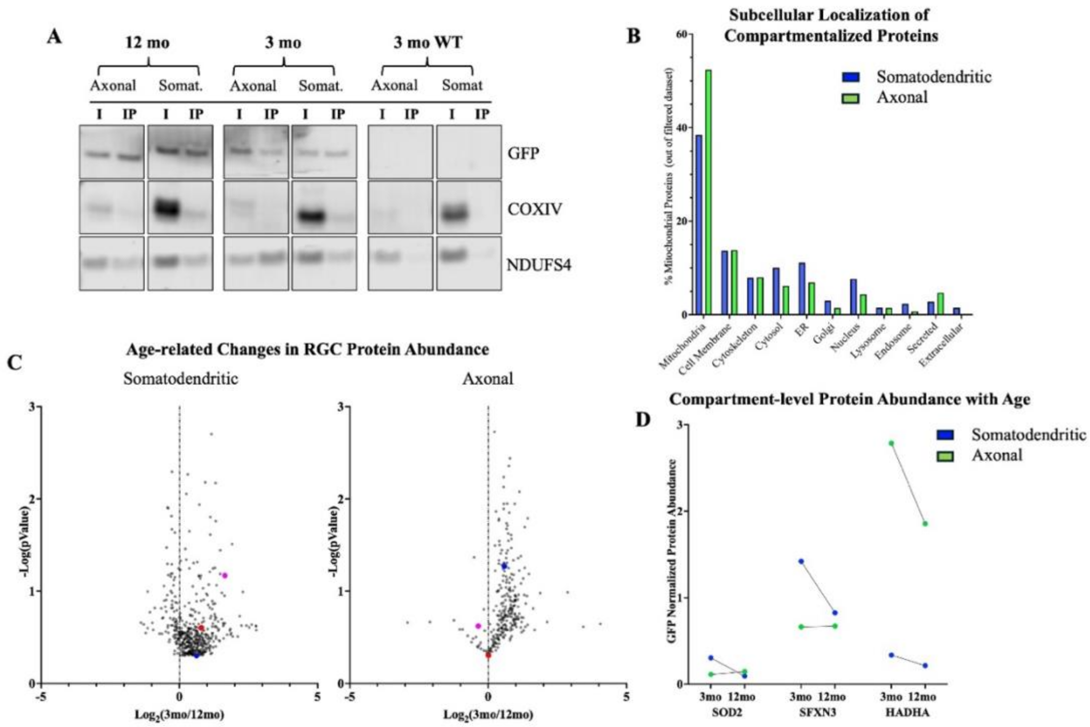

Figure 13. Proteomic profiling of mitochondria isolated from RGC somatodendritic and axonal compartments of young (3 mo) and aged (12 mo) mice. A. Representative western blot showing immunoprecipitation of GFP-OMM-tagged mitochondria from RGC somatodendritic and axonal compartments of 3 mo and 12 mo RGC MitoTAG mice compared to control WT mice lacking the tag. Native mitochondrial proteins COX4, and NDUFS4 co-precipitated in RGC MitoTAG but not WT samples. I, input; IP, immunoprecipitate. B. Assigned subcellular localization of proteins identified across two biological replicates in each compartment. C. Volcano plots showing the relative age-related abundance (3mo/12mo) of proteins identified in both age groups. Proteins to the left of the vertical line are more abundant in 12 mo mice and those to the right are more abundant in 3 mo mice. Colored dots represent proteins of interest: SOD2 (purple), SFXN3 (red), and HADHA (blue). D. Comparison of age-related changes in GFP-normalized protein abundance for SOD2, SFXN3, and HADHA for each compartment. Each dot represents an average between two biological replicates.

3. Fatty Acid Oxidation Enrichment in RGC Axonal Mitochondria

3.1 Study Background and Objectives

Mitochondria can utilize several substrates as inputs into oxidative metabolic pathways. In addition to glucose, amino acids and fatty acids can also be used to generate acetyl-CoA, although through separate biochemical pathways. Fatty acids liberated from triglyceride molecules that circulate in the blood can enter the cell via fatty acid transport proteins on the cell surface. Once within the cell, fatty acids are conjugated with a Coenzyme A (CoA) group by fatty acyl-CoA synthase (FACS). Subsequently, carnitine palmitoyltransferase 1 (Cpt1) converts the fatty acyl-CoA to a fatty acylcarnitine molecule, a precondition for it to be transported across the mitochondrial outer membrane to the intermembrane space by carnitine translocase (CAT). As CAT shuttles fatty acylcarnitine molecules across the OMM , a carnitine molecule is exchanged in the opposite direction. The IMM protein carnitine palmitoyltransferase 2 (Cpt2) converts fatty acylcarnitine molecules back into a fatty acyl-CoA molecule **(Figure 14A)**, allowing it to enter the fatty acid ß-Oxidation (FAO) pathway where one acetyl-CoA molecule is produced for every cycle of oxidation **(Figure 14B)**. The generation of acetyl-CoA removes two carbons from each fatty acyl-CoA molecule; further FAO cycles continue until the fatty acid is completely catabolized. The acetyl-CoA molecule generated by the FAO pathway then enter the TCA cycle in the mitochondrial matrix to follow the same ATP-generating process as acetyl-CoA molecules derived from glucose.

Among the interesting findings from our work described in the previous chapter was the axonal enrichment of mitochondrial proteins related to fatty acid metabolism. HADHA, which we identified as enriched in axonal mitochondria by mass spectrometry and confirmed using immunohistochemical methods, is the α-subunit of the mitochondrial trifunctional protein (MTP) (Liang, Li et al. 2018). It forms a heterotetrameric complex with the β-subunit, HADHB, which we found to be similarly enriched in the axonal compartment of RGCs. The MTP complex catalyzes the final three steps in the mitochondrial FAO pathway to ultimately produce acetyl-CoA molecules(Wiegand and Remington 1986). Among other mitochondrial proteins enriched in the axonal mitochondria in our analysis are very-long-chain-specific acyl-CoA dehydrogenase and 3-hydroxyacyl CoA dehydrogenase, which catalyze the first step of ß-oxidation of very long chain fatty acids and an intermediate step in FAO, respectively.

The constellation of proteins enriched in axonal mitochondria raises the possibility that FAO may be of particular importance to axonal physiology, either as an energy source or for generation of acetyl-CoA as a biosynthetic precursor. Notably, MTP deficiency can lead to a rare, autosomal recessive disorder that causes impaired mitochondrial metabolism of long-chain fatty acids (Purevsuren, Fukao et al. 2009). Among the most frequent disease manifestations of MTP deficiency is peripheral neuropathy, which may indicate a particular sensitivity of projection neurons to aberrant FAO (Ishikawa, Nakamori et al. 2023). The experiments described in the present chapter were designed to test our hypothesis that fatty acid catabolism is of increased in RGC axonal mitochondria and that RGC-specific impairment of FAO may lead to optic atrophy in mice, possibly with axonopathy preceding the death of RGC somas in the retina.

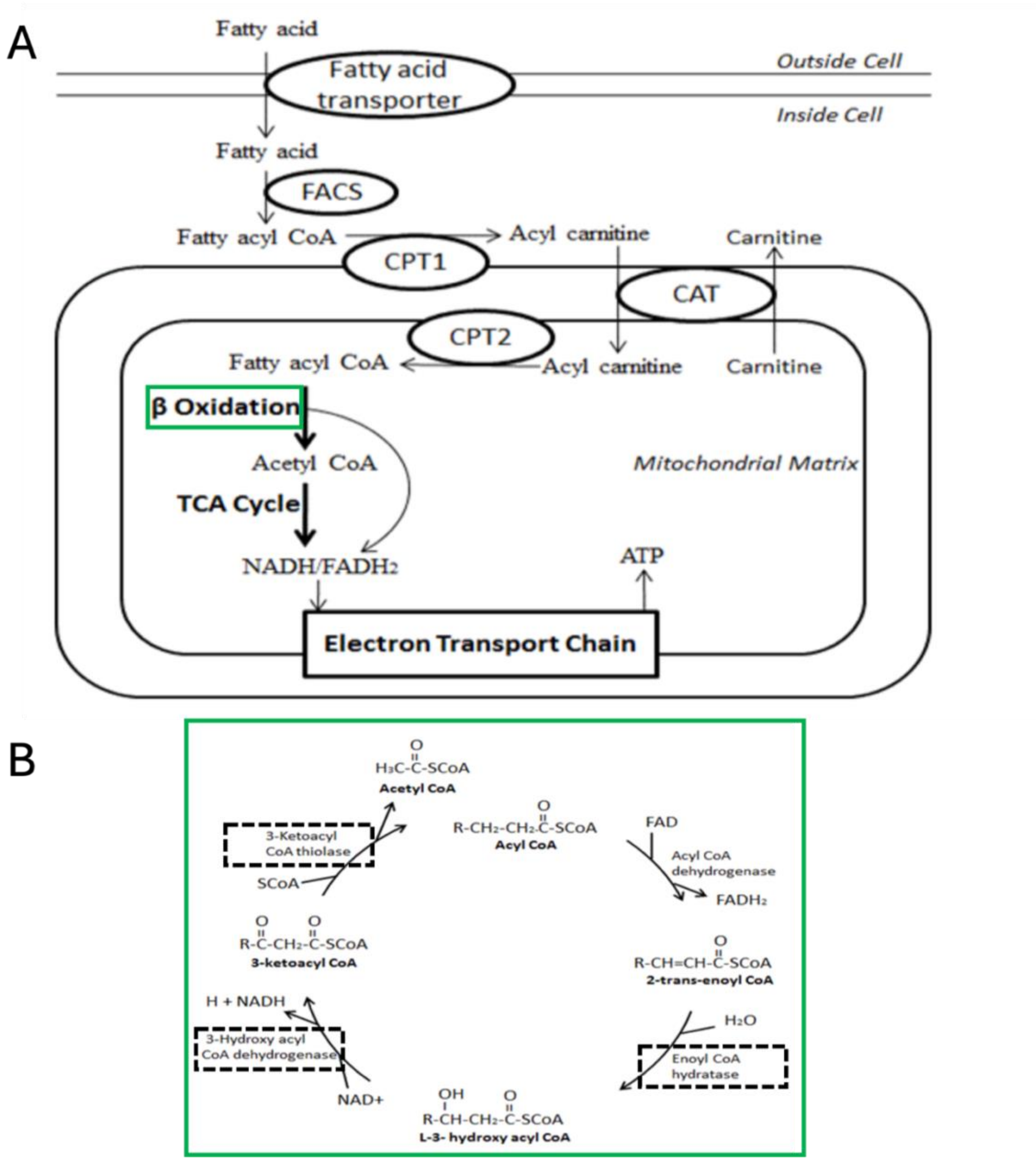

Figure 14. Schematic of fatty acid import and catabolism. (A) Extracellular fatty acids are conjugated with a CoA molecule to generate fatty acyl-CoA to be imported into the cell. Within the cytosol, the CoA moiety is exchanged for a carnitine. This fatty acylcarnitine molecule can then be imported into the mitochondria where the carnitine is exchanged again for a CoA moiety and can be readily catabolized. (B) Schematic of the steps of fatty acid β-oxidation (FAO), which takes place within mitochondria. The Mitochondrial Trifunctional Protein is a heterotetrameric complex comprised of HADHA and HADHB and has enzymatic activities responsible for catalyzing the final three reactions of FAO, highlighted by dotted boxes.

3.2 Results

Metabolomic Profiling of Acylcarnitine species in RGC Compartments

Having validated the expression of HADHA and identified increased enrichment of FAO-related proteins in RGC axonal mitochondria, we set out to further evaluate the compartment-specific importance of fatty acid metabolism through a comparative analysis of acylcarnitine metabolites in isolated axonal and somatodendritic RGC mitochondria **(Figure 15A)**. We performed four separate isolations using optic nerve and retinal inputs from 8 mice/replicate at PD90. After immunoprecipitating RGC-derived somatodendritic and axonal mitochondria as described in the previous chapter, samples were probed for FAO-related proteins and prepared for acylcarnitine metabolite profiling. First, we performed a western blot analysis to quantify GFP-normalized protein expression of HADHA and HADHB in isolated RGC somatodendritic and axonal mitochondria. Consistent with our previous proteomic analysis, we observed a 4-fold and 3-fold enrichment of HADHA and HADHB in axonal mitochondria relative to somatodendritic counterparts **(Figure 15B)**. Then, employing acylcarnitine metabolite profiling, we identified a significant increase in the concentration C16, C16:1, and C18:1 acylcarnitine species in RGC axonal mitochondria **(Figure 15C)**. The increased abundance of long-chain fatty acylcarnitine species suggests that long-chain fatty acids may be an important metabolic substrate for RGC axonal mitochondria.

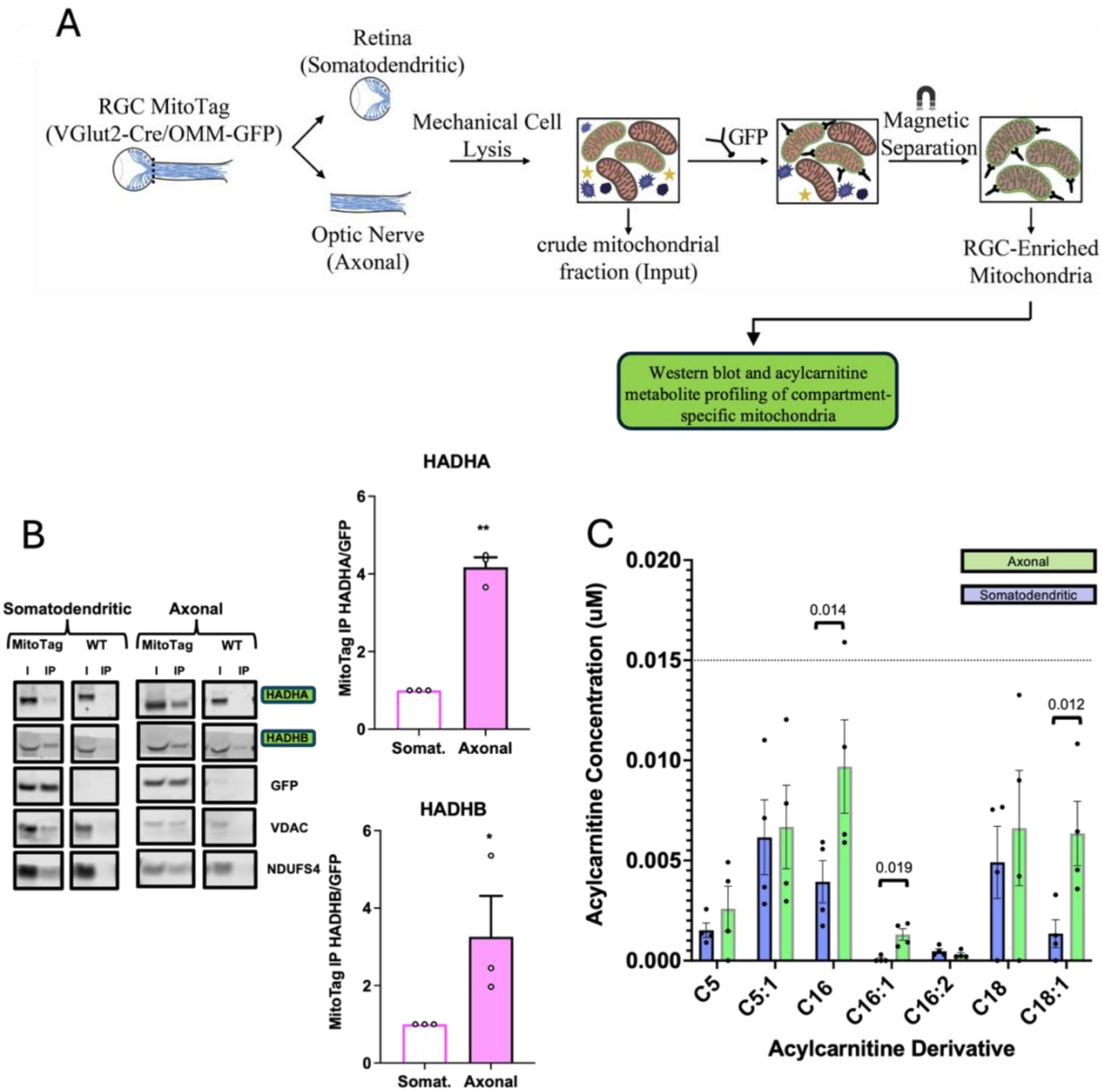

Figure 15. Increased Acylcarnitine Metabolites in RGC Axonal Mitochondria. (A) RGC Mitocapture assay was used to isolate mitochondria from somatodendritic and axonal compartments of RGC MitoTag, which were used for downstream analyses. (B) Representative western blot showing immunoprecipitation of GFP-OMM-tagged mitochondria from RGC somatodendritic and axonal compartments of RGC MitoTAG mice compared to control WT mice lacking the tag. Mitochondrial Trifunctional Proteins, HADHA and HADHB, and native mitochondrial proteins VDAC and NDUFS4 co-precipitated in RGC MitoTag but not WT samples. I, input; IP, immunoprecipitate. The bar graphs to the right depict the GFP-normalized abundance of HADHA and HADHB in axonal mitochondria relative to somatodendritic. (C) Acylcarnitine profile of RGC somatodendritic and axonal mitochondria. RGC axonal mitochondria demonstrate an enrichment of C16, C16:1, and C18:1 acylcarnitine derivatives. Performed in collaboration with Olga Ilkayeva and Dev Muoio (Duke Molecular Physiology Institute).

Functional Loss of FAO Capacity in VGlut2-Cre/Cpt1a$^{fl/fl}$ Mice

After identifying an axon-specific signature of FAO-related proteins and metabolites, we hypothesized that removing the capacity of RGC mitochondria to metabolize fatty acids would trigger a neurodegenerative process that may be particularly severe in axons. Carnitine Palmitoyltransferase 1 (Cpt1) is directly upstream of HADHA/B and is responsible for conjugating carnitine to fatty acyl-CoA molecules, a necessary step to allow influx of fatty acid species into the mitochondria. We decided to genetically ablate Cpt1a in RGCs in order to remove the FAO capacity of RGC mitochondria. *VGlut2-Cre* mice were crossed with *Cpt1a*$^{fl/fl}$ to generate a *VGlut2-Cre/Cpt1a*$^{fl/fl}$ (Cpt1a KO) mouse line. These mice and their control littermates were then aged to 6 months prior to assessing for a degenerative phenotype in the RGCs. At the time of enucleation, retinas and optic nerves were isolated from each mouse. To quantify RGC soma survival, retinal flat mounts were made from Cpt1a KO and control specimens and immunolabeled for Ribosomal Binding Protein Multiple Splicing-1 (RBPMS-1), a highly specific marker for RGC somas **(Figure 16A)**. Cpt1a KO retinas exhibited a trend toward decreased RGC soma density, but it did not reach statistical significance at any of the three distances from the optic nerve head where the somas were quantified **(Figure 16B)**. This was in contrast to a model of mitochondrial optic neuropathy employed by our lab in which mitochondrial complex I deficiency causes profound RGC degeneration, with loss of two-thirds of RGC somas by 3 months of age (Wang, Klingeborn et al. 2020).

To determine whether a degenerative phenotype might be more apparent in RGC axons, we collected optic nerves from Cpt1a KO and control mice and assessed RGC axonal density in optic nerve cross sections. The optic nerves were imaged by light microscopy after staining with methylene blue to highlight myelin and also by electron microscopy. Gross morphology of the Cpt1a KO and control optic nerves **(Figure 17A)** and ultrastructural analysis by electron microscopy **(Figure 17B)** showed no major morphological differences caused by the loss of Cpt1a in RGCs. While occasional myelination patterns appeared abnormal, this was believed to be fixation artifact, as they were observed in the optic nerves of both genotypes **(Figure 17B).** Consistent with our RGC soma counts, there was a trend toward a slight decrease in axon density in the 6-month-old Cpt1a KO optic nerves, but this failed to reach statistical significance ($p=0.076$) **(Figure 17C)**. While the loss of Cpt1a, the gatekeeper for FAO in mitochondria, failed to produce a significant degenerative phenotype in RGCs, it is possible that RGCs may be less able to compensate for this loss when combined with other cellular stressors. Thus, subjecting mice to longer aging (>12mo) or elevated IOP could potentially enhance any deleterious effect(s) resulting from loss of mitochondrial FAO in RGCs.

3.3 Conclusion

In summary, we have obtained preliminary data suggesting that compared to somatodendritic mitochondria, RGC axonal mitochondria have an apparent increase in utilization of long-chain fatty acids as a metabolic substrate. This is consistent with our prior proteomic data indicating that a number of FAO enzymes are enriched in axonal mitochondria. However, genetic ablation of FAO in RGC mitochondria failed to produce any more than a modest decrease in RGC survival and no obvious signs of axonopathy. Whether RGC axonal mitochondria rely more heavily on FAO for generating ATP compared to mitochondria in other compartments remains to be addressed experimentally.

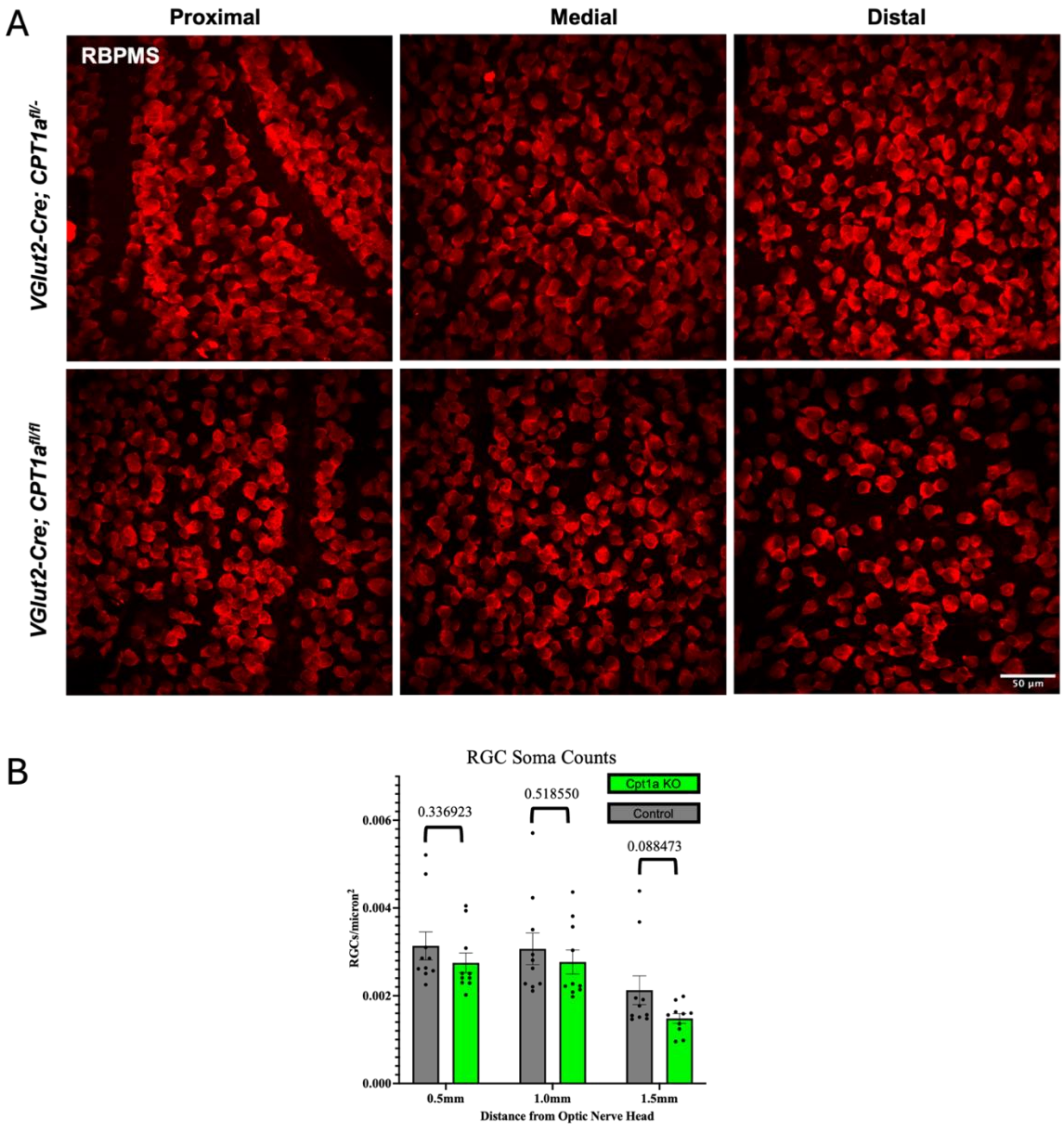

Figure 16. Retinal Ganglion Cell Soma Density in Cpt1a KO mice. (A) Retinal flat mounts of *VGlut2-Cre/Cpt1a*$^{fl/fl}$ (Cpt1a KO) and control littermates were immunolabeled with RBMPS1 at P180 and imaged at distances of 0.5 (proximal), 1.0 (medial), and 1.5 mm (distal) from the optic nerve head. (B) Bar graphs comparing RGC soma density between Cpt KO and WT mice at each distance from the optic nerve head. P-values are depicted above each comparison, with none reaching statistical significance.

4. Discussion

The overall aim of the work in this dissertation was to gain a deeper understanding of compartment-specific differences in RGC mitochondrial protein composition and of any functional significance these differences may imply. The importance of this foundational knowledge is multifaceted. First, our observation of reproducible enrichment of specific proteins and pathways in axonal or somatodendritic mitochondria implies some form of active regulation of mitochondrial protein content, presumably to tailor mitochondria to the needs of specific cellular compartments. The mechanism underlying such regulation is currently a mystery but could be related to local mitochondrial protein translation or degradation within each compartment and/or active trafficking of already-differentiated mitochondria to the cellular compartments for which they are best equipped. Second, the unique sensitivity of RGCs to mitochondrial dysfunction may be a result of mitochondria failing to meet the physiological needs of specific compartments. For instance, understanding whether IOP-induced mitochondrial dysfunction is particularly severe at the lamina cribrosa (glial lamina) and which biological roles are predominantly impacted there could potentially lead to new neuroprotective therapeutic strategies beyond simply lowering IOP. Our proteomics data is a valuable resource for identifying pathways with potential biological relevance in RGC health and disease, paving the way for additional hits to be validated and then perturbed in relevant experimental models as we did for the FAO pathway.

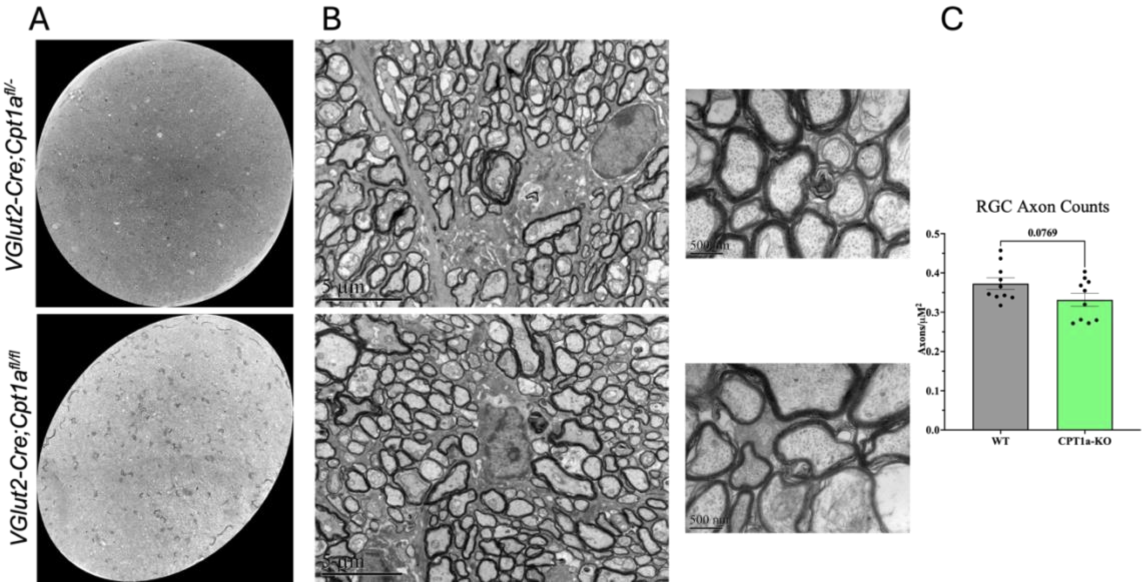

Figure 17. Optic Nerve Axon Density in Cpt1a KO and control mice. (A) Representative light microscopy images of *VGlut2-Cre/Cpt1a*$^{fl/fl}$ and control mouse whole optic nerve cross-sections stained with methylene blue at P180. (B) Representative electron micrographs of *VGlut2-Cre/Cpt1a*$^{fl/fl}$ and control optic nerve cross-sections, demonstrating grossly normal axon abundance and morphology. (C) Bar graphs comparing the densities of RGC axons within the retrolaminar optic nerve of the indicated genotypes. The p-value is depicted above. Scale bar = 5μm (B; left column), 500nm (B; right column).

Methodological considerations

Most of the described work utilized the RGC MitoTag mouse, which we generated in order to tag the OMM of mitochondria specifically within RGCs and thereby facilitate their purification from complex mixtures of mitochondria and other organelles. As described earlier, the RGC MitoTag mouse expresses a cytosol-facing GFP tag that is bound to the outer mitochondrial membrane. Once immuno-isolated via an anti-GFP antibody, the purified mitochondria can be further studied, as exemplified by our proteomic and metabolomic analyses. Additional analyses, including oxygen consumption rate, reactive oxygen species formation, and ATP generation should also be feasible as downstream applications of this purification strategy. The GFP tag is also attractive for its utility in imaging procedures, such as with two-photon laser scanning microscopy (TPLSM) to allow for *in vivo* intraretinal imaging, which could be employed to further characterize the movement and positioning of GFP-tagged mitochondria in the RGCs or other retinal cell types (Quintero, Shiga et al. 2022).

Our approach to achieve compartment-specific purification of mitochondria from a cell type of interest was an adaptation of the strategy of Fecher and colleagues to immuno-isolate cell-specifically tagged mitochondria from tissues (Fecher, Trovò et al. 2019). *In vivo* tagging of mitochondria in genetically modified mouse strains allows for highly specific isolation of mitochondria deriving from a specific cell type regardless of the complexity of the tissue. However, while the immuno-isolation step is critical, the quality of the mitochondrial purification is still highly dependent on the earlier, more crude steps of the preparation. In accordance with Fecher et al. (Fecher, Trovò et al. 2019), we elected to utilize differential centrifugation in obtaining crude mitochondrial fractions, as opposed to gradient-based protocols (Sims and Anderson 2008; Wang, Leverin et al. 2011). While gradient-based isolation methods, such as those using sucrose or Percoll gradients, can result in greater purity of isolated mitochondria, they force mixed populations of mitochondria into closer proximity and increase the likelihood of adherence/fusion amongst mitochondria originating from different cells (de Mello, Fecher et al. 2023). We also employed mechanical rather than detergent-based tissue homogenization in order to better preserve mitochondrial integrity to avoid losing mitochondrial proteins from the sample.

Our data indicate that we successfully purified intact mitochondria from RGCs, as normal morphology was observed with electron microscopy and efficient recovery of both inner and outer mitochondrial membrane proteins was demonstrated by western blotting. We adjusted our protocol to optimize the specificity of the immunoprecipitations, although this level of stringency did come at the cost of some efficiency, as the presence of GFP in the flow-through indicates that a fraction of GFP-tagged RGC mitochondria failed to immunoprecipitate from both compartments **(Figure 10B)**. Using a mixing experiment, we further showed that the Mitocapture procedure avoids significant nonspecific clumping of mitochondria deriving from other cell types. Thus, we conclude that in our approach the intact mitochondria present in the immunoprecipitation overwhelmingly derive from the cell type of interest.

After completing the LC-MS/MS analysis of immuno-isolated mitochondria, our goal was to compare the abundance of proteins recovered from the somatodendritic and axonal compartments, in order to assess for differential compartment-specific regulation of mitochondrial protein composition. As in other mitochondrial proteomic analyses, we identified a large number of ‘non-mitochondrial’ proteins in immuno-isolated mitochondria from both compartments. While in most cases this can be explained by physical attachment between mitochondria and other cellular membranes and the cytoskeleton, it is also conceivable that some of them reflect previously unknown transient mitochondrial interactions (Guo, Zhang et al. 2022).

Two important caveats of our work must be discussed. First is the fact that the most proximal region of RGC axons exists in the innermost surface of the retina (the RNFL), and therefore some RGC axonal mitochondria will necessarily be isolated alongside somatodendritic mitochondria from retinal specimens. This is illustrated in **Figure 12A**, in which RGC expression of the axon-enriched protein HADHA appears to be limited almost exclusively to the RNFL rather than strongly labeling the RGC somas and dendrites like SOD2 and SFNX3. It is unavoidable, therefore, that the presence of the RNFL leads to some 'contamination' of the somatodendritic mitochondrial preparation with some axonal mitochondria, potentially diluting the degree of compartment-specific differences between the mitochondrial proteomes.

The second caveat is the observed expression of the GFP-OMM tag by horizontal cells in the OPL of the RGC MitoTag mouse retina **(Figure 9)**. Because the *Vglut2*-driven Cre is not entirely specific to RGCs, a mitochondrial purification from whole retina will inevitably recover some tagged mitochondria derived from horizontal cells. We previously showed that ~10% of horizontal cells demonstrate Cre-mediated genetic recombination in *Vglut2-Cre* mice, compared to >96% of RGCs (Wang, Klingeborn et al. 2020). Based on the literature, there are approximately 45,000 RGCs and 18,000 horizontal cells per mouse retina (Jeon, Strettoi et al. 1998; Whitney, Raven et al. 2011). If 10% of horizontal cells express Cre recombinase in RGC MitoTag mice, then they should be outnumbered by RGCs by approximately 24:1, which makes their contribution unlikely to significantly obscure compartment-specific mitochondrial proteome differences within RGCs. Nevertheless, due to both of the caveats we raised, it is particularly important that interesting differences identified in our proteomic analyses be validated using immunohistochemical techniques.

Potential biological significance of compartment-specific differences in the protein composition of RGC mitochondria

Within the somatodendritic compartment, we identified and immunohistochemically validated an enrichment of SOD2, a critical mitochondrial antioxidant protein that converts superoxide radicals to hydrogen peroxide (Sheng, Abreu et al. 2014). Another protein enriched in somatodendritic mitochondria is peroxiredoxin-5 (PRDX5), which can reduce hydrogen peroxide to water, among other functions (Kim, Park et al. 2018; Choi, Kim et al. 2019). The abundance of these antioxidant proteins may suggest that the RGC somatodendritic mitochondria are subjected to especially high levels of oxidative stress and/or require particularly efficient antioxidant pathways to scavenge free radicals and avoid oxidative damage. It is notable that a number of mitochondrial optic neuropathies have been associated with RGC oxidative stress (Wong, Cavelier et al. 2002; Beretta, Mattavelli et al. 2004; Samanta, Fariduddin et al. 2012; Formichi, Radi et al. 2015; Klein, Warren et al. 2017; Zhou, Yao et al. 2022).

Consistent with a high degree of sensitivity of the RGC soma to oxidative stress, we have previously shown in a mouse model of RGC-specific NDUFS4 deficiency that the onset of RGC soma degeneration appears to begin prior to loss of axons. *In vivo* work has further shown that adeno-associated virus-mediated overexpression of SOD2 attenuated RGC death in rats with high intraocular pressure (Jiang, Tang et al. 2016). SOD2 overexpression was also observed to inhibit apoptosis, reduce oxidative stress, and increase mitochondrial function in immortalized skin fibroblasts from patients with complex I deficiency and in cultured cells treated with the complex I inhibitor rotenone (Chen, McMillan-Ward et al. 2007; Zhou, Yao et al. 2022). Thus, a better understanding of antioxidant pathways in RGC somas may be of particular therapeutic relevance to mitochondrial optic neuropathies.

Another notable finding is that PRDX5 is enriched in RGC somatodendritic mitochondria, whereas the related protein PRDX3 is very highly enriched in RGC axonal mitochondria. Among all members of the peroxiredoxin family, PRDX3 and 5 are the only proteins that localize to mitochondria (PRDX3 is exclusively mitochondrial, while PRDX5 can also exist in peroxisomes and the cytosol) (Chae, Robison et al. 1994). PRDX3 and 5 are hypothesized to act as ROS sensors and peroxide scavengers in environments of high oxidative stress (De Simoni, Goemaere et al. 2008; Cox, Winterbourn et al. 2009). It is unclear to what extent PRDX3 and 5 are redundant in their functions, but the striking compartmental discrepancy in their abundance within RGC mitochondria is quite intriguing. Genetically modified mouse lines with loss of PRDX3 and PRDX5 have been generated and reportedly have relatively mild signs of systemic mitochondrial dysfunction (Huh, Kim et al. 2012; Kim, Park et al. 2018). It would be interesting to determine whether loss of either protein is associated with early compartment-specific RGC degenerative phenotypes.

It is also striking that we identified a number of components of the electron transport chain, particularly subunits of complex I and ATP synthase, as being enriched in the RGC somatodendritic compartment relative to the axonal compartment. While the relative abundances of these proteins and the relative activity levels of the electron transport chain in the two compartments remain to be validated, it would seem surprising for axonal mitochondria to have a lower ATP-generating capacity than their counterparts in the RGC soma and dendrites. However, recent work in cortical projection neurons has cast doubt on the role of oxidative phosphorylation in providing for the energy needs of axons, potentially indicating that mitochondrial functions other than ATP generation may be of particular importance in neuronal axons (Hirabayashi, Lewis et al. 2024).

Age-related Mitochondrial Proteome Changes and Axonal FAO

Numerous proteins related to FAO and the metabolism of fatty acids were identified as enriched in axonal mitochondria relative to somatodendritic mitochondria. To first validate an axonal signature of fatty acid metabolism, we used metabolomic analysis to identify the relative enrichment of fatty acylcarnitine molecules in RGC somatodendritic and axonal mitochondria. Cpt1a is responsible for conjugating a carnitine molecule to fatty acids in place of the existing

Coenzyme A (CoA). CoA is conjugated to fatty acid molecules through a class of proteins called acyl-CoA synthetases (LEIJ, KRAM et al. 1999; Yan, Yang et al. 2015). Once conjugated and a fatty acylcarnitine molecule is formed, it can be transported across the mitochondrial outer membrane by carnitine O-acetyltransferase, to the mitochondrial matrix (Qu, Zeng et al. 2016). Acylcarnitine metabolomic profiling allows us to view a snapshot of acylcarnitine molecules – primed for FAO – in mitochondria isolated from the somatodendritic and axonal compartments of RGCs. We identified significant increases in the concentration of C16, C16:1, and C18:1 fatty acylcarnitine molecules in RGC axonal mitochondria. It has previously been shown that peroxisomes may form mitochondria contacts and are a source of high FAO activity. It is important to note, however, that only FAO in mitochondria requires the conversion from fatty acyl-CoA to fatty acylcarnitine for mitochondrial import, while peroxisomes can metabolize free fatty acids and fatty acyl-CoA molecules. This suggests that the genetic knockout of Cpt1a in RGCs will only inhibit the import and metabolism of fatty acids in mitochondria, and not in other organelles. Additionally, while we identified an axon-specific enrichment of Very-Long Chain Acyl-CoA Dehydrogenase (VLCAD), it has been demonstrated that mitochondria preferentially metabolize long-chain fatty acids, while peroxisomes prefer shorter chain (He, Pei et al. 2011)

In the context of increased FAO in RGC axonal mitochondria, we decided to generate a genetic knock-out of Cpt1a, the protein responsible for priming fatty acids for mitochondrial import by exchanging carnitine and CoA (fatty acyl-CoA $\rightarrow$ fatty acylcarnitine). After generating the VGlut2-Cre/Cpt1a$^{fl/fl}$ (Cpt1a-KO) mouse, we allowed experimental (Cpt1a-KO) and control (VGlut2-Cre/Cpt1af$^{l/-}$) mice to age to 6-months-old (PD180). Aging Cpt1a-KO and control mice allow use to analyze the effect of age as a stressor on the normal degenerative processes of RGCs. Because we revealed that FAO is enriched in RGC axonal mitochondria, we hypothesized that under challenge from a stressor (age), RGC axons would be unable to sustain relevant mitochondrial functions and would trigger an axon-specific degenerative phenotype.

To understand to what extent Cpt1a loss has on RGCs, we analyzed RGC soma and axon density through microscopy imaging of retinal flat mounts and axon counting, respectively. Through these efforts, we identified that the RGC-specific loss of Cpt1a caused a non-significant decrease in RGC soma and axon density compared to control mice. While the lack of a definitive phenotype could suggest that RGCs are not in fact reliant on FAO under normal physiological conditions, enhanced adverse effects might become more apparent in the context of additional or more extreme cellular stressors. Stressors that would address these questions more clearly include increased aging (12-24 months age), high IOP, traumatic injury, and heritable or environmental insults to oxidative phosphorylation. While a direct and obvious RGC phenotype of degeneration was not apparent in our mice, the lack of FAO in RGC mitochondria could have functional consequences, such as the decreased ability to propagate an action potential. Therefore, assessing visual function in these mice with pattern electroretinography (pERG) or behavioral visual testing might reveal functional effects that are out of proportion to any subtle degenerative phenotype that might be at play.

Future experiments will be needed to further validate the findings outlined in this dissertation, and it would be fruitful to explore the pathophysiological role of compartmentalized mitochondrial functions. While we performed metabolomic analysis on mitochondria derived from RGC somatodendritic and axonal compartments, additional experiments should include a similar metabolomic evaluation of tissues obtained from mice with the genetic ablation of Cpt1a. This would reveal if any predilection for long-chain fatty acid metabolites in RGC axons is abrogated due to the inability to import fatty acids.

5. Conclusions

In conclusion, we optimized and employed a novel approach to isolate and characterize whole and intact mitochondria derived from discretely organized somatodendritic and axonal compartments of RGCs. We utilized liquid chromatography-tandem mass spectrometry to identify differences in the mitochondrial protein composition between RGC compartments. To this end, we identified compartment-specific enrichment of functionally distinct proteins between the two compartments. The enrichment of proteins related to ROS management in RGC somatodendritic mitochondria and FAO in RGC axonal mitochondria suggests the existence of mitochondrial functional differences within the RGC. While we validated the expression of compartment-specific proteins SOD2, SFXN3, and HADHA in RGCs, this approach should be easily adaptable to study the functional relevance of these proteins in RGC and neuronal compartments.

After identifying an axon-enriched signature of mitochondrial FAO proteins, we utilized metabolomics profiling to identify acylcarnitine species of various chain length in RGC-derived mitochondria. Our data suggests that RGC axonal mitochondria have an increase in availability of long-chain fatty acids for use as a metabolic substrate, compared to somatodendritic mitochondria. To understand the physiological relevance of FAO to RGCs, we generated the VGlut2-Cre/Cpt1a$^{fl/fl}$ mouse to genetically ablate the expression of CPT1a – the rate limiting enzyme for the import of fatty acids into mitochondria, where HADHA/HADHB catalyze the final three steps of FAO. Although we did not identify an axon- or RGC-specific phenotype of degeneration due to the loss of fatty acid import capacity to RGC mitochondria, a trend towards decreased RGC survival and axonopathy in knockout mice at 6-months of age was observed. More comprehensive studies examining the metabolic contribution of fatty acids to RGC ATP stores are needed to understand the dependence of RGCs on alternative metabolic substrates. These studies highlight initial understandings of compartmentalized regulation of mitochondrial proteome content in RGCs.

6. Materials and Methods

Animals

All animal experiments adhered to a protocol approved by the Institutional Animal Care and Use Committee of Duke University. Mice were housed under a 12-hour light-dark cycle with *ad libitum* access to food and water, and all experiments were carried out during the day. *Vglut2-Cre;GFP-OMM*$^{fl/fl}$ mice ('RGC MitoTag mice') were generated by crossing *Vglut2-Cre* mice(Vong, Ye et al. 2011) obtained from Jackson Labs (stock no. 028863) with GFP-OMM$^{fl/fl}$ mice(Fecher, Trovò et al. 2019) provided by Dr. Thomas Misgeld, Technical University of Munich. C57Bl/6J mice (Jackson Labs stock no. 000664) were used as wild type (WT) controls for all experiments. *VGlut2-Cre/Cpt1a*$^{fl/fl}$ mice (Cpt-KO) were generated by crossing *Vglut2-Cre* mice(Vong, Ye et al. 2011) obtained from Jackson Labs (stock no. 028863) with Cpt1a$^{fl/fl}$ mice(Raud, Roy et al. 2018) obtained from Jackson Labs (stock no. 032778). Littermate *VGlut2-Cre/Cpt1a*$^{fl/-}$ were used as controls for all Cpt-KO experiments.

Antibodies

The following antibodies with specified dilutions were used for immunofluorescence (IF) and western blot (WB) analyses: goat polyclonal anti-GFP ([1:1000 WB, 1:750 IF]; abcam, ab5450), rabbit polyclonal anti-HADHA (1:50 IF; abcam, ab54477), rabbit polyclonal anti-SOD2/MnSOD (1:50 IF; abcam, ab13534), mouse monoclonal anti-NDUFS4 (1:1000 WB; Santa Cruz Biotechnology, sc-100567), mouse monoclonal anti-Tuj1 (1:500 IF; Fisher Scientific, MAB11905), mouse polyclonal anti-VDAC (1:1000 WB; EMD Millipore, AB10527), rabbit polyclonal anti-SFXN3 (1:50 IF; Sigma, HPA008028), rabbit polyclonal anti-RBPMS (1:1000; Novus, NBP2-20112), rabbit polyclonal anti-HADHB (1:50; abcam, ab230667). Secondary antibodies against the appropriate species conjugated to Alexa Fluor 488 (1:1000), Alexa Fluor 568

(1:1000) or Alexa Fluor 680 (1:1000) were purchased from Invitrogen. Cell nuclei were stained using DAPI (Sigma Aldrich). Secondary antibodies against the appropriate species conjugated to IRDye 800CW or 680RD were purchased from Li-Cor for western blot experiments.

Intravitreal Injection of AAV

The plasmid EF1a-mito-dsRED2 was a gift from Thomas Schwarz (Addgene plasmid # 174541 ; http://n2t.net/addgene:174541 ; RRID:Addgene_174541). It contains a Flex-Switch-MitoDsRed construct under the transcriptional control of the EF-1α promoter. This construct was packaged into adeno-associated virus serotype 2 (AAV2) by the Duke University School of Medicine Viral Vector Core. 1.25uL of AAV2-Flex-Switch-MitoDsRed viral suspension at a concentration of 3.3×10^{12} vg/mL was injected into the vitreous cavity of anesthetized 3-month-old RGC MitoTag mice, followed by harvesting of optic nerve tissue four weeks later.

RGC Mitocapture Assay

Mitochondria were isolated from freshly collected mouse ocular tissues by adapting a previously described protocol(Wettmarshausen and Perocchi 2017; Fecher, Trovò et al. 2019). Adult (P90) RGC MitoTag and WT mice (N=3 each) were euthanized with intraperitoneal administration of a lethal dose of the anesthetic tribromoethanol (Avertin) and transcardially perfused with 1x PBS. Each eye was enucleated and severed at its base from the proximal optic nerve and then placed in 600 μL Isolation Buffer (IB) containing 220 mM Mannitol, 80 mM Sucrose, 10 mM HEPES, 1 mM EDTA, at pH 7.4, and supplemented with 1% essentially fatty acid-free BSA (A7030; Sigma) and 1x protease inhibitors (cOmplete EDTA-free Protease Inhibitor Cocktail; Roche). The calvaria and cortex were removed to expose the optic nerves, which were transected at the optic chiasm and placed into a separate tube containing 600 μL IB. At all stages of the procedure, the samples were kept on ice or at +4°C. Optic nerve tissue was initially minced with Vannas scissors, and retina tissue was dissected and removed from the remaining eye cup. The retina and optic nerve tissues were then separately disrupted in IB with a Dounce glass homogenizer using six up-and-down turns of a Type A pestle. The tissue was then further homogenized with six up-and-down turns of a Type B pestle. The cells were then lysed by nitrogen cavitation using a cell disruption vessel (model 4635; Parr Instrument Company) at 800 PSI, spinning at 80 rpm for 10 minutes. Following a slow pressure release from the nitrogen cavitation vessel, 1x protease inhibitor was added to the resulting tissue homogenate. Nuclei and other cellular debris were removed from the solution by centrifugation at 600 x g for 10 minutes. The supernatant was then transferred to a new tube with IB on ice. Pre-separation filters (#130-041-407; Miltenyi Biotec) were then hydrated with 1 mL of Immunocapture Buffer (ICB) containing 137 mM KCl, 2.5 mM $MgCl_2$, 3 mM KH_2PO_4, 10 mM HEPES, 1 mM EDTA, at pH 7.4, and supplemented with 1% essentially fatty acid-free BSA and 1x Protease Inhibitor cocktail. The transferred supernatant was then passed through the pre-separation filter and washed with 2 mL ICB. The filtered solution was then centrifuged at 13,000 x g for 3 minutes. The supernatant was removed, and the pellet resuspended in 400 uL ICB.

Subsequently, 100 uL of each sample was removed and set aside as representative “crude mitochondrial fraction.” The remaining 300 uL was diluted to 2 mL total with ICB and combined with 60 uL of superparamagnetic microbeads coated with mouse IgG_1 antibodies against GFP (#130-091-125; Miltenyi Biotec). These samples were then placed on a rotating wheel at +4°C for 1 hr. LS Columns (#130-042-401; Miltenyi Biotec) were then placed on a magnetic QuadroMACS separator (#130-090-976; Miltenyi Biotec) and equilibrated with 1 mL ICB. To separate the immunocaptured, GFP microbead-coated mitochondria from the remaining cellular material, the solution was then applied to the columns in 1 mL increments, allowing the solution to fully pass through the column until the remaining portion was applied. Importantly, while LS columns are attached to the QuadroMACS separator, bead-antibody complex, and immunoprecipitated material are trapped by the magnetic field. Once the entire sample had passed through the column, each column was washed with 4 x 4 mL ICB. The solution that passed through the column was designated as the flow-through. LS columns were then removed from the QuadroMACS magnetic separator, and GFP-labeled mitochondria were removed from the LS column with 2 x 3 mL washes with ICB, using a plunger to push the remaining immunoprecipitated sample through the column on the last wash. Mitochondria adherent to the microbeads were pelleted by centrifugation at 13,000 x g for 3 min and washed twice with IB without BSA with subsequent centrifugation at 13,000 x g for 3 min between washes. Pellets were stored at -80°C prior to western blot analysis or sample preparation for proteomic analysis.

Western Blotting

For western blot analysis, mitochondrial pellets were resuspended in RIPA buffer containing 50 mM Tris–HCl, pH 8.0, 150 mM NaCl, 0.1 mM EDTA and 1% Triton X-100, 0.25% Nonidet P-40, 0.1% SDS, as well as 1x Protease Inhibitor cocktail on ice for 30 min with frequent vortexing. Samples were mixed with 1x LDS sample buffer (NP0007; Thermo Fisher Scientific) and heated at 70°C for 10 min. SDS-PAGE was performed on the entire sample, followed by transfer to PVDF membrane pre-activated with methanol. Following transfer, the membrane was blocked with a 1:1 mixture of PBS-Tween (0.0125%) and Li-Cor Intercept Blocking Buffer (Li-Cor, catalogue #927-700001), then incubated overnight at +4°C with primary antibody. After washing, the blot was incubated with secondary antibody for 1 hr at room temperature, washed, and imaged using the Li-Cor Odyssey CLx.

Sample Preparation and LC-MS/MS Analysis

Protein concentration in the samples was determined with a BCA assay (Pierce BCA Protein Assay Kit; Thermo Fisher Scientific) according to the manufacturer's instructions, using BSA as the standard. For each sample, 10 µg of total protein was used to prepare peptide mixtures for proteomic profiling. Proteins were cleaved with the trypsin/endoproteinase LysC mixture (Promega, V5072) using the paramagnetic beads-based method(Hughes, Foehr et al. 2014). Each digest was dissolved in 12 µl of 1/2/97% (by volume) trifluoroacetic acid/acetonitrile/water solution, and 4 µl were injected into a 5 µm, 300 µm × 5 mm PepMap Neo C18 trap column (Thermo Fisher Scientific) in 1% acetonitrile in water for 3 min at 5 µl/min. Analytical separation of peptides was performed on an EasySpray PepMap 2 µm, 75 µm × 250 mm, C18 column (Thermo Fisher Scientific) over 90 min at a flow rate of 0.3 µl/min at 35°C, using Vanquish Neo UPLC (Thermo Fisher Scientific). The 2-30% mobile phase B gradient was used, where phase A was 0.1% formic acid in water and phase B 0.1% formic acid in acetonitrile. Peptides separated by LC were introduced into the Q Exactive HF Orbitrap mass spectrometer (Thermo Fisher Scientific) using positive electrospray ionization at 2000 V and capillary temperature of 275°C. Data collection was performed in the data-dependent acquisition (DDA) mode with 120,000 resolution (at m/z 200) for MS1 precursor measurements. The MS1 analysis utilized a scan from 375-1450 m/z with a target AGC value of 3.0e6 ions, the RF lens set at 30%, and a maximum injection time of 50 ms. Peptides were selected for MS/MS using charge state filtering (2-5), monoisotopic peak detection, and a dynamic exclusion time of 20 sec with a mass tolerance of 10 ppm. MS/MS analysis was performed using Higher-Energy Collisional Dissociation with a collision energy of 30±5% with detection in the ion trap using a rapid scanning rate, AGC target value of 1.0e5 ions, and maximum injection time of 100 ms.

Protein Identification and Quantification

For label-free relative protein quantification, raw mass spectral data files (.raw) were imported into Progenesis QI for Proteomics 4.2 software (Waters Inc.) for duplicate runs alignment of each preparation and peak area calculations. Peptides were identified using Mascot version 2.5.1 (Matrix Science) for searching the UniProt 2019 reviewed mouse database containing 17,008 entrees and supplemented with eGFP amino acid sequence from *Aequorea victoria*. Mascot search parameters were: 10 ppm mass tolerance for precursor ions; 0.025 Da for fragment-ion mass tolerance; one missed cleavage by trypsin; fixed modification was carbamidomethylation of cysteine; variable modification was oxidized methionine and deamidation of asparagine and glutamine. Only proteins identified with 2 or more peptides (peptide false discovery rate (FDR) < 0.5% and protein FDR < 1% calculated using reversed decoy database), were included in the protein quantification analysis. To account for variations in experimental conditions and amounts of protein material in individual LC-MS/MS runs, the integrated peak area for each identified peptide was corrected using the factors calculated by the automatic Progenesis algorithm utilizing the total intensities for all peaks in each run. Values representing protein amounts were calculated as a sum of ion intensities for all identified constituent non-conflicting peptides. Protein abundances were averaged for two technical replicates for each sample, and p-values were calculated for each protein using ANOVA analysis. The abundance ratio between RGC MitoTag and WT control sample was calculated for each protein.

In order to compare somatodendritic and axonal protein abundances, each proteomics dataset was first filtered by removing identified proteins with a Unique Peptide Count < 2, MitoTag/WT $\leq$ 1.5 and a p-value $\geq$ 0.05. We then collated the datasets to identify proteins that appeared in at least 3 of 4 biological replicates. After initial filtering of the datasets and protein identification across replicates, MitoTag protein abundance values were normalized to MitoTag

GFP values for each dataset and subsequently averaged among biological replicates to create an 'average GFP-normalized value' for each protein identified in at least 3 replicates. The ratio between normalized abundances of axonal and somatodendritic proteins was used to identify the relative enrichment of each protein in either compartment. Volcano plots were constructed to highlight the differential abundance of proteins identified in both somatodendritic and axonal compartments. For each identified protein, a t-test was performed to identify significantly enriched proteins in each compartment. Optic nerve to retina (ON/Ret) compartment enrichment ratios and p-values were calculated and plotted on the x and y axes using log_2 and $-log_{10}$ formulas, respectively. An ON/Ret or Ret/ON threshold ≥2 was applied to identify compartmentally-enriched proteins.

Sample Preparation for Acylcarnitine Analysis

Mitochondria were isolated from RGC MitoTag and WT mice (N=8) using the RGC mitocapture assay. Sample protein concentration was determined with a BCA assay according to the manufacturer's instructions, using BSA as the standard. For each sample, 22 µg of total protein was used to prepare peptide mixtures for metabolome profiling. Samples were resuspended in 50ul of 50% methanol in water. Acylcarnitines were analyzed by flow injection electrospray ionization tandem mass spectrometry and quantified by isotope or pseudo-isotope dilution using methods described previously(Newgard, An et al. 2004; Ferrara, Wang et al. 2008). Samples prepared in 50% methanol were spiked with a cocktail of heavy-isotope internal standards (Cambridge Isotope Laboratories, MA, USA; CDN Isotopes, Canada) and deproteinized with methanol. The methanol supernatants were dried under nitrogen and derivatized with acidified methanol for 15 min. at 50 ºC. Mass spectra for acylcarnitines were obtained using a precursor ion scan of *m/z* 99. The data were acquired in the positive ion mode using a Xevo TQD mass spectrometer equipped with

Acquity^{TM} UPLC system, and a data system controlled by MassLynx 4.1 operating system (Waters, Milford, MA). 80% methanol was used as a mobile phase. Ion ratios of analyte to respective internal standard computed from centroided spectra were converted to concentrations using calibrators constructed from authentic aliphatic acylcarnitines (Sigma, MO, USA; Larodan, Sweden) and dialyzed fetal bovine serum (Sigma, MO, USA).

Histological Preparation

For immunofluorescence experiments, RGC MitoTag mouse retina and optic nerve tissues were harvested following euthanasia. Enucleated eyes with optic nerves attached were fixed in 4% paraformaldehyde in PBS for 90 min on ice, followed by removal of the anterior segments to produce a posterior eyecup. After initial fixation, optic nerves were excised from the back of each eye. For retinal and optic nerve cross-sections, tissue samples were cryoprotected in sequential 15% and 30% sucrose solutions for 24 hours each. Tissue samples were frozen in Tissue Freezing Medium (Triangle Biomedical), sectioned at 16 μm on a Leica CM1950 cryostat, and placed on glass slides. Sections were hydrated in 1x PBS and blocked in 3% normal donkey serum in PBS with 0.3% Triton X-100. Sections were stained with primary antibodies diluted in blocking buffer overnight at 4°C in a humidity chamber. Sections were subsequently washed and incubated with secondary antibodies for 2 h at room temperature, followed by washing and mounting in Fluoromount G (Invitrogen).

To assess RGC axons, mouse optic nerve specimens were processed and analyzed as previously described(Li, Farsiu et al. 2014). Briefly, euthanized mice were exsanguinated via transcardial perfusion with 80 mL of ice-cold PBS followed by fixation with 80 mL of 4% PFA. Optic nerves were dissected back to the optic chiasm and fixed in 2% paraformaldehyde and 2% glutaraldehyde overnight, then washed and stored in PBS. Samples were embedded in the Embed-

812 resin mixture and sectioned on an ultramicrotome (LKB Ultratome V; Leica, Paris, France) using a glass knife. Cross-sections of 0.27 µm thickness were stained with 1% methylene blue. Axon counts were obtained using the Nikon Eclipse Ti2 microscope and AxoNet(Ritch, Hannon et al. 2020), an ImageJ plug-in for assessing RGC axons. For each optic nerve, 4 nerve section images were obtained using a 40X objective. Image analysis consisted of manual thresholding to adjust the contrast between myelin ensheathing axons and the axon intracellular area. The final count was divided by the total area sampled to determine mean axon density per nerve.

For quantification of retinal ganglion cell somas in retinal flatmounts, z-stacks through the retinal nerve fiber layer and ganglion cell layer of 45,000 μm^2 in area were obtained in each quadrant at locations of 0.5, 1.0, and 1.5 mm from the optic nerve head. RBPMS1-positive RGC somas were manually counted using the Cell Counter plugin for Fiji(Schneider, Rasband et al. 2012; Schroeder, Dobson et al. 2021). Cell density was averaged among the four quadrants at each distance from the optic nerve head.

Quantification of Protein Abundance by Immunofluorescence

To quantify the intensity of colocalized pixels between each protein of interest (SOD2, SFXN3, or HADHA) and GFP, stained retina and optic nerve sections were imaged on a Nikon Eclipse Ti2 inverted confocal microscope using a Nikon A1 confocal scanner system controlled by Nikon NIS-Elements software (Nikon, Tokyo, Japan). Images were acquired using a 40x objective with oil immersion. An 1800 m^2 region was used to acquire four images across independent retina and optic nerve tissue samples (N=4 of each). The ImageJ “AND” function was used to perform a bitwise comparison between the protein of interest and GFP immunostaining to create a “filtered” image of GFP-colocalized protein, from which the fluorescence intensity was then measured. Filtered fluorescence intensity was averaged across four images for each protein and divided by the average fluorescence intensity of GFP in each region to derive a representation of the abundance of each protein normalized to amount of mitochondrial material.

Electron Microscopy

For ultrastructural analysis, purified mitochondrial pellets from RGC MitoTag retinas and optic nerves obtained via the MitoCapture immunoprecipitation procedure were fixed in a solution of 2% glutaraldehyde and 2% paraformaldehyde in 1x PBS. The specimens were then post-fixed in a solution of 1% osmium tetroxide in 0.1% cacodylate buffer, followed by dehydration with graded ethanol from 30%-100% and propylene oxide. A 1:1 propylene oxide:Embed 812 Resin mixture was infiltrated overnight under a vacuum. Pure Embed 812 Resin was then exchanged on the second day and samples were incubated at 65°C overnight. Ultra-thin sections were then cut at 54-75 nm thickness (Leica EM CU7) and contrast stained with 1% uranyl acetate, 3.5% lead citrate solution. Image acquisition was then performed on a JEM-1400 transmission electron microscope (JEOL) using a Gatan ORIUS (1000) camera.

Statistics

Statistical analysis was performed using GraphPad Prism software. Specific sample size, statistical test and p-values for each experiment are given in the appropriate figure legends. p-values ≤ 0.05 were considered significant. Standard error bars are shown on graphs.

Bibliography

Abu-Remaileh, M., G. A. Wyant, C. Kim, N. N. Laqtom, M. Abbasi, S. H. Chan, E. Freinkman and D. M. Sabatini (2017). "Lysosomal metabolomics reveals V-ATPase- and mTOR-dependent regulation of amino acid efflux from lysosomes." Science (American Association for the Advancement of Science) **358**(6364): 807-813.

Ahier, A., T. Onraet and S. Zuryn (2021). "Cell-specific mitochondria affinity purification (CS-MAP) from Caenorhabditis elegans." STAR Protocols **2**(4): 100952.

Alston, C. L., M. C. Rocha, N. Z. Lax, D. M. Turnbull and R. W. Taylor (2017). "The genetics and pathology of mitochondrial disease." The Journal of Pathology **241**(2): 236-250.

Altmann, R. (1894). Die Elementarorganismen und ihre Beziehungen zu den Zellen, Veit.

Andrews, R. M., P. G. Griffiths, M. A. Johnson and D. M. Turnbull (1999). "Histochemical localisation of mitochondrial enzyme activity in human optic nerve and retina." British journal of ophthalmology **83**(2): 231-235.

Angelova, P. R., N. Esteras and A. Y. Abramov (2021). "Mitochondria and lipid peroxidation in the mechanism of neurodegeneration: Finding ways for prevention." Medicinal research reviews **41**(2): 770-784.

Attwell, D. and S. B. Laughlin (2001). "An energy budget for signaling in the grey matter of the brain." Journal of Cerebral Blood Flow & Metabolism **21**(10): 1133-1145.

Baden, T., T. Euler and P. Berens (2020). "Understanding the retinal basis of vision across species." Nature Reviews Neuroscience **21**(1): 5-20.

Ballabio, A. (2016). "The awesome lysosome." EMBO molecular medicine **8**(2): 73-76.

Ban, T., T. Ishihara, H. Kohno, S. Saita, A. Ichimura, K. Maenaka, T. Oka, K. Mihara and N. Ishihara (2017). "Molecular basis of selective mitochondrial fusion by heterotypic action between OPA1 and cardiolipin." Nature cell biology **19**(7): 856-863.

Bao, Z.-Z. (2008). "Intraretinal projection of retinal ganglion cell axons as a model system for studying axon navigation." Brain research **1192**: 165-177.

Barron, M. J., P. Griffiths, D. M. Turnbull, D. Bates and P. Nichols (2004). "The distributions of mitochondria and sodium channels reflect the specific energy requirements and conduction properties of the human optic nerve head." British journal of ophthalmology **88**(2): 286-290.

Beretta, S., L. Mattavelli, G. Sala, L. Tremolizzo, A. H. V. Schapira, A. Martinuzzi, V. Carelli and C. Ferrarese (2004). "Leber hereditary optic neuropathy mtDNA mutations disrupt glutamate transport in cybrid cell lines." Brain **127**(10): 2183-2192.

Bodenstein, D. F., P. Powlowski, K. A. Zachos, D. El Soufi El Sabbagh, H. Jeong, L. Attisano, L. Edgar, D. C. Wallace and A. C. Andreazza (2023). "Optimization of differential filtration-based mitochondrial isolation for mitochondrial transplant to cerebral organoids." Stem Cell Res Ther **14**(1): 202.

Boiko, T., A. Van Wart, J. H. Caldwell, S. R. Levinson, J. S. Trimmer and G. Matthews (2003). "Functional specialization of the axon initial segment by isoform-specific sodium channel targeting." J Neurosci **23**(6): 2306-2313.

Bonora, M., S. Patergnani, A. Rimessi, E. De Marchi, J. M. Suski, A. Bononi, C. Giorgi, S. Marchi, S. Missiroli, F. Poletti, M. R. Wieckowski and P. Pinton (2012). "ATP synthesis and storage." Purinergic Signal **8**(3): 343-357.

Bouzier-Sore, A.-K. and L. Pellerin (2013). "Unraveling the complex metabolic nature of astrocytes." Frontiers in cellular neuroscience **7**: 179.

Bricker, D. K., E. B. Taylor, J. C. Schell, T. Orsak, A. Boutron, Y.-C. Chen, J. E. Cox, C. M. Cardon, J. G. Van Vranken and N. Dephoure (2012). "A mitochondrial pyruvate carrier required for pyruvate uptake in yeast, Drosophila, and humans." Science **337**(6090): 96-100.

Brickley, K., M. J. Smith, M. Beck and F. A. Stephenson (2005). "GRIF-1 and OIP106, members of a novel gene family of coiled-coil domain proteins: association in vivo and in vitro with kinesin." Journal of Biological Chemistry **280**(15): 14723-14732.

Buono, L. M., R. Foroozan, R. C. Sergott and P. J. Savino (2002). "Is normal tension glaucoma actually an unrecognized hereditary optic neuropathy? New evidence from genetic analysis." Curr Opin Ophthalmol **13**(6): 362-370.

Burns, M. E. and V. Y. Arshavsky (2005). "Beyond Counting Photons: Trials and Trends in Vertebrate Visual Transduction." Neuron (Cambridge, Mass.) **48**(3): 387-401.

Carelli, V., C. La Morgia, F. N. Ross-Cisneros and A. A. Sadun (2017). "Optic neuropathies: the tip of the neurodegeneration iceberg." Human molecular genetics **26**(R2): R139-R150.

Carelli, V., F. N. Ross-Cisneros and A. A. Sadun (2004). "Mitochondrial dysfunction as a cause of optic neuropathies." Progress in retinal and eye research **23**(1): 53-89.

Chae, H. Z., K. Robison, L. B. Poole, G. Church, G. Storz and S. G. Rhee (1994). "Cloning and sequencing of thiol-specific antioxidant from mammalian brain: alkyl hydroperoxide reductase and thiol-specific antioxidant define a large family of antioxidant enzymes." Proc Natl Acad Sci U S A **91**(15): 7017-7021.

Chalecka, M., A. Kazberuk, J. Palka and A. Surazynski (2021). "P5C as an interface of proline interconvertible amino acids and its role in regulation of cell survival and apoptosis." International journal of molecular sciences **22**(21): 11763.

Chang, C.-R. and C. Blackstone (2010). "Dynamic regulation of mitochondrial fission through modification of the dynamin-related protein Drp1." Annals of the New York Academy of Sciences **1201**(1): 34-39.

Chapot, C. A., T. Euler and T. Schubert (2017). "How do horizontal cells 'talk' to cone photoreceptors? Different levels of complexity at the cone-horizontal cell synapse." J Physiol **595**(16): 5495-5506.

Chen, H., S. A. Detmer, A. J. Ewald, E. E. Griffin, S. E. Fraser and D. C. Chan (2003). "Mitofusins Mfn1 and Mfn2 coordinately regulate mitochondrial fusion and are essential for embryonic development." The Journal of cell biology **160**(2): 189-200.

Chen, H., J. M. McCaffery and D. C. Chan (2007). "Mitochondrial fusion protects against neurodegeneration in the cerebellum." Cell **130**(3): 548-562.

Chen, M., C. Luo, J. Zhao, G. Devarajan and H. Xu (2019). "Immune regulation in the aging retina." Progress in retinal and eye research **69**: 159-172.

Chen, Y., E. McMillan-Ward, J. Kong, S. J. Israels and S. B. Gibson (2007). "Mitochondrial electron-transport-chain inhibitors of complexes I and II induce autophagic cell death mediated by reactive oxygen species." J Cell Sci **120**(Pt 23): 4155-4166.

Choi, H. I., D. H. Kim, J. S. Park, I. J. Kim, C. S. Kim, E. H. Bae, S. K. Ma, T. H. Lee and S. W. Kim (2019). "Peroxiredoxin V (PrdxV) negatively regulates EGFR/Stat3-mediated fibrogenesis via a Cys48-dependent interaction between PrdxV and Stat3." Sci Rep **9**(1): 8751.

Cioni, J.-M., J. Q. Lin, A. V. Holtermann, M. Koppers, M. A. H. Jakobs, A. Azizi, B. Turner-Bridger, T. Shigeoka, K. Franze, W. A. Harris and C. E. Holt (2019). "Late Endosomes Act as mRNA Translation Platforms and Sustain Mitochondria in Axons." Cell **176**(1-2): 56-72.e15.

Cohen, Y., Y. A. Klug, L. Dimitrov, Z. Erez, S. G. Chuartzman, D. Elinger, I. Yofe, K. Soliman, J. Gärtner and S. Thoms (2014). "Peroxisomes are juxtaposed to strategic sites on mitochondria." Molecular BioSystems **10**(7): 1742-1748.

Consortium, T. U. (2020). "UniProt: the universal protein knowledgebase in 2021." Nucleic Acids Research **49**(D1): D480-D489.

Cooper, G. M. and K. Adams (2022). The cell: a molecular approach, Oxford University Press.

Cooper, M. L., S. D. Crish, D. M. Inman, P. J. Horner and D. J. Calkins (2016). "Early astrocyte redistribution in the optic nerve precedes axonopathy in the DBA/2J mouse model of glaucoma." Experimental eye research **150**: 22-33.

Cottrell, D. A., E. L. Blakely, M. A. Johnson, P. G. Ince, G. M. Borthwick and D. M. Turnbull (2001). "Cytochrome c oxidase deficient cells accumulate in the hippocampus and choroid plexus with age." Neurobiol Aging **22**(2): 265-272.

Cox, A. G., C. C. Winterbourn and M. B. Hampton (2009). "Mitochondrial peroxiredoxin involvement in antioxidant defence and redox signalling." Biochem J **425**(2): 313-325.

Davis, A. F. and D. A. Clayton (1996). "In situ localization of mitochondrial DNA replication in intact mammalian cells." The Journal of cell biology **135**(4): 883-893.

De Brito, O. M. and L. Scorrano (2008). "Mitofusin 2 tethers endoplasmic reticulum to mitochondria." Nature **456**(7222): 605-610.

de Mello, N. P., C. Fecher, A. M. Pastor, F. Perocchi and T. Misgeld (2023). "Ex vivo immunocapture and functional characterization of cell-type-specific mitochondria using MitoTag mice." Nat Protoc **18**(7): 2181-2220.

De Simoni, S., J. Goemaere and B. Knoops (2008). "Silencing of peroxiredoxin 3 and peroxiredoxin 5 reveals the role of mitochondrial peroxiredoxins in the protection of human neuroblastoma SH-SY5Y cells toward MPP+." Neurosci Lett **433**(3): 219-224.

Debanne, D., E. Campanac, A. Bialowas, E. Carlier and G. Alcaraz (2011). "Axon physiology." Physiological reviews **91**(2): 555-602.

Dhande, O. S., B. K. Stafford, J.-H. A. Lim and A. D. Huberman (2015). "Contributions of Retinal Ganglion Cells to Subcortical Visual Processing and Behaviors." Annual Review of Vision Science **1**(1): 291-328.

Faria-Pereira, A. and V. A. Morais (2022). "Synapses: The Brain's Energy-Demanding Sites." Int J Mol Sci **23**(7).

Fecher, C., L. Trovò, S. A. Müller, N. Snaidero, J. Wettmarshausen, S. Heink, O. Ortiz, I. Wagner, R. Kühn, J. Hartmann, R. M. Karl, A. Konnerth, T. Korn, W. Wurst, D. Merkler, S. F. Lichtenthaler, F. Perocchi and T. Misgeld (2019). "Cell-type-specific profiling of brain mitochondria reveals functional and molecular diversity." Nature neuroscience **22**(10): 1731.

Fedorenko, A., P. V. Lishko and Y. Kirichok (2012). "Mechanism of fatty-acid-dependent UCP1 uncoupling in brown fat mitochondria." Cell **151**(2): 400-413.

Fernandez-Marcos, P. J. and J. Auwerx (2011). "Regulation of PGC-1α, a nodal regulator of mitochondrial biogenesis." The American journal of clinical nutrition **93**(4): 884S-890S.

Ferrara, C. T., P. Wang, E. C. Neto, R. D. Stevens, J. R. Bain, B. R. Wenner, O. R. Ilkayeva, M. P. Keller, D. A. Blasiole, C. Kendziorski, B. S. Yandell, C. B. Newgard and A. D. Attie (2008). "Genetic networks of liver metabolism revealed by integration of metabolic and transcriptional profiling." PLoS genetics **4**(3): e1000034-e1000034.

Firl, A., J.-B. Ke, L. Zhang, P. G. Fuerst, J. H. Singer and M. B. Feller (2015). "Elucidating the role of AII amacrine cells in glutamatergic retinal waves." The Journal of neuroscience **35**(4): 1675-1686.

Flood, D., E. S. Lee and C. T. Taylor (2023). "Intracellular energy production and distribution in hypoxia." The Journal of biological chemistry **299**(9): 105103-105103.

Formichi, P., E. Radi, E. Giorgi, G. N. Gallus, J. Brunetti, C. Battisti, A. Rufa, M. T. Dotti, R. Franceschini, L. Bracci and A. Federico (2015). "Analysis of opa1 isoforms expression and apoptosis regulation in autosomal dominant optic atrophy (ADOA) patients with mutations in the opa1 gene." Journal of the neurological sciences **351**(1): 99-108.

Fransson, Å., A. Ruusala and P. Aspenström (2006). "The atypical Rho GTPases Miro-1 and Miro-2 have essential roles in mitochondrial trafficking." Biochemical and biophysical research communications **344**(2): 500-510.

Friedman, J. R., L. L. Lackner, M. West, J. R. DiBenedetto, J. Nunnari and G. K. Voeltz (2011). "ER tubules mark sites of mitochondrial division." Science **334**(6054): 358-362.

Funai, K., S. A. Summers and J. Rutter (2020). "Reign in the membrane: How common lipids govern mitochondrial function." Curr Opin Cell Biol **63**: 162-173.

Furchgott, R. F. and J. V. Zawadzki (1980). "The obligatory role of endothelial cells in the relaxation of arterial smooth muscle by acetylcholine." nature **288**(5789): 373-376.

Glater , E. E., L. J. Megeath , R. S. Stowers and T. L. Schwarz (2006). "Axonal transport of mitochondria requires milton to recruit kinesin heavy chain and is light chain independent." Journal of Cell Biology **173**(4): 545-557.

Green, D. R. and J. C. Reed (1998). "Mitochondria and Apoptosis." Science (American Association for the Advancement of Science) **281**(5381): 1309-1312.

Guo, J., L. Zhang, Y. Bu, W. Li, J. Hu and J. Li (2022). "Ras-related protein Rab-20 inhibition alleviates cerebral ischemia/reperfusion injury by inhibiting mitochondrial fission and dysfunction." Frontiers in molecular neuroscience **15**: 986710-986710.

Guo, X., E. S. Dason, V. Zanon-Moreno, Q. Jiang, A. Nahirnyj, D. Chan, J. G. Flanagan and J. M. Sivak (2014). "PGC-1α signaling coordinates susceptibility to metabolic and oxidative injury in the inner retina." The American journal of pathology **184**(4): 1017-1029.

Guo, X., J. Zhou, C. Starr, E. J. Mohns, Y. Li, E. P. Chen, Y. Yoon, C. P. Kellner, K. Tanaka, H. Wang, W. Liu, L. R. Pasquale, J. B. Demb, M. C. Crair and B. Chen (2021). "Preservation of vision after CaMKII-mediated protection of retinal ganglion cells." Cell **184**(16): 4299-4314.e4212.

Hattar, S., M. Kumar, A. Park, P. Tong, J. Tung, K. W. Yau and D. M. Berson (2006). "Central projections of melanopsin-expressing retinal ganglion cells in the mouse." Journal of Comparative Neurology **497**(3): 326-349.

He, M., Z. Pei, A.-W. Mohsen, P. Watkins, G. Murdoch, P. P. Van Veldhoven, R. Ensenauer and J. Vockley (2011). "Identification and characterization of new long chain Acyl-CoA dehydrogenases." Molecular genetics and metabolism **102**(4): 418-429.

Herzig, S., E. Raemy, S. Montessuit, J.-L. Veuthey, N. Zamboni, B. Westermann, E. R. Kunji and J.-C. Martinou (2012). "Identification and functional expression of the mitochondrial pyruvate carrier." Science **337**(6090): 93-96.

Hirabayashi, Y., T. L. Lewis, Jr., Y. Du, D. M. Virga, A. M. Decker, G. Coceano, J. Alvelid, M. A. Paul, S. Hamilton, P. Kneis, Y. Takahashi, J. T. Gaublomme, I. Testa and F. Polleux (2024). "Most axonal mitochondria in cortical pyramidal neurons lack mitochondrial DNA and consume ATP." bioRxiv.

Hönscher, C., M. Mari, K. Auffarth, M. Bohnert, J. Griffith, W. Geerts, M. van der Laan, M. Cabrera, F. Reggiori and C. Ungermann (2014). "Cellular metabolism regulates contact sites between vacuoles and mitochondria." Developmental cell **30**(1): 86-94.

Huberman, A. D., W. Wei, J. Elstrott, B. K. Stafford, M. B. Feller and B. A. Barres (2009). "Genetic identification of an On-Off direction-selective retinal ganglion cell subtype reveals a layer-specific subcortical map of posterior motion." Neuron **62**(3): 327-334.

Hughes, C. S., S. Foehr, D. A. Garfield, E. E. Furlong, L. M. Steinmetz and J. Krijgsveld (2014). "Ultrasensitive proteome analysis using paramagnetic bead technology." Mol Syst Biol **10**(10): 757.

Huh, J. Y., Y. Kim, J. Jeong, J. Park, I. Kim, K. H. Huh, Y. S. Kim, H. A. Woo, S. G. Rhee, K. J. Lee and H. Ha (2012). "Peroxiredoxin 3 is a key molecule regulating adipocyte oxidative stress, mitochondrial biogenesis, and adipokine expression." Antioxid Redox Signal **16**(3): 229-243.

Indo, H. P., M. Davidson, H.-C. Yen, S. Suenaga, K. Tomita, T. Nishii, M. Higuchi, Y. Koga, T. Ozawa and H. J. Majima (2007). "Evidence of ROS generation by mitochondria in cells with impaired electron transport chain and mitochondrial DNA damage." Mitochondrion **7**(1-2): 106-118.

Ishihara, N., Y. Fujita, T. Oka and K. Mihara (2006). "Regulation of mitochondrial morphology through proteolytic cleavage of OPA1." The EMBO journal **25**(13): 2966-2977.

Ishikawa, R., M. Nakamori, M. Takenaka, S. Aoki, Y. Yamazaki, A. Hashiguchi, H. Takashima and H. Maruyama (2023). "Case report: Mitochondrial trifunctional protein deficiency caused by HADHB gene mutation (c.1175C>T) characterized by higher brain dysfunction followed by neuropathy, presented gadolinium enhancement on brain imaging in an adult patient." Front Neurol **14**: 1187822.

Islinger, M., G. H. Lüers, H. Zischka, M. Ueffing and A. Völkl (2006). "Insights into the membrane proteome of rat liver peroxisomes: microsomal glutathione-S-transferase is shared by both subcellular compartments." Proteomics **6**(3): 804-816.

Ito, Y. A. and A. Di Polo (2017). "Mitochondrial dynamics, transport, and quality control: A bottleneck for retinal ganglion cell viability in optic neuropathies." Mitochondrion **36**: 186-192.

Jeon, C.-J., E. Strettoi and R. H. Masland (1998). "The Major Cell Populations of the Mouse Retina." The Journal of neuroscience **18**(21): 8936-8946.

Jiang, W., L. Tang, J. Zeng and B. Chen (2016). "Adeno-associated virus mediated SOD gene therapy protects the retinal ganglion cells from chronic intraocular pressure elevation induced injury via attenuating oxidative stress and improving mitochondrial dysfunction in a rat model." Am J Transl Res **8**(2): 799-810.

Kiedrowski, L. and E. Costa (1995). "Glutamate-induced destabilization of intracellular calcium concentration homeostasis in cultured cerebellar granule cells: role of mitochondria in calcium buffering." Molecular pharmacology **47**(1): 140-147.

Kim, M. H., S. J. Park, J. H. Kim, J. B. Seong, K. M. Kim, H. A. Woo and D. S. Lee (2018). "Peroxiredoxin 5 regulates adipogenesis-attenuating oxidative stress in obese mouse models induced by a high-fat diet." Free Radic Biol Med **123**: 27-38.

Kissová, I., M. k. Deffieu, S. Manon and N. Camougrand (2004). "Uth1p is involved in the autophagic degradation of mitochondria." Journal of Biological Chemistry **279**(37): 39068-39074.

Klein, K. A., A. K. Warren, C. R. Baumal and r. T. R. Hedges (2017). "Optical coherence tomography findings in methanol toxicity." International Journal of Retina and Vitreous **3**(1): 36-36.

Koentjoro, B., J.-S. Park and C. M. Sue (2017). "Nix restores mitophagy and mitochondrial function to protect against PINK1/Parkin-related Parkinson's disease." Scientific reports **7**(1): 44373.

Kole, Maarten H. P. and Greg J. Stuart (2012). "Signal Processing in the Axon Initial Segment." Neuron (Cambridge, Mass.) **73**(2): 235-247.

Lascaratos, G., K.-Y. Chau, H. Zhu, D. Gkotsi, R. King, I. Gout, D. Kamal, P. J. Luthert, A. H. V. Schapira and D. F. Garway-Heath (2015). "Resistance to the most common optic neuropathy is associated with systemic mitochondrial efficiency." Neurobiology of Disease **82**: 78-85.

Lee, E. J., J. C. Han and C. Kee (2017). "A novel hypothesis for the pathogenesis of glaucomatous disc hemorrhage." Progress in retinal and eye research **60**: 20-43.

Lee, S., L. Sheck, J. G. Crowston, N. J. Van Bergen, E. C. O'Neill, F. O'Hare, Y. X. G. Kong, V. Chrysostomou, A. L. Vincent and I. A. Trounce (2012). "Impaired Complex-I-Linked Respiration and ATP Synthesis in Primary Open-Angle Glaucoma Patient Lymphoblasts." Investigative Ophthalmology & Visual Science **53**(4): 2431-2437.

LEIJ, F. R. V. D., A. M. KRAM, B. BARTELDS, H. ROELOFSEN, G. B. SMID, J. TAKENS, V. A. ZAMMIT and J. R. KUIPERS (1999). "Cytological evidence that the C-terminus of carnitine palmitoyltransferase I is on the cytosolic face of the mitochondrial outer membrane." Biochemical Journal **341**(3): 777-784.

Li, G., S. Farsiu, J. Qiu, A. Dixon, C. Song, S. J. McKinnon, F. Yuan, P. Gonzalez and W. D. Stamer (2014). "Disease progression in iridocorneal angle tissues of BMP2-induced ocular hypertensive mice with optical coherence tomography." Molecular vision **20**: 1695-1709.

Liang, K., N. Li, X. Wang, J. Dai, P. Liu, C. Wang, X.-W. Chen, N. Gao and J. Xiao (2018). "Cryo-EM structure of human mitochondrial trifunctional protein." Proceedings of the National Academy of Sciences - PNAS **115**(27): 7039-7044.

Liao, S., L. Chen, Z. Song and H. He (2022). "The fate of damaged mitochondrial DNA in the cell." Biochimica et Biophysica Acta (BBA) - Molecular Cell Research **1869**(5): 119233.

Libby, R. T., Y. Li, O. V. Savinova, J. Barter, R. S. Smith, R. W. Nickells and S. W. John (2005). "Susceptibility to neurodegeneration in a glaucoma is modified by Bax gene dosage." PLoS Genet **1**(1): 17-26.

Lorincz, A. and Z. Nusser (2008). "Cell-Type-Dependent Molecular Composition of the Axon Initial Segment." The Journal of neuroscience **28**(53): 14329-14340.

Losón, O. C., Z. Song, H. Chen and D. C. Chan (2013). "Fis1, Mff, MiD49, and MiD51 mediate Drp1 recruitment in mitochondrial fission." Molecular Biology of the Cell **24**(5): 659-667.

Maddison, D. C., B. Malik, L. Amadio, D. M. Bis-Brewer, S. Züchner, O. M. Peters and G. A. Smith (2023). "COPI-regulated mitochondria-ER contact site formation maintains axonal integrity." Cell reports (Cambridge) **42**(8): 112883-112883.

Masland, R. H. (2012). "The neuronal organization of the retina." Neuron **76**(2): 266-280.

Mayoral, S. R., A. Etxeberria, Y. A. Shen and J. R. Chan (2018). "Initiation of CNS Myelination in the Optic Nerve Is Dependent on Axon Caliber." Cell Rep **25**(3): 544-550.e543.

Meeusen, S., J. M. McCaffery and J. Nunnari (2004). "Mitochondrial Fusion Intermediates Revealed in vitro." Science (American Association for the Advancement of Science) **305**(5691): 1747-1752.

Mikelberg, F. S., S. M. Drance, M. Schulzer, H. M. Yidegiligne and M. M. Weis (1989). "The normal human optic nerve: axon count and axon diameter distribution." Ophthalmology **96**(9): 1325-1328.

Misgeld, T. and T. L. Schwarz (2017). "Mitostasis in Neurons: Maintaining Mitochondria in an Extended Cellular Architecture." Neuron (Cambridge, Mass.) **96**(3): 651-666.

Morita, M., J. Prudent, K. Basu, V. Goyon, S. Katsumura, L. Hulea, D. Pearl, N. Siddiqui, S. Strack and S. McGuirk (2017). "mTOR controls mitochondrial dynamics and cell survival via MTFP1." Molecular cell **67**(6): 922-935. e925.

Nakabeppu, Y., D. Tsuchimoto, H. Yamaguchi and K. Sakumi (2007). "Oxidative damage in nucleic acids and Parkinson's disease." Journal of neuroscience research **85**(5): 919-934.

Naon, D., M. Zaninello, M. Giacomello, T. Varanita, F. Grespi, S. Lakshminaranayan, A. Serafini, M. Semenzato, S. Herkenne and M. I. Hernández-Alvarez (2016). "Critical reappraisal confirms that Mitofusin 2 is an endoplasmic reticulum–mitochondria tether." Proceedings of the National Academy of Sciences **113**(40): 11249-11254.

Narendra, D., A. Tanaka, D.-F. Suen and R. J. Youle (2008). "Parkin is recruited selectively to impaired mitochondria and promotes their autophagy." The Journal of cell biology **183**(5): 795-803.

Newgard, C. B., J. An, D. M. Muoio, M. Shiota, Y. Fujimoto, G. W. Cline, G. I. Shulman, T. R. Koves, R. Stevens and D. Millington (2004). "Hepatic expression of malonyl-CoA decarboxylase reverses muscle, liver and whole-animal insulin resistance." Nature medicine **10**(3): 268-274.

Norat, P., S. Soldozy, J. D. Sokolowski, C. M. Gorick, J. S. Kumar, Y. Chae, K. Yağmurlu, F. Prada, M. Walker, M. R. Levitt, R. J. Price, P. Tvrdik and M. Y. S. Kalani (2020). "Mitochondrial dysfunction in neurological disorders: Exploring mitochondrial transplantation." npj Regenerative medicine **5**(1): 22-22.

Novak, I., V. Kirkin, D. G. McEwan, J. Zhang, P. Wild, A. Rozenknop, V. Rogov, F. Löhr, D. Popovic and A. Occhipinti (2010). "Nix is a selective autophagy receptor for mitochondrial clearance." EMBO reports **11**(1): 45-51.

Nunnari, J. and A. Suomalainen (2012). "Mitochondria: In Sickness and in Health." Cell **148**(6): 1145-1159.

Pagliarini, D. J., S. E. Calvo, B. Chang, S. A. Sheth, S. B. Vafai, S.-E. Ong, G. A. Walford, C. Sugiana, A. Boneh, W. K. Chen, D. E. Hill, M. Vidal, J. G. Evans, D. R. Thorburn, S. A. Carr and V. K. Mootha (2008). "A Mitochondrial Protein Compendium Elucidates Complex I Disease Biology." Cell **134**(1): 112-123.

Parolisi, R. and E. Boda (2018). "NG2 glia: novel roles beyond Re-/Myelination." Neuroglia **1**(1): 151-175.

Peeters, A., A. B. Shinde, R. Dirkx, J. Smet, K. De Bock, M. Espeel, I. Vanhorebeek, A. Vanlander, R. Van Coster and P. Carmeliet (2015). "Mitochondria in peroxisome-deficient hepatocytes exhibit impaired respiration, depleted DNA, and PGC-1α independent proliferation." Biochimica et Biophysica Acta (BBA)-Molecular Cell Research **1853**(2): 285-298.

Pekkurnaz, G. and X. Wang (2022). "Mitochondrial heterogeneity and homeostasis through the lens of a neuron." Nature Metabolism **4**(7): 802-812.

Perelli, R. M., M. L. O'Sullivan, S. Zarnick and J. N. Kay (2021). "Environmental oxygen regulates astrocyte proliferation to guide angiogenesis during retinal development." Development (Cambridge) **148**(9).

Piantadosi, C. A., M. S. Carraway, A. Babiker and H. B. Suliman (2008). "Heme oxygenase-1 regulates cardiac mitochondrial biogenesis via Nrf2-mediated transcriptional control of nuclear respiratory factor-1." Circulation research **103**(11): 1232-1240.

Purevsuren, J., T. Fukao, Y. Hasegawa, H. Kobayashi, H. Li, Y. Mushimoto, S. Fukuda and S. Yamaguchi (2009). "Clinical and molecular aspects of Japanese patients with mitochondrial trifunctional protein deficiency." Mol Genet Metab **98**(4): 372-377.

Qi, Y., L. Yan, C. Yu, X. Guo, X. Zhou, X. Hu, X. Huang, Z. Rao, Z. Lou and J. Hu (2016). "Structures of human mitofusin 1 provide insight into mitochondrial tethering." J Cell Biol **215**(5): 621-629.

Qu, Q., F. Zeng, X. Liu, Q. J. Wang and F. Deng (2016). "Fatty acid oxidation and carnitine palmitoyltransferase I: emerging therapeutic targets in cancer." Cell Death & Disease **7**(5): e2226-e2226.

Quigley, H. A. D. (2011). "Glaucoma." The Lancet (British edition) **377**(9774): 1367-1377.

Quintela-López, T., H. Shiina and D. Attwell (2022). "Neuronal energy use and brain evolution." Current biology **32**(12): R650-R655.

Quintero, H., Y. Shiga, N. Belforte, L. Alarcon-Martinez, S. El Hajji, D. Villafranca-Baughman, F. Dotigny and A. Di Polo (2022). "Restoration of mitochondria axonal transport by adaptor Disc1 supplementation prevents neurodegeneration and rescues visual function." Cell Rep **40**(11): 111324.

Raimondi, V., F. Ciccarese and V. Ciminale (2020). "Oncogenic pathways and the electron transport chain: a dangeROS liaison." British Journal of Cancer **122**(2): 168-181.

Rasband, M. N. (2010). "The axon initial segment and the maintenance of neuronal polarity." Nature reviews. Neuroscience **11**(8): 552-562.

Rath, S., R. Sharma, R. Gupta, T. Ast, C. Chan, T. J. Durham, R. P. Goodman, Z. Grabarek, M. E. Haas, W. H. W. Hung, P. R. Joshi, A. A. Jourdain, S. H. Kim, A. V. Kotrys, S. S. Lam, J. G. McCoy, J. D. Meisel, M. Miranda, A. Panda, A. Patgiri, R. Rogers, S. Sadre, H. Shah, O. S. Skinner, T. L. To, M. A. Walker, H. Wang, P. S. Ward, J. Wengrod, C. C. Yuan, S. E. Calvo and V. K. Mootha (2021). "MitoCarta3.0: an updated mitochondrial proteome now with sub-organelle localization and pathway annotations." Nucleic Acids Res **49**(D1): D1541-d1547.

Raud, B., D. G. Roy, A. S. Divakaruni, T. N. Tarasenko, R. Franke, E. H. Ma, B. Samborska, W. Y. Hsieh, A. H. Wong, P. Stüve, C. Arnold-Schrauf, M. Guderian, M. Lochner, S. Rampertaap, K. Romito, J. Monsale, M. Brönstrup, S. J. Bensinger, A. N. Murphy, P. J. McGuire, R. G. Jones, T. Sparwasser and L. Berod (2018). "Etomoxir Actions on Regulatory and Memory T Cells Are Independent of Cpt1a-Mediated Fatty Acid Oxidation." Cell Metab **28**(3): 504-515.e507.

Richard, M. A., G. G. Philip, A. J. Margaret and M. T. Douglass (1999). "Histochemical localisation of mitochondrial enzyme activity in human optic nerve and retina." British Journal of Ophthalmology **83**(2): 231.

Ritch, M. D., B. G. Hannon, A. T. Read, A. J. Feola, G. A. Cull, J. Reynaud, J. C. Morrison, C. F. Burgoyne, M. T. Pardue and C. R. Ethier (2020). "AxoNet: A deep learning-based tool to count retinal ganglion cell axons." Scientific Reports **10**(1): 8034.

Ronnett, G. V., E. K. Kim, L. E. Landree and Y. Tu (2005). "Fatty acid metabolism as a target for obesity treatment." Physiol Behav **85**(1): 25-35.

Rosenberg, T., S. Nørby, M. Schwartz, J. Saillard, P. J. Magalhães, D. Leroy, E. C. Kann and M. Duno (2016). "Prevalence and Genetics of Leber Hereditary Optic Neuropathy in the Danish Population." Investigative ophthalmology & visual science **57**(3): 1370-1375.

Rueden, C. T., J. Schindelin, M. C. Hiner, B. E. DeZonia, A. E. Walter, E. T. Arena and K. W. Eliceiri (2017). "ImageJ2: ImageJ for the next generation of scientific image data." BMC Bioinformatics **18**(1): 529.

Samanta, S. K., K. Fariduddin, N. Mahapatra, J. Bhunia and P. Mondal (2012). "Hooch blindness: a community study report on a few indoor patients of toxic optic neuropathy following consumption of adulterated alcohol in West Bengal." Nepalese journal of ophthalmology **4**(1): 162-164.

Schneider, C. A., W. S. Rasband and K. W. Eliceiri (2012). "NIH Image to ImageJ: 25 years of image analysis." Nature methods **9**(7): 671-675.

Schroeder, A. B., E. T. A. Dobson, C. T. Rueden, P. Tomancak, F. Jug and K. W. Eliceiri (2021). "The ImageJ ecosystem: Open-source software for image visualization, processing, and analysis." Protein science **30**(1): 234-249.

Schwarz, T. L. (2013). "Mitochondrial trafficking in neurons." Cold Spring Harbor perspectives in biology **5**(6): a011304.

Schweers, R. L., J. Zhang, M. S. Randall, M. R. Loyd, W. Li, F. C. Dorsey, M. Kundu, J. T. Opferman, J. L. Cleveland and J. L. Miller (2007). "NIX is required for programmed mitochondrial clearance during reticulocyte maturation." Proceedings of the National Academy of Sciences **104**(49): 19500-19505.

Sheng, Y., I. A. Abreu, D. E. Cabelli, M. J. Maroney, A.-F. Miller, M. Teixeira and J. S. Valentine (2014). "Superoxide Dismutases and Superoxide Reductases." Chemical Reviews **114**(7): 3854-3918.

Sims, N. R. and M. F. Anderson (2008). "Isolation of mitochondria from rat brain using Percoll density gradient centrifugation." Nature protocols **3**(7): 1228-1239.

Sohal, R. S. and B. H. Sohal (1991). "Hydrogen peroxide release by mitochondria increases during aging." Mech Ageing Dev **57**(2): 187-202.

Soubannier, V., P. Rippstein, B. A. Kaufman, E. A. Shoubridge and H. M. McBride (2012). "Reconstitution of mitochondria derived vesicle formation demonstrates selective enrichment of oxidized cargo." PloS one **7**(12): e52830.

Stowers, R. S., L. J. Megeath, J. Górska-Andrzejak, I. A. Meinertzhagen and T. L. Schwarz (2002). "Axonal transport of mitochondria to synapses depends on milton, a novel Drosophila protein." Neuron **36**(6): 1063-1077.

Sun, D., M. Lye-Barthel, R. H. Masland and T. C. Jakobs (2009). "The morphology and spatial arrangement of astrocytes in the optic nerve head of the mouse." Journal of Comparative Neurology **516**(1): 1-19.

Sundaramurthy, S., A. SelvaKumar, J. Ching, V. Dharani, S. Sarangapani and P. Yu-Wai-Man (2021). "Leber hereditary optic neuropathy—new insights and old challenges." Graefe's archive for clinical and experimental ophthalmology **259**(9): 2461-2472.

Tal, R., G. Winter, N. Ecker, D. J. Klionsky and H. Abeliovich (2007). "Aup1p, a yeast mitochondrial protein phosphatase homolog, is required for efficient stationary phase mitophagy and cell survival." Journal of Biological Chemistry **282**(8): 5617-5624.

Tanaka, M., S. A. Kovalenko, J. S. Gong, H. J. Borgeld, K. Katsumata, M. Hayakawa, M. Yoneda and T. Ozawa (1996). "Accumulation of deletions and point mutations in mitochondrial genome in degenerative diseases." Ann N Y Acad Sci **786**: 102-111.

Torres, N., S. Tobón-Cornejo, L. A. Velazquez-Villegas, L. G. Noriega, G. Alemán-Escondrillas and A. R. Tovar (2023). "Amino Acid Catabolism: An Overlooked Area of Metabolism." Nutrients **15**(15).

Ušaj, M. M., M. Brložnik, P. Kaferle, M. Žitnik, H. Wolinski, F. Leitner, S. Kohlwein, B. Zupan and U. Petrovič (2015). "Genome-wide localization study of yeast Pex11 identifies peroxisome–mitochondria interactions through the ERMES complex." Journal of molecular biology **427**(11): 2072-2087.

Van Bergen, N. J., J. G. Crowston, J. E. Craig, K. P. Burdon, L. S. Kearns, S. Sharma, A. W. Hewitt, D. A. Mackey and I. A. Trounce (2015). "Measurement of systemic mitochondrial function in advanced primary open-angle glaucoma and leber hereditary optic neuropathy." PloS one **10**(10): e0140919.

Varma, R., T. S. Vajaranant, B. Burkemper, S. Wu, M. Torres, C. Hsu, F. Choudhury and R. McKean-Cowdin (2016). "Visual Impairment and Blindness in Adults in the United States: Demographic and Geographic Variations From 2015 to 2050." JAMA ophthalmology **134**(7): 802-809.

Vong, L., C. Ye, Z. Yang, B. Choi, S. Chua, Jr. and B. B. Lowell (2011). "Leptin action on GABAergic neurons prevents obesity and reduces inhibitory tone to POMC neurons." Neuron **71**(1): 142-154.

Vos, M., E. Lauwers and P. Verstreken (2010). "Synaptic mitochondria in synaptic transmission and organization of vesicle pools in health and disease." Frontiers in synaptic neuroscience **2**: 139.

Wang, J. T., Z. A. Medress and B. A. Barres (2012). "Axon degeneration: molecular mechanisms of a self-destruction pathway." J Cell Biol **196**(1): 7-18.

Wang, L., J. Dong, G. Cull, B. Fortune and G. A. Cioffi (2003). "Varicosities of intraretinal ganglion cell axons in human and nonhuman primates." Investigative ophthalmology & visual science **44**(1): 2-9.

Wang, L., M. Klingeborn, A. M. Travis, Y. Hao, V. Y. Arshavsky and r. S. M. Gospe (2020). "Progressive optic atrophy in a retinal ganglion cell-specific mouse model of complex I deficiency." Scientific reports **10**(1): 16326-16326.

Wang, X., A. L. Leverin, W. Han, C. Zhu, B. R. Johansson, E. Jacotot, V. S. Ten, N. R. Sims and H. Hagberg (2011). "Isolation of brain mitochondria from neonatal mice." Journal of neurochemistry **119**(6): 1253-1261.

Wang, Y., E. Xu, P. R. Musich and F. Lin (2019). "Mitochondrial dysfunction in neurodegenerative diseases and the potential countermeasure." CNS neuroscience & therapeutics **25**(7): 816-824.

Wässle, H. (2004). "Parallel processing in the mammalian retina." Nature Reviews Neuroscience **5**(10): 747-757.

Wettmarshausen, J. and F. Perocchi (2017). Isolation of Functional Mitochondria from Cultured Cells and Mouse Tissues. Methods in molecular biology (Clifton, N.J.). New York, NY, Springer New York. **1567:** 15-32.

Whitney, I. E., M. A. Raven, D. C. Ciobanu, R. A. PochÃ©, Q. Ding, Y. Elshatory, L. Gan, R. W. Williams and B. E. Reese (2011). "Genetic modulation of horizontal cell number in the mouse retina." Proceedings of the National Academy of Sciences - PNAS **108**(23): 9697-9702.

Wiegand, G. and S. J. Remington (1986). "Citrate synthase: structure, control, and mechanism." Annual review of biophysics and biophysical chemistry **15**(1): 97-117.

Wilkison, S. J., C. L. Bright, R. Vancini, D. J. Song, H. M. Bomze and R. Cartoni (2021). "Local Accumulation of Axonal Mitochondria in the Optic Nerve Glial Lamina Precedes Myelination." Frontiers in neuroanatomy **15**: 678501-678501.

Williams, P. A., J. M. Harder, N. E. Foxworth, B. H. Cardozo, K. E. Cochran and S. W. M. John (2017). "Nicotinamide and WLDS Act Together to Prevent Neurodegeneration in Glaucoma." Frontiers in neuroscience **11**: 232-232.

Williams, P. A., J. M. Harder, N. E. Foxworth, K. E. Cochran, V. M. Philip, V. Porciatti, O. Smithies and S. W. M. John (2017). "Vitamin B_3 modulates mitochondrial vulnerability and prevents glaucoma in aged mice." Science (American Association for the Advancement of Science) **355**(6326): 756-760.

Wong, A., L. Cavelier, H. E. Collins-Schramm, M. F. Seldin, M. McGrogan, M.-L. Savontaus and G. A. Cortopassi (2002). "Differentiation-specific effects of LHON mutations introduced into neuronal NT2 cells." Human molecular genetics **11**(4): 431-438.

Yakes, F. M. and B. Van Houten (1997). "Mitochondrial DNA damage is more extensive and persists longer than nuclear DNA damage in human cells following oxidative stress." Proceedings of the National Academy of Sciences **94**(2): 514-519.

Yan, S., X.-F. Yang, H.-L. Liu, N. Fu, Y. Ouyang and K. Qing (2015). "Long-chain acyl-CoA synthetase in fatty acid metabolism involved in liver and other diseases: an update." World Journal of Gastroenterology: WJG **21**(12): 3492.

Yang, Y., Y. Ogawa, K. L. Hedstrom and M. N. Rasband (2007). "βIV spectrin is recruited to axon initial segments and nodes of Ranvier by ankyrinG." The Journal of cell biology **176**(4): 509-519.

Yazdankhah, M., P. Shang, S. Ghosh, S. Hose, H. Liu, J. Weiss, C. S. Fitting, I. A. Bhutto, J. S. Zigler, Jr., J. Qian, J. A. Sahel, D. Sinha and N. A. Stepicheva (2021). "Role of glia in optic nerve." Prog Retin Eye Res **81**: 100886.

Youle, R. J. and D. P. Narendra (2011). "Mechanisms of mitophagy." Nature reviews Molecular cell biology **12**(1): 9-14.

Yu, D.-Y., S. J. Cringle, C. Balaratnasingam, W. H. Morgan, P. K. Yu and E.-N. Su (2013). "Retinal ganglion cells: Energetics, compartmentation, axonal transport, cytoskeletons and vulnerability." Progress in retinal and eye research **36**: 217-246.

Yu, F., R. Courjaret, L. Assaf, A. Elmi, A. Hammad, M. Fisher, M. Terasaki and K. Machaca (2024). "Mitochondria-ER contact sites expand during mitosis." iScience **27**(4): 109379-109379.

Yu, S. B. and G. Pekkurnaz (2018). "Mechanisms Orchestrating Mitochondrial Dynamics for Energy Homeostasis." Journal of Molecular Biology **430**(21): 3922-3941.

Yu Wai Man, C. Y., P. F. Chinnery and P. G. Griffiths (2005). "Optic neuropathies--importance of spatial distribution of mitochondria as well as function." Medical hypotheses **65**(6): 1038.

Yu-Wai-Man, P., P. G. Griffiths, N. Howell, D. M. Turnbull and P. F. Chinnery (2016). "The Epidemiology of Leber Hereditary Optic Neuropathy in the North East of England." American journal of human genetics **98**(6): 1271-1271.

Yu-Wai-Man, P., M. I. Trenell, K. G. Hollingsworth, P. G. Griffiths and P. F. Chinnery (2011). "OPA1 mutations impair mitochondrial function in both pure and complicated dominant optic atrophy." Brain (London, England : 1878) **134**(Pt 4): e164-e164.

Zanna, C., A. Ghelli, A. M. Porcelli, M. Karbowski, R. J. Youle, S. Schimpf, B. Wissinger, M. Pinti, A. Cossarizza, S. Vidoni, M. L. Valentino, M. Rugolo and V. Carelli (2008). "OPA1 mutations associated with dominant optic atrophy impair oxidative phosphorylation and mitochondrial fusion." Brain (London, England : 1878) **131**(2): 352-367.

Zhou, Q., S. Yao, M. Yang, Q. Guo, Y. Li, L. Li and B. Lei (2022). "Superoxide dismutase 2 ameliorates mitochondrial dysfunction in skin fibroblasts of Leber's hereditary optic neuropathy patients." Frontiers in neuroscience **16**: 917348-917348.

Biography

Liam Lewis was born in Fredericksburg, Virginia. After graduating from Luray High School, in Luray, VA, he attended Virginia Commonwealth University and majored in Bioinformatics with concentrations in Biology and Chemistry. Liam worked at Inboden Environmental Services in Mt. Jackson, VA, and participated in an NIH-sponsored Post-Baccalaureate Research Education program at VCU (VCU PREP) in the years following college. After being admitted to the Cell & Molecular Biology program at Duke University in 2018, Liam subsequently joined the emerging lab of Romain Cartoni, PhD, in the Pharmacology Department to study the fascinating world of mitochondrial biology in Retinal Ganglion Cells. After joining the lab of Sidney Gospe, III, MD, PhD in 2023, Liam worked with Sid and Vadim Arshavsky to complete his project to shed light on the emerging concept of compartmentalized mitochondrial functions in RGCs. Liam is enthusiastic to begin a post-academic career in Life Sciences Consulting.